

Estimating Lake Evaporation Using Meteorological Data & Remote Sensing

**A Case Study of Lake Naivasha
Central Rift Valley, Kenya**

Ashfaque Ahmed

April, 1999

Estimating Lake Evaporation Using Meteorological Data & Remote Sensing

A Case Study of Lake Naivasha, Central Rift Valley, Kenya

**By
Ashfaque Ahmed**

Thesis submitted to the International Institute for Aerospace Survey and Earth Sciences (ITC), Enschede, The Netherlands, in partial fulfillment of the requirements for the degree of Master of Science in Water Resources Survey with emphasis on Watershed Management and Conservation.

Degree Assessment Board:

Prof. Dr. A.M.J. Meijerink (Chairman of the Examination Board)
Dr. H.A.R. de Bruin (External Examiner)
Dr. W.G.M. Bastiaanssen (Main Supervisor)
G.N. Parodi, MSc (2nd Supervisor)



APRIL, 1999

INTERNATIONAL INSTITUTE FOR AEROSPACE SURVEY AND EARTH SCIENCES
ENSCHDEDE, THE NETHERLANDS

In the name of Allah
The Merciful, The Compassionate

Dedication

This work is dedicated to my wife and my late son Ahmed Munaz Ashfaque

ACKNOWLEDGEMENTS

First of all I thank the almighty Allah whom through his Grace and Blessing has sustained me for all these years. The completion of this study has been made possible through the love support, sacrifice and encouragement of many to whom I shall be eternally indebted.

First and foremost, I would like to express my thanks to Dutch government for the fellowship grant and the rare opportunity given to me to study at ITC. I highly appreciate the full support by provided my organization and my colleagues at the Bangladesh Water Development Board during the whole duration of my study.

I sincerely thank Dr. W.G.M. Bastiaanssen who has been a supervisor, mentor and friend to me. He has been quite patient with me and prodding to me the right track. His support and advice at all stages of this work have been invaluable. My gratitude also goes to my second supervisor G.N. Parodi for his valuable suggestions.

I am most grateful to Prof. Dr. A.M.J. Meijerink, Head of Water Resources and Environmental Studies Division, for his interest in my work and for his useful suggestions and comments. All staff of the Water Resources and Environmental Studies Division has been helpful and my appreciation goes to them all.

I am indebted to Mr. Farah, O. Hossain of Moi University, Kenya, who helped me during fieldwork and continued to send me data even on my return to Netherlands. I am also grateful to Dr. Sylvia J. M. Barlag, Head Satellite data Division, KNMI, for reports, Journals and data she provided for the study.

My course mates have provided a wonderful atmosphere for study and several suggestions. In particular I wanted to convey my gratitude to Mr. Antonio L. Querido (Cape Verde), Anthony Duah (Ghana), Ahmad M. Salah (Egypt), Behar Hossain (Ethiopia), Fathi A. Hamouda (Egypt), Jorge Salazar (Bolivia), Julian Gressando (Indonesia), Mekonnen G. Michael (Ethiopia), Robert R. Hernandez (Cuba), Samuel G. Mmbui (Kenya) and Mrs. Zhen Xu Tang (China).

Special thanks to my wife for her confidence and never ending support and encouragement. My parents, family and friends have also encouraged me and above all prayed for me. I owe a great deal for the spiritual support you gave.

Last but not least, I am grateful to the people of Kenya, where my fieldwork was done. I am grateful to the staff of the Kenyan Wildlife services Training Center, Naivasha, especially Mr. Litondo, Principal of the Training Center, who helped me by providing boat and car for data collection during my fieldwork.

Finally I wish to express my sincere appreciate to countless friend-far and near- and members of my extended family who encouraged and gave me immeasurable physical, moral and spiritual support in my endeavors.

ABSTRACT

Evaporation from the lake Naivasha, Kenya is a major component of water balance. This study examines the evaporation losses from this lake evaluated by the energy balance method with other two approaches (Penman method and Priestley Taylor approach) by using meteorological data from lake surface as well as data from weather station and also by remotely sensed spectral data. Energy budget calculation shows that the sensible heat flux and the water heat flux in the lake is negligibly small and on average almost all of the daily net radiation is utilized in the evaporative process over the lake. From the comparison of the two methods with the energy balance approach, Priestley-Taylor approach with coefficient $\alpha=1.26$, was found very close to energy balance approach. From instantaneous evaporation to daily estimation, evaporative fraction method was used and the value of evaporative fraction ≈ 1 was obtained above the lake surface. For the net longwave radiation calculations, a simple equation given by Slob was tested and compared with a commonly used equation, which comprises many variables. A high correlation ($r^2 = 0.995$) was obtained for long-term comparison and the result shows that, evaporation can be calculated within $\pm 5\%$ from the lake using this equation. From the satellite images and field observations, negligible spatial variation of evaporation, surface temperature and albedo was found in the lake. For remote sensing evaporation estimation, TM image of 21st January 1995 was used. The daily total evaporation from the lake was found 5.95 mm using evaporative fraction approach and Slob's equation for daily net longwave radiation. Whereas from pan data the estimated average evaporation was 5.46 mm for 21st January with a standard deviation of 1.28 mm for the period of 1957-1990. In this thesis also a new remote sensing approach, TOVS (TIROS Operational Vertical Sounder) and its applicability in evaporation calculation has discussed.

Table of Contents

Dedication	iii
Acknowledgements	iv
Abstract	v
Table of Contents	vi
List of Figures	viii
List of Tables	x
List of Frequently Used Symbols	xi
List of Acronyms	xiv
Chapter 1: Introduction	1
1.1 General	1
1.2 Importance of the Study	1
1.3 Conflicting Evaporation values of lake Naivasha	2
1.4 Objective of the Study	3
1.5 Methodology	3
1.5.1 Field method	3
1.5.2 Remote sensing	3
1.6 Sources of data	4
Chapter 2: The Study Area	5
2.1 Kenya Rift Valley	5
2.2 Geology of the Area	5
2.3 Location and Description of the Lake Naivasha	6
2.3.1 The Lake	6
2.3.2 Climate	7
2.4 Water Balance of Lake Naivasha	11
Chapter 3: Theory of Open Water Evaporation	13
3.1 Radiation Balance	13
3.2 Surface Energy Balance	16
3.3 Bowen Ratio Method	18
3.4 Penman Equation	19
3.5 Priestley and Taylor Equation	19
3.6 Remote sensing	20
3.6.1 Net Shortwave Radiation	20
3.6.2 Net Longwave Radiation	20
3.7 Data collection and Instruments	21

Chapter 4: Remote sensing Evaporation, TOVS Application	23
4.1 General	23
4.2 TOVS Application	24
4.2.1 Shortwave radiation	25
4.2.2 Longwave radiation	27
4.2.3 Air Temperature, Vapor pressure, and Vapor Pressure Deficit	29
Chapter 5: Data Analysis and Results	31
5.1 Field Campaign October 1998	31
5.2 Annual Evaporation from field data	40
5.2.1 Lake Evaporation using Ndabibi station data	42
5.2.2 Long-term evaporation from Ndabibi Met. Station data	44
5.3 Remote sensing	45
5.3.1 TOVS Application	45
5.3.2 Thematic Mapper Application	46
Chapter 6: Conclusions	48
REFERENCES	50
APPENDICES	
APPENDIX A : Climatic data	A-1
AI : General Climatic Data of Naivasha	A-1
AII : Mean Rainfall figure for selected Station	A-1
AIII: Daily Insolation	A-2
AIV: Temperature data for Naivasha Vet. Expt. Station	A-2
APPENDIX B : Water Balance of Lake Naivasha	A-3
BI : Water Balance determined by Gaudet and Maleck (1979)	A-3
BII : Water Balance determined by LNROA (1993)	A-4
APPENDIX C : Evaporative demand of the atmosphere (Standard micro- meteorological expression required for evaporation calculation)	A-5
CI : Water Vapor	A-5
CII : Radiation	A-7
APPENDIX D : Evapotranspiration from Water Hyacinth	A-10
APPENDIX E : TOVS	A-14
EI : TOVS Sensors	A-14
EII : Data availability, Geographic location & coverage, Parameters	A-18
EIII: TOVS atmospheric profile	A-20
APPENDIX F : Thematic Mapper Application	A-22
APPENDIX G : Field data and Analysis	A-24

List of Figures

<i>Figure 1.1:</i> Monthly total and accumulated evaporation using pan data from 1957-1990	2
<i>Figure 2.1:</i> Great Kenyan Rift Valley	5
<i>Figure 2.2:</i> Location Map	6
<i>Figure 2.3:</i> A general trend of climatic data of Naivasha Town	7
<i>Figure 2.4:</i> Locations of different meteorological stations	8
<i>Figure 2.5:</i> General trend of wind velocity in Naivasha area (1937-54)	8
<i>Figure 2.6:</i> Rainfall variation of two stations around Lake Naivasha	9
<i>Figure 2.7:</i> Daily average evaporation from Class A land Pan data using Pan coefficient 1.0.	9
<i>Figure 2.8:</i> Monthly means of daily Insolation of Kedong Met. Station (0°55' S, 36°30' E, 1961-68)	10
<i>Figure 2.9:</i> Temperature variation of Naivasha meteorological stations (1937-1954)	10
<i>Figure 2.10:</i> General trend of monthly mean Cloud cover in Naivasha area (Kedong 0°55' S, 36°30' E, 1961-68)	11
<i>Figure 2.11:</i> General trend of Cloud cover in daytime above the Lake Naivasha (8 th October 1998)	11
<i>Figure 4.1:</i> Atmospheric temperature profile and perceptible water content in the atmosphere derived from TOVS sensors	24
<i>Figure 4.2:</i> Comparison of mean daily solar radiation derived from satellite observations with ground measurements for 4 seasonal months	25
<i>Figure 4.3:</i> Comparison of mean monthly air temperature derived from satellite measurements (TOVS) and surface observations)	29
<i>Figure 4.4:</i> Comparison of mean monthly vapor pressure derived from satellite measurements (TOVS) and surface observations	30
<i>Figure 4.5:</i> Comparison of mean monthly vapor pressure deficit derived from satellite measurements (TOVS) and surface observations	30
<i>Figure 5.1:</i> Effect of cloud and atmosphere on incoming solar radiation	31
<i>Figure 5.2:</i> Variation of Albedo of lake water surface with local time	32
<i>Figure 5.3:</i> Diurnal variation of longwave (LW) radiation	33
<i>Figure 5.4:</i> Variation of Net radiation with local time	33
<i>Figure 5.5:</i> Comparison of net radiation (Slob approaches Vs Calculated)	35

<i>Figure 5.6:</i> Variation of radiation fluxes with local time	35
<i>Figure 5.7:</i> Variation of Sensible heat flux in daytime	36
<i>Figure 5.8:</i> Variation of water temperature with depth and local time	37
<i>Figure 5.9:</i> Variation of Latent heat flux, R_n , G_o and H with Local Time	38
<i>Figure 5.10:</i> The variations of evaporative fraction with the daytime	39
<i>Figure 5.11:</i> Comparison of Bowen ratio, Penman equation and Priestley- Taylor equation with Energy balance (residual) approach	40
<i>Figure 5.12:</i> Variation of incoming solar radiation and net longwave at two stations	41
<i>Figure 5.13:</i> Variation of Evaporation at two stations	42
<i>Figure 5.14:</i> Daily evaporation by two methods	42
<i>Figure 5.15:</i> Comparison of Slob's approach with the field (Smith approach) method	42
<i>Figure 5.16:</i> Fluctuation of daily average incoming solar radiation at Ndabibi met. Station	44
<i>Figure 5.17:</i> Trend of the variation of solar radiation and difference of daily max and min temperature over time at Ndabibi met station	44
<i>Figure 5.18:</i> Comparison of long-term mean incoming shortwave radiation and evaporation (Kedong Met. Station, 0°55' S, 36°30' E, 1961-68) data with 1 year (1998-1999) Ndabibi data	45
<i>Figure 5.19:</i> Spatial variation of daily evaporation [mm] from lake surface derived from TM image (9 ⁴⁵ AM, 21 st January 1995)	46
<i>Figure 5.20:</i> Surface temperature of lake Naivasha derived from TM image (9 ⁴⁵ AM, 21 st January 1995)	47
<i>Figure 5.21:</i> Instantaneous latent heat flux from the lake using energy balance equation (9 ⁴⁵ AM, 21 st January 1995)	47
<i>Figure 5.22:</i> Instantaneous latent heat flux from the lake using Priestley-Taylor equation (9 ⁴⁵ AM, 21 st January 1995)	47

List of Tables

Table 2.1: Four component of Lake Naivasha	7
Table 2.2: Water balance of Lake Naivasha	12
Table 3.1: Instruments used for data collection during the field campaign in October 1998	22
Table 4.1: The TOVS meteorological product description	24
Table 5.1: Sensible heat flux at different daytime (8 th October 1998)	36
Table 5.2: Water heat flux in daytime (8 th October '98)	37
Table 5.3: Variation of Latent heat flux, R_n , G_o and H with Local Time (8 th October 1998)	38
Table 5.4: Comparison of three methods with Energy balance method	40
Table 5.5: Monthly Average value of Evaporation and other climatic parameters (Ndabibi Meteorological Station)	43
Table 5.6: Long term evaporation using Kedong Met. Station data (1961-68)	46

List of Frequently Used Symbols

Symbols	Interpretation	Unit
α	Priestley- Taylor coefficient	[-]
γ	Psychrometric Constant	[mbar. K ⁻¹]
β	Bowen ratio	[-]
Δ	Slope of saturated vapor pressure curve	[mbar. K ⁻¹]
λ	Latent heat of vaporization	[J.kg ⁻¹]
λ	The wavelength	[μ m]
λ_w	Thermal conductivity of the water	[W.m ⁻¹ .K ⁻¹]
Γ	Adiabatic lapse rate	[K.m ⁻¹]
σ	Stephan Boltzmann constant	[W.m ⁻² .K ⁻⁴]
δ	Solar declination	[rad]
ω_a	Instantaneous Solar hour angle	[rad]
ω	Solar hour angle representing the 24 hour solar radiation	[rad]
Λ	Evaporative fraction	[-]
A_{inst}	Instantaneous evaporative fraction	[-]
$A_{24\ hours}$	Integrated daily evaporative fraction	[-]
ρ_a	Moist air density	[kg. m ⁻³]
ρ_d	Dry air density	[kg. m ⁻³]
ρ_v	Actual vapor density	[kg. m ⁻³]
ρ_w	Density of water	[kg. m ⁻³],
ϵ_a	Emissivity of air	[-]
ϵ_a^{avg}	Average emissivity of the atmosphere	[-]
ϵ_λ	Emissivity of the natural body in wavelength λ .	[-]
ϵ_o	Broadband surface emissivity	[-]
λE	Latent heat flux	[W. m ⁻²]
Ψ_{sh}	Integrated stability function for sensible heat	[-]
Ψ_{sm}	Integrated stability function for momentum transfer	[-]
ϕ_{su}	Solar zenith angle	[rad]
τ_{sw}	Atmospheric shortwave transmittance	[-]
τ_{sw}''	Two-way transmittance for broadband	[-]
τ_{sw}^{avg}	Average atmospheric shortwave transmittance	[-]
τ_6	Atmospheric transmittance in the region of thermal channel TM6[-]	
B	Bandwidth	[μ m]

Symbols	Interpretation	Unit
BB	Broadband albedo	[-]
D	Vapor pressure deficit	[mbar]
cos	Cosine function	[rad]
c_p	Specific heat of moist air	[J.kg ⁻¹ .K ⁻¹]
d	Displacement height	[m]
d_s	Relative distance between earth and sun	[AU]
E	Evaporation	[m. s ⁻¹]
E_o	Eccentricity correction factor	[-]
e_a	Actual vapor pressure	[mbar]
e_s	Saturated vapor pressure	[mbar]
e_1	Vapor pressure at height z_1	[mbar]
e_2	Vapor pressure at height z_2	[mbar]
G_o	Soil or water heat flux	[W. m ⁻²]
H	Sensible heat flux	[W. m ⁻²]
h	Plant height	[m]
J	Day number of the year	[-]
k	Von karman's constant	[-]
$K\downarrow$	Incoming short wave solar radiation	[W. m ⁻²]
$K\uparrow$	Outgoing short wave solar radiation	[W. m ⁻²]
K^*	Net shortwave radiation	[W. m ⁻²]
KB^{-1}	Roughness for momentum/heat flux density ratio	[-]
$L(T_o)\uparrow$	Outgoing longwave radiation from the natural surface	[W. m ⁻²]
$L\downarrow$	Incoming long wave radiation	[W. m ⁻²]
$L\uparrow$	Outgoing long wave radiation	[W.m ⁻²]
$L_\lambda(T_o)$	Longwave radiation of the natural bodies	[W.m ⁻²]
L_λ^{bb}	Blackbody energy emission	[W.m ⁻² . μm^{-1}]
L^*	Net long wave thermal radiation	[W. m ⁻²]
L_6^{atm}	Longwave radiation emitted from the top of atmosphere upward	[W. m ⁻²]
L_6^{surf}	Emitted radiance at the land surface from thermal channel TM6	[W. m ⁻²]
L_6^{TOA}	Emitted radiance at TOA from thermal channel TM6	[W. m ⁻²]
L_i^{TOA}	Reflectance of band i at top of atmosphere (TOA)	[W. m ⁻²]
lat	Latitude	[rad]
n	Total number of spectral bands	[-]
n	Actual hours of sunshine	[Hours]

Symbols	Interpretation	Unit
N	Maximum possible sunshine hours	[Hours]
P	Total pressure	[mbar]
R_a	Daily Extra-terrestrial short wave solar radiation	[W. m ⁻²]
R_n	Net radiation	[W. m ⁻²]
$R_{n24\ hour}$	Average net radiation for the day	[W. m ⁻²]
R_{ai}	Instantaneous Extra-terrestrial short wave solar radiation	[W. m ⁻²]
r_a	Lowest planetary albedo at all pixels	[-]
r_{ah}	Aerodynamic resistance to heat transport	[s. m ⁻¹]
r_o	Broad band albedo	[-]
r_o	Surface albedo	[-]
r_p	Broadband planetary albedo	[-]
r_s	canopy resistance	[s.m ⁻¹]
sin	Sine function which should be in radian mode	[-]
T	Average of surface and air temperature	[K]
T_{dry}	Dry bulb temperature	[K]
T_{wet}	Wet bulb temperature	[K]
T_1	Air temperature at height z_1	[K]
T_2	Air temperature at height z_2	[K]
T_a	Air temperature at observation height	[K]
T_o	Water surface temperature	[K]
T_w	Temperature of water	[K]
U	Relative Humidity	[-]
u	Velocity of air	[m . s ⁻¹]
Z	Elevation	[m]
z	Height	[m]
z_o	Roughness height	[m]
z_{oh}	Roughness height for heat transport	[m]
z_{om}	Roughness height for momentum transport	[m]

List of Acronyms

AMSL	Above Mean Sea Level
AMSU	Advanced Microwave Sounding Unit
ATOVS	Advanced TIROS Operational Vertical Sounder
AVHRR	Advanced Very High Resolution Radiometer
BB	Broad Band
DFL	Downward Longwave Fluxes
DO	District Office
ECMWF	European Centre for Medium range Weather Forecasts
HIRS/2	High resolution InfraRed Sounder version 2
LE	Latent heat flux for Evaporation
LW	Long Wave
MSU	Microwave Sounding Unit
NOAA	National Oceanic and Atmospheric Administration
RMS	Root Mean Square
SEE	Standard Error of Estimate
SW	Short Wave
TIR	Thermal InfraRed
TM	Thematic Mapper
TOA	Top of Atmosphere
TOVS	TIROS Operational Vertical Sounder
UTM	Universal Transverse Mercator
WDD	Water Development Department
WH	Water Hyacinth
WS	Water Surface

Chapter 1

Introduction

1.1 General

Evaporation is a significant component of hydrologic cycles. The sun provides the large amount of energy required for transformation but the amount of solar energy received at the earth's surface is not the only important element involved. There will be no evaporation without water. It has been found that four principle meteorological factors, solar radiation, air temperature, humidity and wind movement must be determined for a satisfactory estimation of rate of evaporation if the presence of water is not limiting. The latitudinally average evaporation has a maximum near the equator and near zero at the pole. The general pattern is similar to that of radiation balance and temperature, reflecting the importance and of the availability of energy to supply the latent heat that accompanies the phase change.

In catchment scale hydrology, it is often necessary to estimate evaporation rate that will occur in a reservoir or naturally formed lake. In this thesis, an attempt was made to estimate evaporation from the Lake Naivasha, Kenya, by field measurements and remote sensing approach. For field measurements, the surface energy balance approach was used.

1.2 Importance of the Study

Lake Naivasha is one of the important fresh water lakes of Kenya. It is a fresh water lake at 1887-m altitude surrounded by the alkaline lakes of Elmenteita, Nakuru, Magadi and Bogoria. Over the last fifteen to twenty years, there has been tremendous agricultural and geothermal power development based on the extraction of water from the lake. The lake is the major source for domestic and industrial water supply. It is very important to know how much water losses from the lake through evaporation for the availability of fresh water to the agricultural, domestic and industrial sector.

Research on lake evaporation is needed, also because empirical methods to estimate evaporation are not necessarily correct. The uncertainties related to various empirical methods such as pan evaporation and evapometers can be best evaluated by comparison to an accurate standard; therefore it is desirable to develop a physically based solution, such as the energy balance method. Hoy and Stephens (1977 p iii, as cited by Assoline and Marher 1993) states that “ The energy budget method is known to give the most reliable estimate of lake evaporation”. Also this method is considered to be the most accurate method to estimate lake evaporation by many of other researchers and generally used as reference method [Reis and Dias, 1998; Choudhury. B. J., 1994; Rosenberry. et. al. 1993; Assouline and Marher, 1993; Sturrock et. al. 1992; Stewart and. Rose, 1976; Simons and Mero, 1985; Robertson and Berry, 1985; de Bruin, 1982; Keijman, 1981; Keijman, 1974]

1.3 Conflicting Evaporation values of lake Naivasha

The estimation of actual evaporation remains a difficult issue. In the case of Lake Naivasha, limited available data together with the general problem of estimating evaporation from the pan observation makes any estimate unreliable. Various figures are used for evaporation from free water surface of Lake Naivasha. Ase (1986) has pointed out that it is difficult to arrive at an accurate figure. The average annual figure calculated from pan evaporation was $1865 \pm 106 \text{mm}$ for 1965-1982 using pan coefficient 1. Usually this method over estimates actual evaporation due to the wall of the pan giving an extra heating effect. Moreover pans are usually installed onshore. From a study by Brind and Robertson (1958) it is suggested that the pan factor of Naivasha D.C. varies between 0.84-1.04 but Ase (1986) suggested a multiplication factor of 0.8 for lake evaporation which is related to reference crop and normally used for the class-A pan in Kenya and then he calculated an evaporation of 1492mm per annum. A monthly variation of evaporation of Naivasha meteorological station from a class- A pan is shown in Figure 1.1 using pan coefficient 1.0.

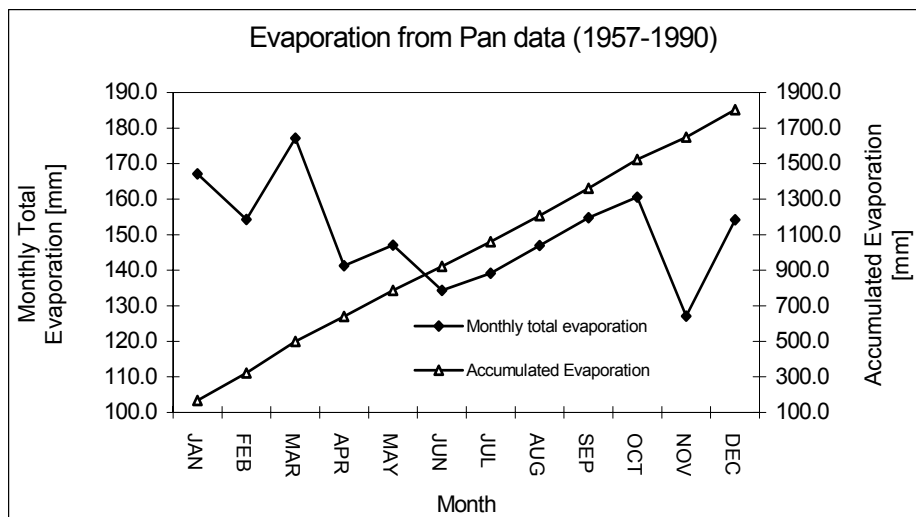


Figure. 1.1: Monthly total and accumulated evaporation using pan data from 1957-1990.

Tetley (1948) considered that the evaporation of Lake Naivasha varies between 1555mm and 2287 mm with an average annual figure of 1830mm. Chance (1944, after LNROA, 1993) the irrigation adviser in the ministry of Agriculture at that time regarded evaporation for the lake as 1850mm. England and Robertson (1959) using a different formula calculated the evaporation rate at $63.6 \pm 10\%$ equivalent to 1358mm.

The District Council Irrigation sub-committee (1950, after LNROA, 1993) used different evaporation figures for the lake from the year 1960 to 1964, but there is no record of how they arrived at this data.

Year	Evaporation in feet
1960	6.22 (1866mm)
1961	6.26 (1878mm)
1962	5.38 (1614mm)
1963	5.45 (1635mm)
1964	5.23 (1569mm)

LNROA (1993) in their environmental study used a value of 1500mm for open water and 60% of this (i.e. 900mm) for swamp area. Lake Naivasha Riparian Association within the Lake management Plan (LNROA, 1996) use 1529mm for open water evaporation and 2141mm for swamp area, although this physically rather unlikely. A brief explanation and calculations using the data collected during the fieldwork is presented in Appendix D.

Hence it is obvious that a more accurate method is required for estimating lake evaporation.

1.4 Objective of the study:

- 1) To determine the temporal variations in Lake Naivasha evaporation for the period May 1998 to January 1999.
- 2) Estimate evaporation from remote sensing devices, which create the opportunity of retrieving longer time series.

1.5 Methodology:

1.5.1 Field Method:

Meteorological data were collected from the surface of the lake in order to calculate instantaneous evaporation. The following Methods were used:

- Residual Method of the Surface energy Balance Equation
- Bowen Ratio Method
- Penman Equation
- Priestley-Taylor Equation

1.5.2 Remote sensing:

To estimate lake evaporation using remotely sensed spectral data, a TM image of 21st January, 1995 was used. Instantaneous latent heat flux and daily total evaporation was calculated using surface energy balance equation and for daily evaporation, evaporative fraction approach was followed. Also a new remote sensing approach, i.e. TOVS data was used to calculate net radiation.

1.6 Sources Data

Field Measurement data, October 1998.

Pan evaporation data from Meteorological Dept. Kenya (Period: 1957-1990)

Data from unofficial met station Loldia (Period: 14th July'98 to 12th October 1998)

Data from unofficial met station Ndabibi (Period: 14th May to January 1999)

Different Reports and Research papers about the Lake (See list of references)

TOVS atmospheric profile (Period: July 1998)

Satellite images of the Lake area (TM image, 21st January, 1995)

Hydrology textbooks & hand books

Chapter 2

The Study Area

2.1 Kenya Rift Valley

The Study area is concentrated in the Kenyan Rift valley. The central rift valley of Kenya, shown in Figure 2.1 is of moderate altitude (2000m AMSL). The area forms a catchment for the drainage from two extensive forest stands on both margins of the rift; the Nyandarua Mountains (Aberdara Range) on the East rise to about 3960m and Mau Escarpment on the West to above 3000m. The catchment presently includes three lakes: Naivasha, Nauru and Elmenteita.

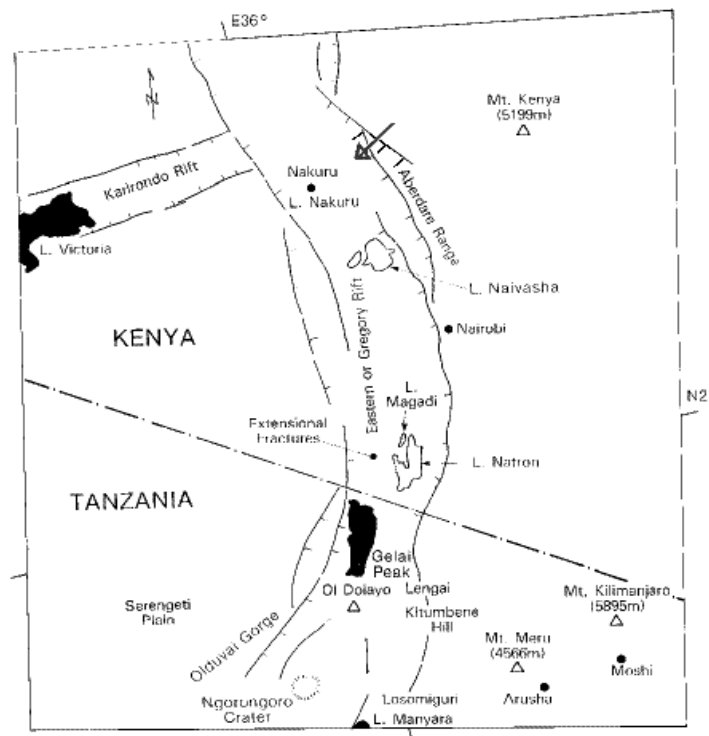


Figure 2.1: Great Kenyan Rift Valley

The floor of the rift valley around the lake Naivasha belongs to Tertiary- Quaternary volcanic suite with associated alkaline sediments. It is characterized by exceptionally long and intense volcanic activity from middle Pleistocene to the last hundred years.

2.2 Geology of the Area

The Lake Naivasha is situated in the Eastern or Gregory Rift, part of Great Rift Valley, which stretched from Jordan in the Middle East to Mozambique in southeast Africa. The Rift Valley was formed through many episodes of faulting and volcanism some 30M years ago. In geologic terms, the lake is very young, and there is still much evidence of volcanic activities. The geological map of the Naivasha area does not include any formation older than Quaternary, in fact these are not older than lower Pleistocene. Especially the area

around the Mount Longonot has very recent features like parasitic cone, the lava field of which is not yet fully covered by the vegetation.

Naivasha Lake is the highest part of the Rift Kenya (1887m AMSL). The older lake sediments are composed of a mixture of volcanic ash and reworked volcanic strata. Soils of the lacustrine plains around the lake have developed from the volcanic ashes. Soils can vary from well to poorly drained, fine to sandy silt and clay loams of varying color, but often pale.

2.3 Location and Description of Lake Naivasha

2.3.1 The Lake

The lake situated in the southwest of Kenya, map reference 0°45' S and 36°20' E, 80 kms south of the equator and 70 kms northwest of Nairobi the capital of Kenya (Fig. 2.2). Lake Naivasha is situated in the bottom of the eastern or Gregory Rift valley, in the middle of three major centers of geothermal activity- the Eburru hills to the northwest, Mount Longonot to the southeast, and Olkaria to the south. The lake is the highest and the freshest of all Rift valley Lakes in eastern Africa. Administratively the lake and its immediate environs are situated in the Naivasha division of the Nakuru District in the rift valley province of Kenya. Although Lake Naivasha is generally referred to as one lake, it has been general practice in the scientific literature to distinguish between four components shown in Table 2.1.

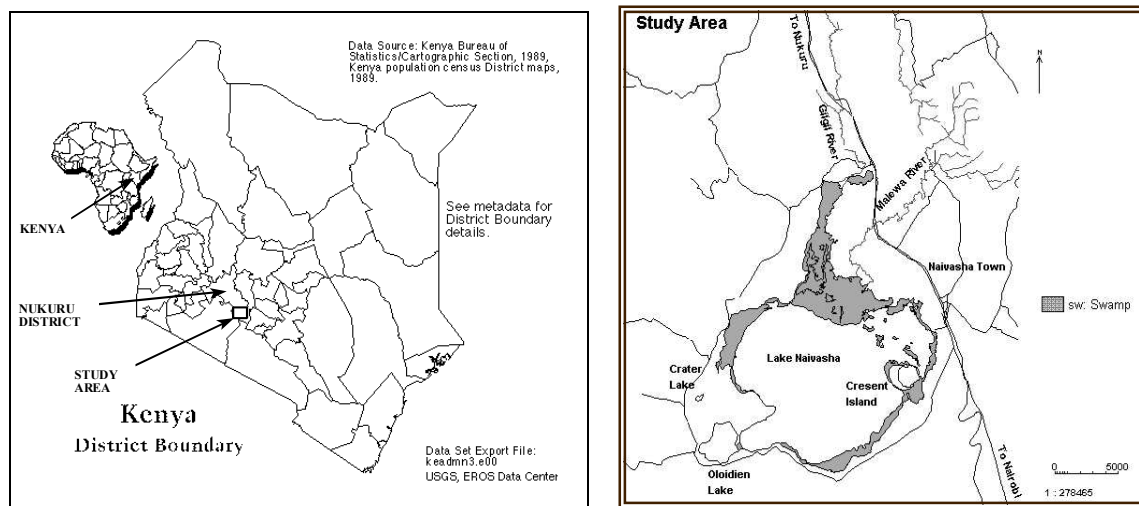


Figure 2.2: Location Map

Table 2.1: Four components of Lake Naivasha

<i>component of Lake Naivasha</i>	<i>Area (km²)</i>	<i>Volume (m³×10⁶)</i>	<i>Mean depth (m)</i>
Lake Naivasha	145	680	4.7
Crescent Island basin	2.1	23	11.0
Oloidien	5.5	31	5.6
Sonachi (Crater lake)	0.6	0.62	3.8
<i>Total</i>	<i>153.2</i>	<i>734.62</i>	

Source: LNROA, 1993.

The boundaries of the four bodies have been formed by the tectonic activity associates and with the formation of the Rift Valley (Richardson and Richardson, 1972).

In the most resent history the lake has shown tremendous change in depth, area and volume. From 1909 to 1969 the lake's area has varied from 216.27 to 88.08 km², and the capacity from 1702.23×10⁶ to 148.02×10⁶ cubic meters. In all a fluctuation in area is of 245% and in volume 1150%. However, the general trend for both parameters are downward (LNROA, 1993).

2.3.2 Climate

The climate of the region is semi arid but locally the climate in the valley varies due to the altitude. Although the lake is located within one degree of equator but it generally experiences cool conditions because of the altitude. A general trend of the climatic data of Naivasha town is presented in Figure 2.3. For numerical value see Appendix AI. The locations of the different meteorological stations are presented in Figure 2.4.

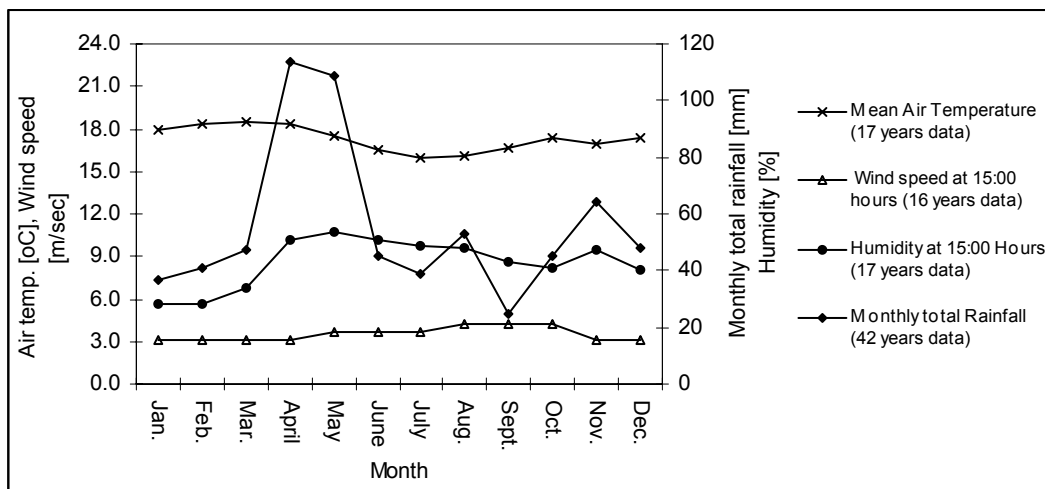


Figure 2.3: A general trend of climatic data of Naivasha Town. (Met. Station: Naivasha DO)

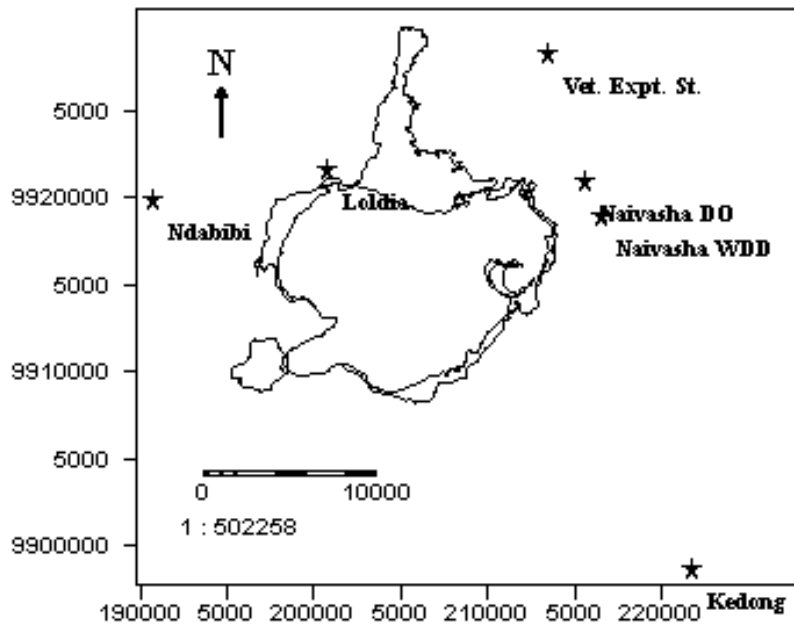


Figure 2.4: Locations of different meteorological stations. (Note: Map coordinate system: UTM, Zone: 37)

Winds:

Winds over the Lake Naivasha are generally weak and come from varying directions in the mornings. In the afternoon winds of 1-2.5 m/sec are typical. Winds are strongest in August to October when they reach a speed of 6 m/sec. There are often violent storms over the lakes leading to serious water movement and high wind speeds. The direction of winds is mainly from the southeast and northeast depending on season. Wind over the lake in the afternoon cause mixing of water down the column, and result in well oxygenated water with equalized temperature from top to bottom. Temporary thermal stratification occurs in calm weather. A general trend of the wind magnitude of different months is presented in Figure 2.5.

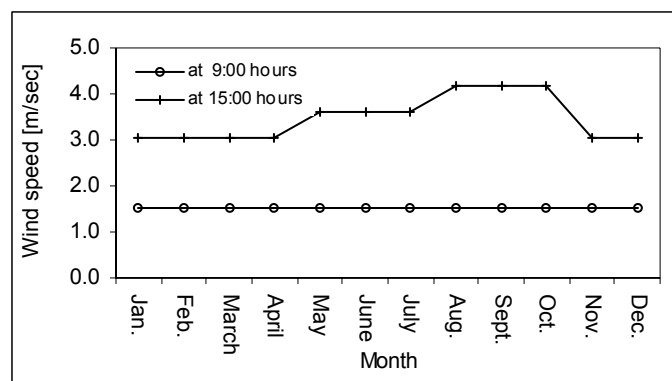


Figure 2.5: General trend of wind velocity in Naivasha area, 1937-54. (Met. Station: Naivasha DO). Source of data: East African Meteorological Dept. 1964, after LNROA, 1993.

Rainfall:

Lake Naivasha is situated in the highest part of Rift valley but in spite of this, the lake and its drainage basin are in rain shadow of winds coming from both the west and, more

importantly from the east. Rainfall is bimodal with main pulses in April/ May and again in November (Fig. 2.6). The Average rainfall of the lake for the period 1931-1960 was 608mm with a variation round the mean from 443 to 939mm (East African Meteorological Dept.1966, after Ase 1986). Rainfall records of two stations around the lake area are given in Appendix AII.

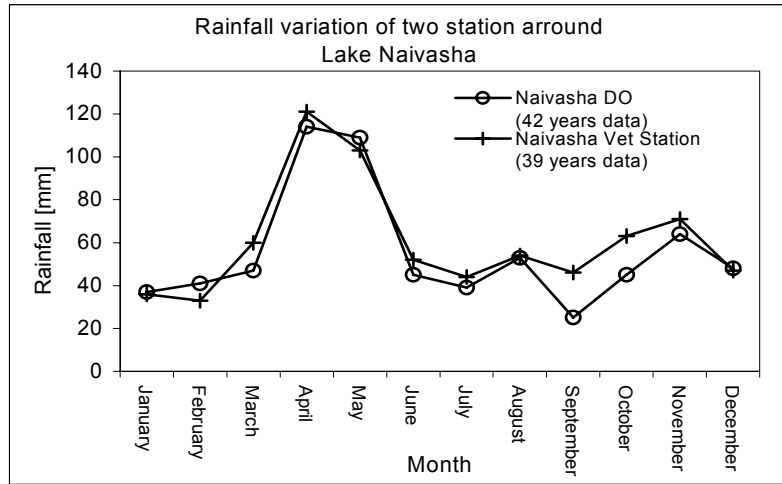


Figure 2.6. Rainfall variation of two stations around Lake Naivasha.

Evaporation:

It is always difficult to estimate evaporation. For Lake Naivasha there are limited records for evaporation measurements. However a general trend of free water surface evaporation by using pan data from Naivasha meteorological station are presented in the Figure 2.7.

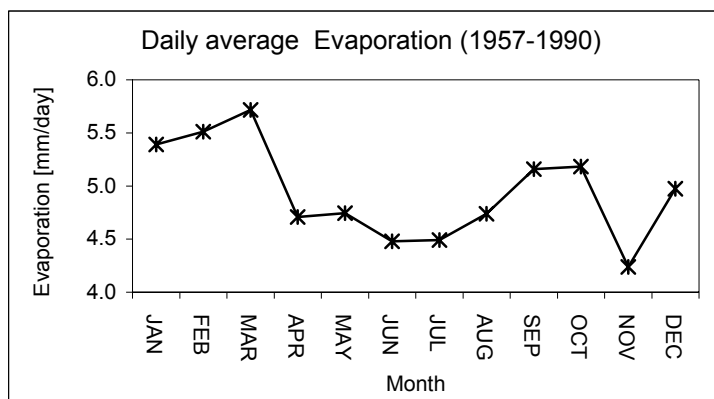


Figure 2.7: Daily average evaporation from Class A land Pan data using Pan coefficient 1.0 (Met. Station: Naivasha WDD)

Insolation:

Melack (1976) has reported that monthly means of daily insolation near the lake area (Kedong Ranch 0°55' S, 36°30' E) varies from 302 W/m² to 66 W/m² (during 1961-68). Highest levels were in January- February, and lowest in July and August. A monthly

variation of solar radiation based on 7 years mean from 1961 to 1968 recorded at Kedong Meteorological station are shown in (Figure 2.8).

It seems that the measured values at the surface are unlikely low as shortwave atmospheric transmittance is about 0.55 only. Data on daily insolation for Naivasha are given in Appendix AIII

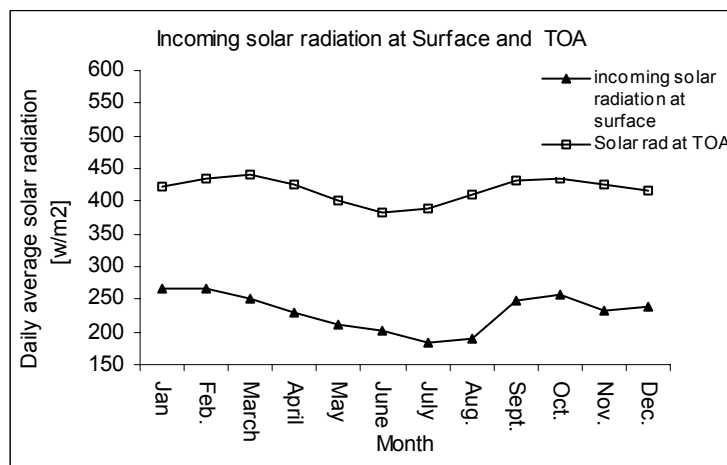


Figure 2.8: Monthly means of daily Insolation of Kedong Met. Station (0°55' S, 36°30' E, 1961-68) Source of data: LNROA, 1993.

Ambient Temperature:

Mean maximum, mean minimum and mean ambient temperatures for Naivasha are given in Appendix AIV. Mean maximum temperatures are ranges from 24.6 to 28.3 °C with the highest temperatures in January and February. Mean minimum ranges from 6.8 to 8.0 °C with coldest month in July and August, although the coldest monthly mean ever recorded is 1.7 °C in September. Mean monthly temperature ranges from 15.9 to 17.8 °C. There is a quite big diurnal variation and a definite cold season as a result of cold air coming down from the Nyandarun range. Temperature variation of Naivasha area is presented in Figure 2.9.

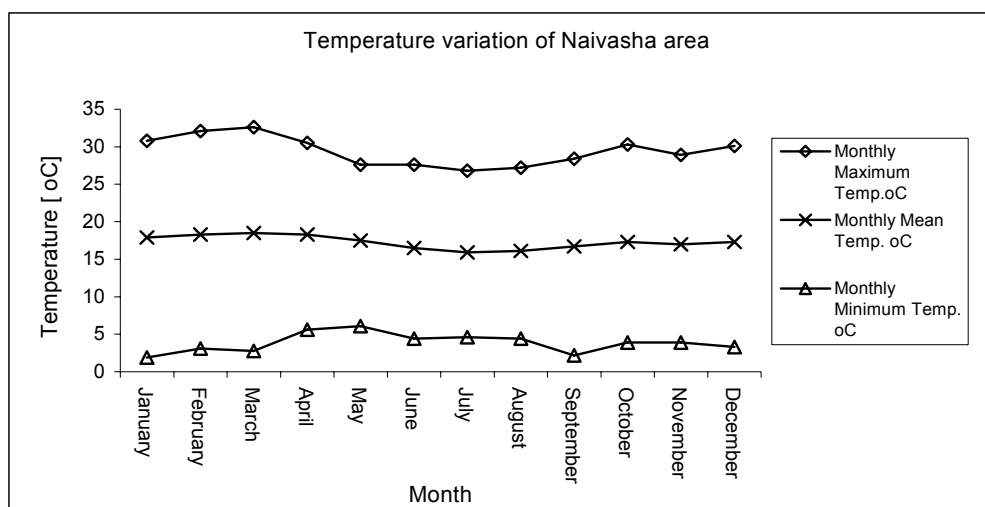


Figure 2.9: Temperature variation of Naivasha Town, 1937-1954, (Met. Station: Naivasha DO). Source of data: East African meteorological Dept, 1964, after LNROA, 1993.

Cloud cover:

Clouds play a critical role in the earth's hydrologic cycle and in the energy balance of the climate system. Changes in surface and air temperature are highly sensitive to cloud amount and type. In the shortwave range clouds reflect more incoming solar radiation than the clear sky surfaces and this effect serves to cool the earth surface and in the longwave range clouds act like a green house gases, they absorb a large fraction of radiation emitted from the surface at high temperature but reemit less of it to space due to low temperature at the cloud tops thus heating the earth surface atmospheric system (Stuhlmann, 1996).

As there are no data about the cloud cover around Naivasha area, it can be indirectly measured from the comparison of solar radiation at TOA and the surface using the data provided in Figure 2.8. A general pattern of the cloud cover around the Naivasha area is presented in Figure 2.10 and 2.11.

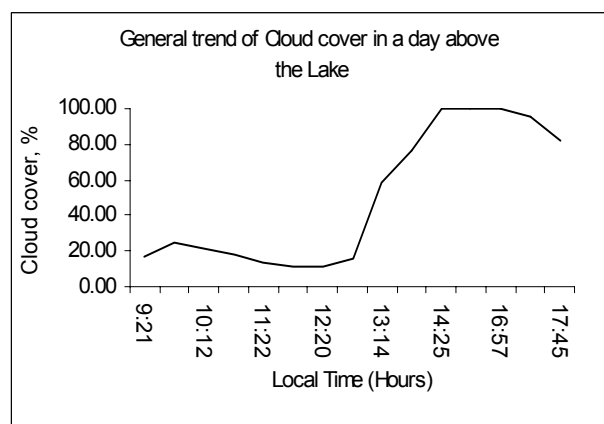
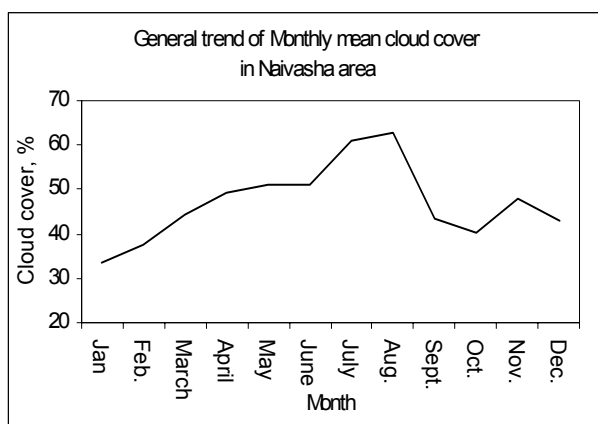


Figure 2.10: General trend of monthly mean Cloud cover in Naivasha area (Kedong 0°55' S, 36°30' E, 1961-68), Source of data: East African meteorological Dept, after LNROA, 1993.

Figure 2.11: General trend of Cloud cover in daytime above the Lake Naivasha (8th October 1998). Source of data: Field campaigns October 1998.

From the daily cloud cover graph it is seen that in the morning time the sky is cloud free and in the afternoon time there is cloud and again it reduces. It is typical for Lake Naivasha.

2.4 Water Balance of Lake Naivasha

The water balance of Lake Naivasha is complicated. Lake Naivasha catchment has an internal drainage system. There is no surface outlet. It has underground water inflows and outflows and the freshness of the water can only result of outflows, otherwise the lake must have been salinized. Several attempts have been made at calculating water balance over the last 30-40 years. Many of these have been unsuccessful due to the fact that there are no accurate estimates of how much water goes in and out of the lake underground and how much is evaporating into atmosphere. The Lake Naivasha Riparian Owners Association (LNROA, 1996) in their Lake management Plan, 1996, estimates preliminary water budgets for the area. The results are shown in the Table 2.2. Also some other Water balance determined by the different researcher are presented in the Appendix B.

Table 2.2: Water balance of Lake Naivasha

Variables	Wet condition	Mean condition	Dry condition
Direct Rainfall on the lake [mm]	939	608	442
Open Water Evaporation [mm]	1529	1529	1743
Transpiration from swamp [mm]	2141	2141	2440
Area of Swamp [km ²]	18	12	9
Area of lake [km ²]	150	120	102
Lake storage [m ³ ×10 ⁶]	600	320	50
Average lake level [m]	1888.3	1885.0	1882.3

Inputs	Wet condition	Mean condition	Dry condition
Direct Rainfall over lake [m ³ ×10 ⁶]	140.8	72.9	45.0
Malewa River [m ³ ×10 ⁶]	378	153	53
GilGil River [m ³ ×10 ⁶]	74	24	3.2
Karati River [m ³ ×10 ⁶]	6.5	2.1	0.28
Ungaged area of the watershed [m ³ ×10 ⁶]	117.8	77.9	34.2
Seepage in [m ³ ×10 ⁶]	54	54	32
TOTAL INPUTS [m³×10⁶]	771.1	383.9	167.7
Outputs	Wet condition	Mean condition	Dry condition
Loss due to Evapotranspiration [m ³ ×10 ⁶]	38.5	26.7	21.9
Evaporation Loss[m ³ ×10 ⁶]	229	183.5	177.8
Seepage- out [m ³ ×10 ⁶]	54	54	32
Abstraction [m ³ ×10 ⁶]	33.8	44.6	53.2
TOTAL OUTPUTS [m³×10⁶]	355.3	308.8	284.9
BALANCE [m³×10⁶]	415.8	75.1	-117.2

Chapter 3

Theory of Open Water Evaporation

3.1 Radiation Balance

Historical and recent studies of evaporation clearly show, where water for evaporation is not limiting like open water evaporation or irrigated land surface evaporation, the primary variable controlling the rate of evaporation is solar radiation impinging on the evaporative surfaces (Allen. et. al., 1996). Part of the solar radiation, $K\downarrow$, is reflected back to the atmosphere as $K\uparrow$ and part of that which is absorbed by the surface is radiated back as long wave radiation, also this loss of energy is partly compensated by the incoming long wave radiation from the sky, $L\downarrow$. The radiation balance determined the net radiant energy, R_n , available at the evaporative surface. Many studies have shown that daily net radiation is closely related to daily rate of evaporation from shallow water bodies, especially in warm to hot subhumid and humid climates (Allen. et. al., 1996)

The net radiation is made up of the following components:

$$R_n = K\downarrow - K\uparrow + L\downarrow - L\uparrow \quad [\text{W.m}^{-2}] \quad (3.1)$$

Where R_n is net radiation of upwelling and downwelling radiative fluxes at the surface. K means shortwave radiation (visible radiation) and L is long wave radiation (Thermal radiation). The arrow \downarrow denotes incoming and the arrow \uparrow outgoing. The sun emits the shortwave radiation within the wavelength interval 0.3 and 3.0 μm . The longwave radiation is emitted by the earth surface and certain components of the atmosphere as cloud particles and the gaseous water vapor and carbon dioxides. Longwave thermal radiation emitted between wavelength 3 and 100 μm .

Shortwave solar radiation

The principal source of heat energy is solar radiation. When measured at the earth surface, solar radiation includes both direct and diffused shortwave radiation and their sum may be called global radiation. The sun's energy is electromagnetic radiation with wavelength less than 4 μm but most of the energy is concentrated between 0.5 and 1.0 μm wavelength (Dingman, 1994). The amount of incoming solar radiation which reaches the earth surface can be determined by knowing extraterrestrial solar radiation, atmospheric condition or cloudiness factor and by earth surface configuration. Details of derivation for shortwave solar radiation is presented in Appendix CII. The outgoing shortwave radiation, $K\uparrow$, is the portion of the visible energy, which is reflected back to the atmosphere. It is characterized by the albedo (r_o). The amount of reflected radiant energy depends on the incidental angle, the wavelength, the diffused or direct radiation fraction and the surface characteristics of the body. The net shortwave radiation K^* is estimated as:

$$K^* = (1-r_o). K\downarrow \quad [\text{W.m}^{-2}] \quad (3.2)$$

Koberg (1964) proposed an empirical relation giving the albedo of water surface as a function of $K\downarrow$:

$$r_o = 0.127 \exp(-0.00108 K\downarrow) \quad [\text{W.m}^{-2}] \quad (3.3)$$

Longwave Radiation

The surface radiation balance has a longwave component. The plank function describes the emission of electromagnetic radiation at a given temperature and a given wavelength. A theoretical body (black body) having kinetic temperature T_o [K] emits wave length energy that responds to Plank's law:

$$L_{\lambda}^{bb}(T_o) = \frac{3.74 \times 10^8}{\lambda^5} \times \frac{1}{[e^{\frac{1.44 \times 10^4}{\lambda T_o}} - 1]} \quad [\text{W.m}^{-2}.\mu\text{m}^{-1}] \quad (3.4)$$

Where,

L_{λ}^{bb} is the blackbody energy emission in $\text{W.m}^{-2}.\mu\text{m}^{-1}$ and λ is the reference wavelength in μm . The blackbody has an emissivity equal to one. A natural body does not emit longwave radiation 100 percent, then in the thermal range, the relation between the black and natural bodies is simplified by the emissivity:

$$L_{\lambda}(T_o) = \epsilon_{\lambda} \cdot L_{\lambda}^{bb}(T_o) \quad [\text{W.m}^{-2}.\mu\text{m}^{-1}] \quad (3.5)$$

Where, $L_{\lambda}(T_o)$ is the longwave radiation of the natural bodies, ϵ_{λ} is the emissivity of the natural body in wave length λ . The spectral integration reads:

$$L(T_o) \uparrow = \int_0^{\infty} \epsilon_{\lambda} \cdot L_{\lambda}^{bb}(T_o) d\lambda = \sigma \cdot \epsilon_o \cdot T_o^4 \quad [\text{W.m}^{-2}] \quad (3.6)$$

Where, $L(T_o) \uparrow$ is outgoing longwave radiation from the natural surface, $\sigma = 5.67 \times 10^{-8} [\text{W.m}^{-2}.\text{K}^{-4}]$ is the Stephan Boltzman constant and ϵ_o is a broadband surface emissivity. ' ϵ_o ' can be derived from the surface properties, and T_o is derived from the radiant temperature T_{rad} in combination with the estimated value of ϵ_o .

The incoming longwave radiation, $L\downarrow$, is more difficult to estimate since it must be an integrated value based on variations in water vapor and temperature, with elevation above the ground surface, degree of cloud cover and temperature of the cloud. For clear skies, the notion of effective thermal infrared emissivity of the atmosphere (ϵ_a) introduced an overall emissivity value for all constituents (Brutsaert, 1975; Brunt, 1932; Swinbank, 1963).

Then, having the air temperature T_a at screen level, $L\downarrow$ is estimated as:

$$L\downarrow = \sigma \cdot \epsilon_a \cdot T_a^4 \quad [\text{W.m}^{-2}] \quad (3.7)$$

A portion of this energy reaching a terrestrial object is reflected back to the atmosphere. Since ϵ_o describes the emissivity of a body in the thermal range, $(1-\epsilon_o)$ account for reflection.

Then, the final expression for R_n is:

$$R_n = (1-r_o) K\downarrow + \sigma \cdot \epsilon_a \cdot T_a^4 - (1-\epsilon_o) \cdot \sigma \cdot \epsilon_a \cdot T_a^4 - \sigma \cdot \epsilon_o \cdot T_o^4 \quad [\text{W.m}^{-2}] \quad (3.8)$$

The radiation terms for daily totals

The *daily shortwave radiation* can be directly measured at agrometeorological stations with pyranometers, although is not very common. If only sunshine data is available, the daily incoming shortwave radiation, $K\downarrow$, can be obtained from the following empirical relationship proposed by FAO (Doorenbos and Pruitt, 1977):

$$K\downarrow = (a_s + b_s \cdot n/N) \cdot R_a \quad [\text{W.m}^{-2}] \quad (3.9)$$

Where, a_s [-] is the fraction of the extraterrestrial radiation reaching the ground in a completely overcast day ($n=0$). $a_s + b_s$ [-] is the fraction of the extraterrestrial radiation reaching the ground in a completely clear day ($n = N$). n is the bright sunshine hours per day [hour]. N is the total daytime length [hours]. R_a is the extraterrestrial shortwave solar radiation at top of atmosphere [W.m^{-2}].

Local instrumentation can be used to estimate a_s and b_s for local condition. When there is no available value for a_s and b_s for local condition, then $a_s = 0.25$ and $b_s = 0.50$ can be used (Doorenbos and Pruitt, 1977). For Kenya, Glover et. al. (1958, after Doorenbos and Pruitt, 1977) proposed the value for $a_s = 0.24$ and $b_s = 0.59$. R_a can be estimated using equation (C13a) presented in Appendix C.

Alternately, Hargreaves and Samani (1982) proposed estimating $K\downarrow$ from the range in daily air temperature:

$$K\downarrow = K_{RS} \cdot (T_x - T_n)^{0.5} \cdot R_a \quad [\text{W.m}^{-2}] \quad (3.10)$$

Where, T_x and T_n are maximum and minimum air temperature in Kelvin. K_{RS} is an empirical coefficient equal to about 0.16 for interior regions and about 0.19 for coastal regions.

The *daily longwave radiation* exchange between the land surface and the atmosphere is very significant since on average the surface emits more energy than the atmosphere. So there is a net loss of energy as thermal radiation from the ground. The average value of net longwave radiation could be estimated using equations (3.6) and (3.7), assuming the daily values of surface and air temperature to be known.

The emissivity of the atmosphere for clear sky condition is usually estimated using an equation from Brutsaert, 1975:

$$\epsilon_a = 1.24 \cdot (e_a / T_a)^{1/7} \quad [-] \quad (3.11)$$

Where, T_a is the air temperature [K], e_a is the actual vapor pressure [mbar], everything measured at screen level. Croley (1989) gave another equation, being based on the formulation originally proposed by Brunt (1932):

$$\varepsilon_a = 0.53 + 0.065 e_a^{0.5} \quad [-] \quad (3.12)$$

For cloudy sky the emissivity of the atmosphere will be different because the clouds behave like blackbodies emitting longwave radiation which is depends on vertical distribution of moisture in the atmosphere and its temperature. The presence of cloud greatly increases the emissivity of the atmosphere. Croley (1989) proposed an empirical equation for emissivity of the air ε_a in cloudy conditions:

$$\varepsilon_a = (0.53 + 0.065 e_a^{0.5})(1 + 0.40C) \quad [-] \quad (3.13)$$

Where, C is the cloud fraction [i.e. $C = (N-n)/ N$]. Daily net longwave thermal radiation can be calculated using equation given by Smith. et. al. (1991).

$$L^* = 5.67 \times 10^{-8} (0.1 + 0.9 n/N) (0.34 - 0.14 e_a^{0.5}) . T_a^4 \quad [\text{W m}^{-2}] \quad (3.14)$$

Where, L^* is net longwave thermal radiation [W.m^{-2}], T_a is air temperature at observation height [K] and e_a is the actual vapor pressure [mbar].

Also Slob (after de. Bruin, 1987) developed an empirical formula to estimate net longwave radiation, L^* for “wet” conditions, which is:

$$L^* = -110. \frac{K \downarrow}{R_a} \quad [\text{W.m}^{-2}] \quad (3.15)$$

Where, $K \downarrow$ is the incoming solar radiation [W.m^{-2}] and R_a is the extraterrestrial shortwave solar radiation [W.m^{-2}] at the top of atmosphere.

3.2 Surface Energy Balance

The energy balance method for estimating evaporation from the Lake and reservoir is considered by many to be the most accurate method [Reis and Dias, 1998; Choudhury, 1994; Rosenberry. et. al. 1993; Robertson and Berry, 1985; Sturrock et. al. 1992; Stewart and. Rose, 1976; Assouline and Marher, 1993; Simons and Mero, 1985; de Bruin, 1982; Keijman, 1981; Keijman, 1974] and is generally used as the reference method to which calculated evaporation rate are compared. The energy balance procedure as applied to lakes is based upon the conservation of energy principles. Evaporation is computed as residual. The energy balance of the water surface can be expressed as:

$$\lambda E = R_n - G_o - H \quad [\text{W.m}^{-2}] \quad (3.16)$$

Where λE is latent heat flux [W.m^{-2}] (positive during evaporation), E is evaporation and λ is the latent heat of vaporization, R_n is net radiation flux [W.m^{-2}] at the water surface, G_o is water heat flux [W.m^{-2}] (positive if water is warming) and H is sensible heat flux [W.m^{-2}] from water surface to air (positive if air is warming).

The calculation of net radiation R_n has been discussed in section 3.1. Description and calculation for G_o and H is discussed in the following section.

Water Heat Flux, G_o

The magnitude of water heat storage or release is usually small from day to day for shallow lake because heat stored early in the day as the water warms is lost late in the day or at night when water cools. The instantaneous rate of heat storage or release at any depth z can be expressed by:

$$G_o = \lambda_w \frac{dT_w}{dz} \quad [\text{W.m}^{-2}] \quad (3.17)$$

Where, λ_w is the thermal conductivity of water which is $0.607 \text{ W.m}^{-1}.\text{K}^{-1}$ (at 25°C), $\frac{dT_w}{dz}$ is the gradient of temperature in the water, T_w is the temperature of water [K], z in meter.

Sensible Heat Flux, H

The sensible heat H is the part of the surface energy that is used to heat up the planetary boundary layer. Mathematical formulation of the sensible heat flux is based on the theory of mass transport of heat and momentum between the surface and near surface environment. Mathematically the sensible heat flux can be expressed as:

$$H = \frac{\rho_a c_p}{r_{ah}} (T_o - T_a) \quad [\text{W.m}^{-2}] \quad (3.18)$$

Where, ρ_a is air density [kg.m^{-3}], c_p is specific heat of moist air, $1004 \text{ [J.kg}^{-1}.\text{K}^{-1}]$, r_{ah} is aerodynamic resistance to heat transport [s.m^{-1}], T_o is water surface temp. [K], and T_a is the air temperature at observation height [K].

The calculation of r_{ah} goes not without difficulties. r_{ah} varies with wind speed and the intensity and the direction of H itself. The aerodynamic resistance to heat transport between the surface and the reference height z can be estimated by:

$$r_{ah} = \frac{1}{k^2 u} \left[\ln\left(\frac{z-d}{z_{om}}\right) - \Psi_{sm} \right] \left[\ln\left(\frac{z-d}{z_{oh}}\right) - \Psi_{sh} \right] \quad [\text{s.m}^{-1}] \quad (3.19)$$

Where, d is zero plane displacement, k is Von karman's constant ($= 0.41$), u is velocity of air [m s^{-1}], z is observation height, z_{om} is surface roughness length for momentum transfer [m], z_{oh} is the surface roughness length for sensible heat transfer [m], Ψ_{sh} and Ψ_{sm} are the integrated stability functions for describing effect of buoyancy or stability between the surface and height z on sensible heat and momentum transfer. For neutral condition ($T_o = T_a$, hence $H=0$), $\Psi_{sm} = \Psi_{sh} = 0$ and for simplicity one can assume $z_{oh} = z_{om} = z_o$. This assumption gives comparatively small errors in combination formula (Thom, 1972). So the simplified Eq. is

$$r_{ah} = \frac{1}{k^2 u} \left[\ln\left(\frac{z}{z_o}\right) \right]^2 \quad [\text{s m}^{-1}] \quad (3.20)$$

For water surface, $d = 0$, $z_{om} = 0.0001\text{m}$ (Allen. et.al, 1996), Brutsaert (1982) suggested a value for $z_o = 0.00023\text{m}$ over typical water surface. Penman assumes a roughness length

$z_0 = 0.00137\text{m}$. (Thom and Oliver, 1977). Sverdrup (1945) quotes roughness height, $z_0 = 0.006\text{m}$ for moderate wind velocity over the sea. As Penman equation was developed to estimate open water evaporation, we can take roughness length $z_0 = 0.00137\text{m}$ for our calculation. The difference between using 0.0001m and 0.00137m is approximately 5 percent, which is well within the application accuracy.

Daily Total from Instantaneous Evaporation

To find the daily total evaporation from instantaneous latent heat flux, Brutsaert and Sugita (1992) used evaporative fraction, which is the energy used for the evaporation process, divided by the total amount of energy available for evaporation process.

$$\Lambda = \frac{\lambda E}{\lambda E + H} = \frac{\lambda E}{R_n - G_o} \quad [-] \quad (3.21)$$

Where Λ is evaporative fraction. Although the sensible heat and the latent heat fluxes are fluctuating strongly on daily basis, evaporative fraction behaves steady during daytime (Bastiaanssen et. al., 1996a; Crago, 1996; Shuttleworth et. al., 1989). Then the instantaneous and the integrated daily evaporative fraction can be hold similar:

$$A_{inst} = A_{24\text{ hours}} \quad [-] \quad (3.22)$$

For shallow lakes, daily average water heat flux G_o can be ignored, which will introduce a small error and be compensated when accumulating evaporation over time. So the daily evaporation from Eq. (3.21) and (3.22) is:

$$E_{24\text{ hours}} = \frac{8.64 \times 10^7 \times \Lambda_{24\text{ hours}} \times R_{n_{24\text{ hours}}}}{\lambda \times \rho_w} \quad [\text{mm.day}^{-1}] \quad (3.23)$$

Where λ is the latent heat of vaporization $2.45 \times 10^6 \text{ [J.kg}^{-1}]$ (at a temperature 23°C) and ρ_w is the density of water $1000 \text{ [kg.m}^{-3}]$, and $R_{n_{24\text{ hours}}}$ is the average net radiation for the day $\text{[W.m}^{-2}]$

3.3 Bowen Ratio Method

The Bowen ratio energy balance rearranges the energy balance equation in order to cancel out the aerodynamic transport terms. This allows calculation of λE by measuring air temperature and vapor pressure at two elevations above the surface in addition to R_n and G_o . In Bowen ratio method λE can be calculated as:

$$\lambda E = \frac{R_n - G_o}{1 + \beta} \quad [\text{W.m}^{-2}] \quad (3.24)$$

Where Bowen ratio β [-] is the ratio of H and λE . Considering the transport coefficients (inverse of aerodynamic resistances) are equal for H and λE , β can be expressed as:

$$\beta = \frac{H}{\lambda E} = \gamma \frac{[T_2 - T_1 + \Gamma(z_2 - z_1)]}{e_2 - e_1} \quad [-] \quad (3.25)$$

Where T_1 [K] and e_1 [mbar] are air temperature and vapor pressure at height z_1 [m] and T_2 [K] and e_2 [mbar] are air temperature and vapor pressure at height z_2 [m], γ is the psychrometric constant [mbar. K⁻¹] and Γ is the adiabatic lapse rate, generally taken as 0.01 K.m⁻¹. Γ can be neglected if the distance between the Bowen ratio measurement height is less than 2m. So the final equation used for interpretation of field measurements is:

$$\beta = \frac{H}{\lambda E} = \gamma \frac{[T_2 - T_1]}{e_2 - e_1} \quad [-] \quad (3.26)$$

3.4 Penman equation

Penman (1948a, 1948b) was the first to introduce the combination method of transfer equation and energy budget principle. He combined the vertical transfer of sensible heat and water vapor with surface energy balance equation to estimate evaporation from open water surface. Many studies have shown that evaporation estimates made with the combination approach compare well with those determined by other methods.

$$\lambda E = \frac{\Delta R_n + \rho_a c_p (e_s - e_a) / r_{ah}}{\Delta + \gamma} \quad [\text{W.m}^{-2}] \quad (3.27)$$

Where, Δ is vapor pressure gradient [mbar. K⁻¹], e_s is saturated vapor pressure at observation height [mbar] and e_a is actual vapor pressure at observation height [mbar] Calculations of different terms are presented in Appendix C.

3.5 Priestley and Taylor Equation

With the simplification of Penman equation, Priestley and Taylor (1972) proposed an equation for estimating evaporation from the saturated surface. From micrometeorological observations over well-watered surface, they found that evaporation or evapotranspiration depends strongly on net radiation and the second term (aerodynamic term) of Penman equation is typically one-fourth of the first term (radiation term). They proposed evaporation as:

$$\lambda E = \alpha \frac{\Delta(R_n - G_o)}{\gamma + \Delta} \quad [\text{W.m}^{-2}] \quad (3.28)$$

Where α is a coefficient of value between 1.2 –1.3. In advection free conditions Priestley and Taylor found an average value of $\alpha = 1.26$ both for water surface and saturated land surface. Several authors have confirmed this value: Reis and Dias (1998), de Bruin and Keijman (1979); Stewart and Rouse (1976); de Bruin (1981); Ferguson and Den Hartog (1975) and Stricker (1981). Some of these authors found the same value for small, shallow lakes, e. g. Stewart and Rouse (1976).

3.6 Remote Sensing

Equation 3.1 can be solved using partial remote sensing data (r_o , ϵ_o , T_o) in combination with ancillary ground data on $K\downarrow$ and $L\downarrow$ (i.e. Bastiaanssen, 1995; Tuzet, 1990; Jackson et. al., 1985; Moran et. al., 1989; Kustas et. al. 1994; Pelgrum and Bastiaanssen, 1996) or entirely from remote sensing (i.e. Zhang, Rossow, and Lacis, 1995; Rossow and Zhang 1995; Darnell et. al., 1992; Darnell et. al., 1988; Tarpley, 1979; Nunez Hart and Kalma, 1984; Li, and Leighton, 1993; Frouin, et. al., 1988; Schmetz, J., Schmetz J. and Raschke, 1986). However a partial method is described below, as some ground data ($K\downarrow$, r_o , τ_{sw}) are available from the study area.

3.6.1 Net shortwave radiation

The net shortwave radiation K^* is estimated as equation (3.2):

$$K^* = (1-r_o) \cdot K\downarrow \quad [\text{W.m}^{-2}]$$

The broadband incoming solar radiation at the earth surface $K\downarrow$ can be estimated using the general algorithm of Bastiaanssen (1995).

$$K\downarrow = R_a \cdot \tau_{sw} \quad [\text{W.m}^{-2}] \quad (3.29)$$

Where τ_{sw} is the atmospheric shortwave transmittance, R_a is the incoming solar radiation at the top of atmosphere (Extraterrestrial solar radiation).

In absence of data on $K\downarrow$ or degree of cloudiness to find τ_{sw} from local measurements, two-way transmittance τ_{sw}'' for broadband solar radiation (0.3-3.0 μm) of equation (3.30) (Zhong and Li, 1988) can be used to determine τ_{sw} :

$$\tau_{sw} = (\tau_{sw}'')^{0.5} = \left(\frac{r_p - r_a}{r_o} \right)^{0.5} \quad [\text{W.m}^{-2}] \quad (3.30)$$

Where r_p [-] is the broadband planetary albedo, r_o [-] is the surface albedo and r_a [-] is the lowest planetary albedo at all pixels (i.e. r_p^{min}). If r_o is measured at a few specific location in the study area, τ_{sw}'' can be obtained by combining r_p from remote sensing measurements and r_o from these in situ measurements. If τ_{sw} is measured, r_o can be derived from r_p and τ_{sw}'' directly. The broadband planetary albedo r_p can be calculated as:

$$r_p = \int_{0.3}^{3.0} r_p(\lambda) d\lambda = \sum_{i=1}^n C(b)_i \cdot r_p(b)_i \quad [\text{W.m}^{-2}] \quad (3.31)$$

Where n is the total number of spectral bands, C(b) is the weighing factor accounts for the uneven distribution of spectral incoming solar radiation at different bands.

3.6.2 Net longwave radiation

At surface incoming longwave radiation $L\downarrow$ can be calculated using Equation (3.7). The average emissivity of the atmosphere ϵ_a can be calculated from the empirical relationship (Bastiaanssen, 1995):

$$\varepsilon_a^{avg} = 1.08(-\ln \tau_{sw}^{avg})^{0.265} \quad [-] \quad (3.32)$$

Where τ_{sw}^{avg} is the average atmospheric shortwave transmittance. For water body we can assume the air temperature at 2m height is same as water surface temperature and the water surface temperature can be estimated using remote sensing technique.

The outgoing longwave radiation $L\hat{\uparrow}$ from the water surface can be calculated using Equation (3.6) where $L\hat{\uparrow}$ is a function of surface temperature T_o and the surface emissivity ε_o . A water body is normally considered as a blackbody so we can assume $\varepsilon_o=1$.

To get surface temperature from the satellite measurements, different algorithms are proposed for Thematic Mapper (TM). The thermal channel TM6 measured the spectrally emitted radiance between 10.6 to 12.4 μm at the top of atmosphere, L_6^{TOA} . The spectral radiances at the top of atmosphere measured by the satellite are related to the spectrally emitted radiances at the land surface L_6^{surf} (Schmugge et. al., 1998):

$$L_6^{TOA} = L_6^{surf} \cdot \tau_6 + L_6^{atm} \quad [\text{W}\cdot\text{m}^{-2}] \quad (3.33)$$

Where L_6^{atm} is the longwave radiation emitted from the top of atmosphere upward (i.e. thermal path radiance) and τ_6 is the atmospheric transmittance in the region of wavelength 10.6 to 12.4 μm . L_6^{atm} and τ_6 can be determined by the atmospheric radiation models or from a limited number of surface temperature T_o field measurements taken at the same moment of the satellite overpass. The spectral radiances at surface level were after atmospheric correction converted into radiometric surface temperature through the inversion of Planck's law:

$$T_o = \frac{14388}{11.5 \ln\left[\left(\frac{\varepsilon_o \times B \times 3.7427 \times 10^8}{L_6^{surf} \cdot (11.5)^5}\right) + 1\right]} \quad [\text{K}] \quad (3.34)$$

Where B is the bandwidth of thermal channel (12.4-10.6 = 1.8 μm), ε_o [-] is the thermal infrared surface emissivity in the spectral range of TM band 6 and T_o [K] is the radiometric surface temperature corrected for gray body effects.

Shortwave and longwave radiation at the surface can be estimated also by using physical approaches which allows relatively fast computation and can use the latest cloud and meteorological data available from satellite sources. Such an approach is describe in Darnell et.al. (1992) and Darnell et.al.(1989) for shortwave radiation and Gupta (1989) for longwave radiation.

3.7 Data collection and Instruments

During the field campaign (October'98) different meteorological data were collected at two level 10cm and 1.5m above the water surface of the lake. A list of instruments, which were used during the field campaign, are presented in Table 3.1 and datasheets are attached in Appendix G.

Table 3.1: Instruments used for data collection during the field campaign in October 1998

Name of Instruments	Use
<u>Pyranometer</u> Sensitivity: $9.07 \mu\text{V}/\text{watt}/\text{m}^2$ Measuring range: 0.305-2.8 μm .	To measure incoming and outgoing solar radiation, Albedo
<u>Thermal Infrared thermometer</u> Accuracy: 0.01 $^{\circ}\text{C}$	To measure the radiant temperature of the air and the water surface in order to calculate the incoming and outgoing longwave radiation.
<u>Psychrometer</u> Measuring range : -30°C to $+45^{\circ}\text{C}$ Accuracy: $\pm 0.2^{\circ}\text{C}$.	To measure the physical temperature, vapor pressure and humidity above the water surfaces.
<u>Anemometer</u> Measuring range: 0-12 m/s 0-20 km/h	To measure the local wind speed
<u>Water quality checker</u> Accuracy: 0.01 $^{\circ}\text{C}$.	To measure the water temperature at different depth.

Chapter 4

Remote sensing Evaporation TOVS Application

4.1 General

The TIROS Operational Vertical Sounder (TOVS) is a successor to the sounding instruments that are flown on the previous generations of polar-orbiting meteorological satellites. The TOVS system consists of three separate and independent instruments and the data from them are combined for the computation of atmospheric profiles. The three instruments are: High Resolution Infrared Radiation Sounder Version 2 (HIRS/2); Microwave Sounding Unit (MSU) and Stratospheric Sounding Unit (SSU). Each instrument has different characteristics, resolutions, scan properties. The HIRS/2 instrument is a step-scanned multi-channel spectrometer with 20 channels primarily in the infrared region of the spectrum including both longwave (15-micron) and shortwave (4.3 micron), plus one channel in the visible (0.69-micron) region. The MSU instrument is a passive scanning microwave spectrometer with four channels in the 5.5-micron oxygen region. The SSU is a step-scanned infrared spectrometer with 3 channels in the 15-micron CO₂ band. The 3 SSU channels have the same frequency but different cell pressures. This system is onboard the NOAA 6 through NOAA 14 and TIROS-N satellites.

TOVS was designed so that the data from the HIRS/2, SSU and MSU instruments could be combined to compute:

- 1) atmospheric temperature profiles from the surface to 10 millibars (mbar),
- 2) water vapor content at three levels of the atmosphere, and
- 3) Total ozone content.

This information was traditionally obtained from radiosondes. Radiosondes have the advantage that they measure the atmospheric profile of pressure, temperature, and humidity directly. But the spatial coverage of the earth is irregular so it cannot give the accurate spatial variation of those data. A satellite sounding system has the advantage of giving much more regularly spaced coverage. The disadvantage of the satellite sounding instruments is that they do not measure the required meteorological parameters directly. They are basically low-resolution scanners and the meteorological parameters have to be retrieved by a complicated inversion procedure. However by the satellite sounding system, improved accuracy of retrieval profiles and a better definition of the water vapor profile even in the presence of clouds, is possible with the availability of data from many more spectral regions, combined with data from the MSU (which is generally unaffected by non-precipitating clouds) make these objectives possible. A brief description about the TOVS sensors, availability of the data and a sample atmospheric profile derived from TOVS sensors are presented in Appendix E. Table 4.1 and Figure 4.1 presents TOVS atmospheric profile of an area closed to Naivasha.

Table 4.1: The TOVS meteorological product description
(37.35° E, 0.62° N, Solar elevation 48.27 °, 14th July 1998)

Parameters	Description	value
Surface pressure	P_s	920 [mbar]
Surface temperature	T_s	289.5 [K]
15-layer temperature profile	Surface - 850 mbar, T_1	288.5 [K] (from interpolation)
	850-700 mbar, T_2	287.9 [K]
	700-500 mbar, T_3	275.2 [K]
	500-400 mbar, T_4	262.4 [K]
	400-300 mbar, T_5	249.6 [K]
	300-200 mbar, T_6	229.9 [K]
	200-100 mbar, T_7	206.0 [K]
	100-70 mbar, T_8	198.3 [K]
	70-50 mbar, T_9	204.1 [K]
	50-30 mbar, T_{10}	212.7 [K]
	30-10 mbar, T_{11}	224.5 [K]
	10-5 mbar, T_{12}	238.2 [K]
	5-2 mbar, T_{13}	251.5 [K]
	2-1 mbar, T_{14}	258.0 [K]
	1-0.4 mbar, T_{15}	252.4 [K]
3- layer water vapor profile	Surface - 700 mbar, W_1	22 [pr-mm]
	700 - 500 mbar, W_2	7 [pr-mm]
	500 - 300 mbar, W_3	1 [pr-mm]
Total ozone content	U_{O_3}	273 Dobson
Cloud cover	A_c	100%
Cloud top pressure	P_{ct}	Missing

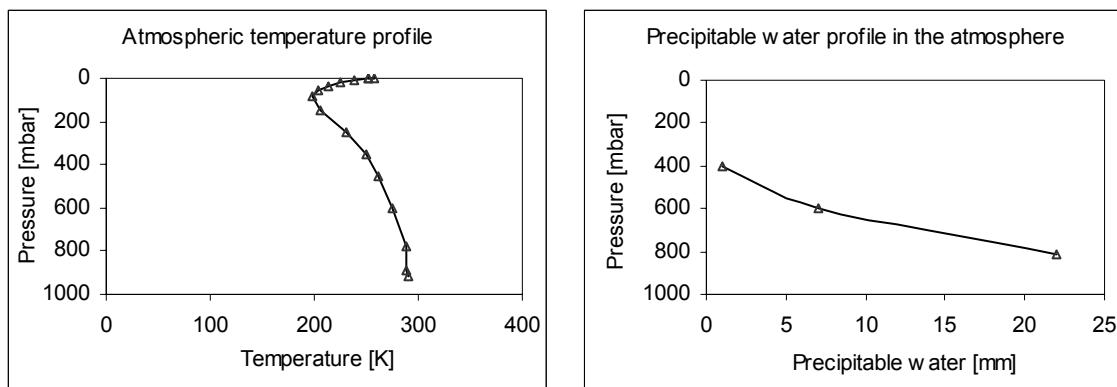


Figure 4.1: Atmospheric temperature profile and perceptible water content in the atmosphere derived from TOVS sensors (37.35° E, 0.62° N, Solar elevation 48.27 °, 14th July 1998)

4.2 TOVS Application

Net solar radiation, net longwave fluxes, fractional cloud cover, air temperature vapor pressure and vapor pressure deficit can be estimated using satellite born sounders data (i.e. TOVS data).

4.2.1 Shortwave radiation:

Darnell et. al., 1988; Darnell et. al., 1992; Darnell et. al., 1996; Li and Leighton, 1993; Zhang, Rossow and Lacis, 1995, used TOVS atmospheric profile in their model to estimate net solar radiation absorbed at the surface. The spatial resolution of these data is about 250 km. When compared with the surface observations, the derived solar radiation using sounder data has a root mean square error less than 18 W/m^2 (c. 0.6 mm/day) and bias less than 9 W/m^2 (i.e. 0.3 mm/day) (Darnell et. al., 1996; Whitlock, et. al., 1995). One should note that even in surface measurements, there are 5-20% uncertainties in daily solar radiation estimation (Stanhill, 1983). Figure 4.2 from Darnell et. al. 1992, shows a comparison of mean daily insolation derived from satellite observations with pyranometer data for globally distributed locations.

Figure 4.2: Comparison of mean daily solar radiation derived from satellite observations with ground measurements for 4 seasonal months (Darnell et. al., 1992)

In the present study a general model of Darnell et.al. (1988), hereinafter D88 to estimate instantaneous incoming shortwave radiation at the surface, $K\downarrow$, was used.

$$K\downarrow = T_C \times T_A \times S \times \text{Cos}\phi_{su} \quad [\text{W.m}^{-2}] \quad (4.1)$$

Which is now also expressed as:

$$K\downarrow = T_C \times [1 + 0.065P \times r_o] \times \text{Exp}(-D\phi_{su}) \times S \times \text{Cos}\phi_{su} \quad [\text{W.m}^{-2}] \quad (4.2)$$

Where T_C and T_A are cloud and atmospheric transmittances respectively and for clear sky condition $T_C = 1$; S is the distance corrected instantaneous solar radiation at the TOA; $D\phi_{su}$ is the effective clear sky broadband optical depth at solar zenith angle ϕ_{su} . The product term involves surface albedo, r_o , and surface pressure, P [atmos], accounts for the atmospheric back scattering of the surface reflected rays. It was shown in D88, that $D\phi_{su}$ can be expressed as a function of vertical optical depth D_o , by

$$D\phi_{su} = D_o \cdot (\text{Sec } \phi_{su})^N \quad [-] \quad (4.3)$$

Where $(\text{Sec } \phi_{\text{su}})^N$ is an angular power functions accounts for the change of optical depth with solar zenith angle and N is approximated as:

$$N = 1.1 - 2.D_0 \quad [-] \quad (4.4)$$

Values for D_0 are determined as:

$$D_0 = D_{\text{H}_2\text{O}} + D_{\text{O}_3} + D_{\text{O}_2} + D_{\text{CO}_2} + D_{\text{Ray}} + D_{\text{Alb}} + D_{\text{Aeros}} \quad [-] \quad (4.5)$$

The first 4 components represent solar radiation absorption due to atmospheric water vapor, ozone, oxygen and carbon dioxide respectively. They can be expressed individually as:

$$D_{\text{H}_2\text{O}} = 0.104 (U_{\text{H}_2\text{O}})^{0.30} \quad [-] \quad (4.6)$$

$$D_{\text{O}_3} = 0.038 (U_{\text{O}_3})^{0.44} \quad [-] \quad (4.7)$$

$$D_{\text{O}_2} = 0.0075 (P)^{0.87} \quad [-] \quad (4.8)$$

$$D_{\text{CO}_2} = 0.104 (P)^{0.29} \quad [-] \quad (4.9)$$

Where $U_{\text{H}_2\text{O}}$ is Satellite-derived perceptible water vapor burden [pr-cm], U_{O_3} is Satellite-derived ozone burden [atm-cm], and P is nominal surface air pressure [atm]. Eq. (4.6) and (4.7) are approximations provided by Lacis and Hansen (1974) and Eq. (4.8) and (4.9) are from Yamamoto (1962).

The Rayleigh scattering component D_{Ray} , is given by

$$D_{\text{Ray}} = 0.038P \quad [-] \quad (4.10)$$

Where 0.038 is the value derived by Lacis and Hansen (1974). The albedo term D_{Alb} , represents atmospheric back scattering of the surface reflected flux and has been approximated as:

$$D_{\text{Alb}} = -0.065 P. r_0 \quad [-] \quad (4.11)$$

Where r_0 is the surface albedo and coefficient 0.065 is average of value given by Lacis and Hansen (1974) and Hoyt (1978). A value of $r_0 = 0.14$ was used for present study based on work by Kondrat'ev (1972) for no snow condition.

The remaining component of Eq. (4.5) D_{Aeros} was determined by a residual technique in D88, as the satellite measurements are not available from which to compute D_{Aeros} .

$$D_{\text{Aeros}} = 0.03 + 0.013 U_{\text{H}_2\text{O}} \quad [-] \quad (4.12)$$

For all sky conditions the cloud transmittance factor T_C is not 1 and it can be determined from TOA albedo and T_C relationship as given by D88, where

$$T_C = 1 - r_n \quad [-] \quad (4.13)$$

Where T_C is an estimated effective daily cloud transmittance and r_n is a normalized albedo parameter defined as:

$$r_n = (A - A_1) / (A_0 - A_1) \quad [-] \quad (4.14)$$

Where A is the area averaged TOA albedo value, and A_1 and A_0 are regression-determined values of TOA albedo for limiting conditions of $T_C = 1$ and 0 (totally clear and totally overcast), respectively. An alternative technique is also proposed by D88 to calculate A_1 and A_0 through use of histograms of the measured daily TOA albedo taken over any region of interest. In the histogram technique, considering the practical case it is assumed that the minimum $T_C = 0.1$ and the A_0 is replaced by $A_{0.1}$, where

$$A_{0.1} = 0.9A_0 + 0.1 A_1 \quad [-] \quad (4.15)$$

$$A_1 = A_1' + 0.03 \quad [-] \quad (4.16)$$

Where A_1' is the minimum value of the histogram curve. The range of $A_{0.1}$ values is quite small and they suggested a value 0.68 for $A_{0.1}$ as a global constant.

4.2.2 Longwave radiation:

To estimate the net longwave fluxes at the surface from satellite sounder (TOVS) data, several attempts have been made (Darnell et. al., 1992; Darnell et. al., 1988; Gupta, 1983; Frouin et.al. 1988; Zhang, Rossow and Lacis, 1995). TOVS contain both infrared and microwave bands that can provide measurements of variation of atmospheric characteristics at several levels within the atmosphere to compute longwave fluxes with an estimated error of 18 W/m² at spatial resolution of 250 km (Darnell et. al. 1992).

The longwave model used in the analysis [Gupta, 1989] (hereinafter G89) is a model for computing the downward longwave fluxes (DFL) at the surface under partly cloudy condition from meteorological parameters available from TOVS. The DFL, denoted by the $L\downarrow$ was expressed in G89 as:

$$L\downarrow = C_1 + C_2 \cdot A_c \quad [W \cdot m^{-2}] \quad (4.17)$$

Where C_1 is clear sky DFL, C_2 represents the cloud effect and A_c is the fractional cloud amount. The clear sky DFL, C_1 was computed as:

$$C_1 = (A_0 + A_1 V + A_2 V^2 + A_3 V^3) \cdot T_e^{3.7} \quad [W \cdot m^{-2}] \quad (4.18)$$

Where $V = \ln W_s$ and W_s is the vapor burden of the atmosphere in perceptible millimeters ($W_s = W_1 + W_2 + W_3$, where W_1 , W_2 and W_3 are the three levels perceptible water in the atmosphere which can be derived from TOVS atmospheric profile). T_e is an effective emitting temperature of the atmosphere and A_0 , A_1 , A_2 and A_3 are regression coefficients as given in G89 ($A_0 = 1.791 \times 10^{-7}$, $A_1 = 2.093 \times 10^{-8}$, $A_2 = -2.748 \times 10^{-9}$ and $A_3 = 1.184 \times 10^{-9}$). T_e was computed as weighted sum of TOVS- derived temperature as:

$$T_e = K_s T_s + K_1 T_1 + K_2 T_2 \quad [K] \quad (4.19)$$

Where T_s is the surface temperature [K], T_1 [K] and T_2 [K] are the temperature of the first and second atmospheric layer just above the surface, K_s , K_1 and K_2 are weighting factor and the values are 0.5, 0.4 and 0.1 respectively. The expression for the cloud factor, C_2 was derived in G89 as:

$$C_2 = T_{cb}^4 / (B_0 + B_1 W_c + B_2 W_c^2 + B_3 W_c^3) \quad [W.m^{-2}] \quad (4.20)$$

Where T_{cb} is the cloud base temperature [K] which is the corresponding temperature of cloud base pressure, P_{cb} . W_c is the water vapor burden of the atmosphere below the cloud base (in pr-mm), and B_0 , B_1 , B_2 and B_3 are regression coefficient and the values are 4.990×10^7 , 2.688×10^6 , -6.147×10^3 and 8.163×10^2 respectively.

Cloud base pressure, P_{cb} can be estimated as:

$$P_{cb} = P_{ct} + \text{cloud thickness in mbar} \quad [\text{mbar}] \quad (4.21)$$

Where P_{ct} is the cloud top pressure, and cloud thickness can be assumed from the following assumptions as given by G89:

Condition	Cloud thickness
1. For low clouds $P_{ct} > 700$ mbar	50 mbar 500-600 m (in lower atmosphere)
2. For medium clouds $700 \text{ mbar} > P_{ct} > 400$ mbar	100 mbar (for tropical area, 30N-30S) 50 mbar (for mid and high latitude)
3. For high clouds $P_{ct} < 400$ mbar	50 mbar 1 km (in the upper atmosphere)

Breon et.al. (1991) showed that the use of Eq.(4.20) with the above regression coefficient would produce overestimation of C_2 and DFL when cloud base pressure $P_{cb} \geq 800$ mbar or essentially when $(P_s - P_{cb}) \leq 200$ mbar (P_s is the surface pressure). They pointed out that the maximum possible value of C_2 is limited by the condition when cloud base is located in the surface (i.e. $P_s - P_{cb} = 0$) and the correction is applied when $(P_s - P_{cb}) \leq 200$ mbar.

When cloud base is located at the surface:

$$L\downarrow = \sigma \cdot T_{cb}^4 \quad [W.m^{-2}] \quad (4.22)$$

Under those conditions, however $T_{cb} = T_s$ and $W_c = 0$. For overcast condition ($A_c=1$) therefore:

$$L\downarrow = C_1 + C_2 = \sigma \cdot T_s^4$$

$$C_2 = \sigma \cdot T_s^4 - C_1 \quad [W.m^{-2}] \quad (4.23)$$

Also under this conditions, from Equation (4.20)

$$C_2 = T_{cb}^4 / B_0' \text{ as } W_c = 0 \quad [W.m^{-2}] \quad (4.24)$$

Where B_0' is the modified value of regression coefficient B_0 . From equation (4.23) and (4.24),

$$B_0' = T_s^4 / (\sigma \cdot T_s^4 - C_1) \quad [-] \quad (4.25)$$

4.2.3 Air Temperature, Vapor pressure, and Vapor Pressure Deficit

Air temperature, vapor pressure, and vapor pressure deficit can be also derived from (TOVS) data. For monthly mean vapor pressure e_a [mbar] from TOVS observations, Choudhury (1996) derived a semiempirical equation relating vapor pressure to precipitable water vapor W [pr-mm]:

$$e_a = 0.77(W-1.2)/(1+0.006W) \quad [\text{mbar}] \quad (4.26)$$

with explained variance of 0.95 and standard error of estimate (SEE) as 1.7 mbar. Figure 4.4 (adopted from Choudhury, 1997) shows a scattered plot of e_a from surface measurements and those derived from Eq. 4.26 using TOVS observations for W . The W values derived from TOVS observations have an uncertainty of about 30% (Kidwell, 1984). Choudhury (1997) also mentioned that in hot deserts both W and e_a are overestimated. The over estimated e_a will over estimate the net radiation but will under estimate vapor pressure deficit D , and thus partly compensate the error in estimating evaporation (Choudhury, 1997).

Algorithm for retrieval of air temperature from TOVS data are described in Choudhury (1997) and if air temperature is known saturated vapor pressure and the vapor pressure deficit can be calculated using Eq. (C1) and (C2a) given in Appendix C. Figure 4.3, 4.4 and 4.5 from Choudhury (1997) shows a comparison of mean monthly air temperature, vapor pressure and vapor pressure deficit derived from TOVS data and surface observations respectively. Results show a high correlation coefficients (r^2) and a low value of standard error of estimates (SEE).

Figure 4.3: Comparison of mean monthly air temperature derived from satellite measurements (TOVS) and surface observations (Choudhury 1997).

Figure 4.4: Comparison of mean monthly vapor pressure derived from satellite measurements (TOVS) and surface observations (Choudhury 1997).

Figure 4.5: Comparison of mean monthly vapor pressure deficit derived from satellite measurements (TOVS) and surface observations (Choudhury 1997).

Chapter 5

Data Analysis and Results

This chapter will present the results of field data analysis for daily, monthly and seasonal variation of evaporation as well as discuss the evaporation estimates using remote sensing spectral data (TOVS and TM).

5.1 Field Campaign October 1998

For estimating lake evaporation energy balance approach was taken as standard method consequently following approaches: Bowen ratio, Penman and Priestley-Taylor method for evaporation calculation were compared with the energy balance method. In the energy balance approach evaporation (Latent heat flux, LE) was calculated as residual, the other components are net radiation, sensible heat flux and water heat flux. The diurnal variation of these components are discussed below.

Radiation Budget

From the data set of different days it can be observed that the incoming solar radiation is strongly related to the atmospheric properties and the cloudiness (see Figure 5.1).

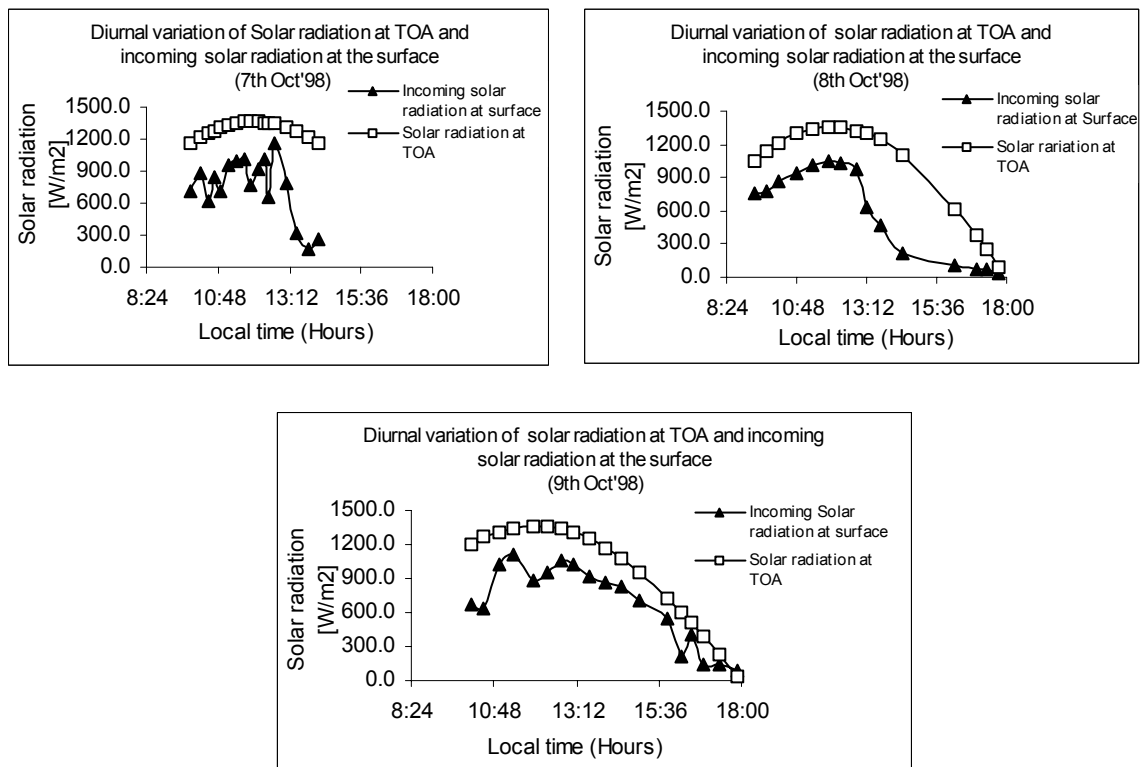


Figure 5.1: Effect of cloud and atmosphere on incoming solar radiation

The reflected shortwave radiation ($K\uparrow$) is relatively small due to the very low albedo, r_o of the water surface (Daily average $r_o = 0.06$, for diurnal variation see Figure 5.2). Albedo of the water surface was also estimated by the approach given by Koberg (1964) [i.e. Eq. 3.3] and a same daily average $r_o = 0.06$ was obtained. However the diurnal variation of albedo estimated by two methods are presented in Figure 5.2. The albedo of the water surface is not constant. In particular it depends upon the angle at which the direct beam strikes the surface. With cloudless skies and higher solar altitude, water is one of the most effective absorbing surfaces ($r_o = 0.03$ to 0.08). When sun is closed to horizon near sunrise and sunset the reflection is mirror like, this accounts for dazzling effect at this time. Under cloudy skies the diffused solar radiation forms a large portion of the incoming solar radiation ($K\downarrow$) and the effect of solar altitude is completely damped. The altitude dependence is also modified by the roughness of the water surface (waves).

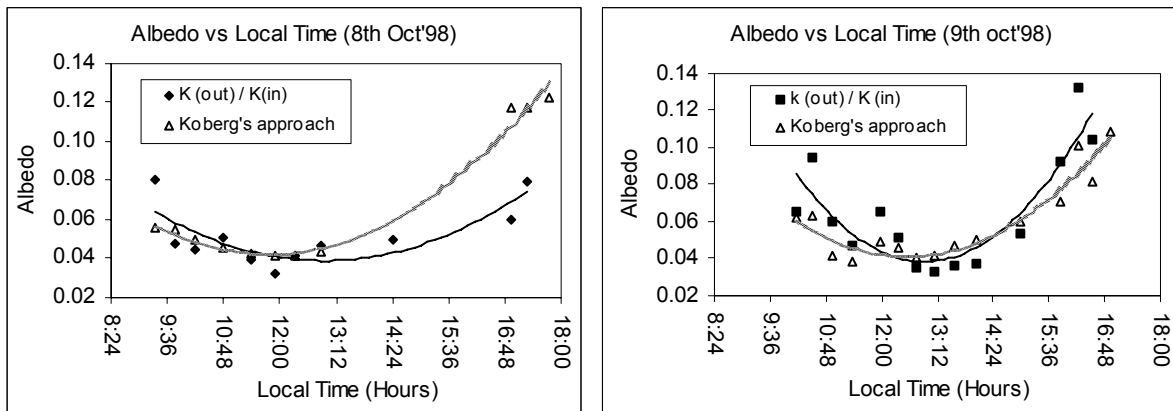


Figure 5.2: Variation of Albedo of lake water surface with local time

With a roughened surface (waves) and high solar altitudes there is a greater probability that the incident beam will hit a sloping rather than a horizontal surface, thereby tending to increase albedo, r_o ; whereas at low altitudes instead of grazing the surface the beam is likely to encounter a wave slope at a local angle which is more conducive to absorption, hence decreasing r_o in comparison to smooth water. In all cases the albedo includes reflection from the water as well as from the surface.

The outgoing longwave radiation from lake water body is distinguished from other natural surfaces by being virtually constant throughout the day (see Figure 5.3) This is due to small diurnal variation of water surface temperature. Also as there is a mixing of lake water down the column which will cool the temperature continuously. Longwave radiation from the atmosphere ($L\downarrow$) is completely absorbed at a water surface with no significant reflection or transmission. In a cloudy sky the radiant temperature of the sky increases which causes the high incoming longwave radiation because the longwave radiation increases exponentially with the temperature. So for water surface the variation of net longwave radiation is mainly due to the variation of incoming longwave radiation. The variations of net longwave radiation with the local time are presented in the Figure 5.3.

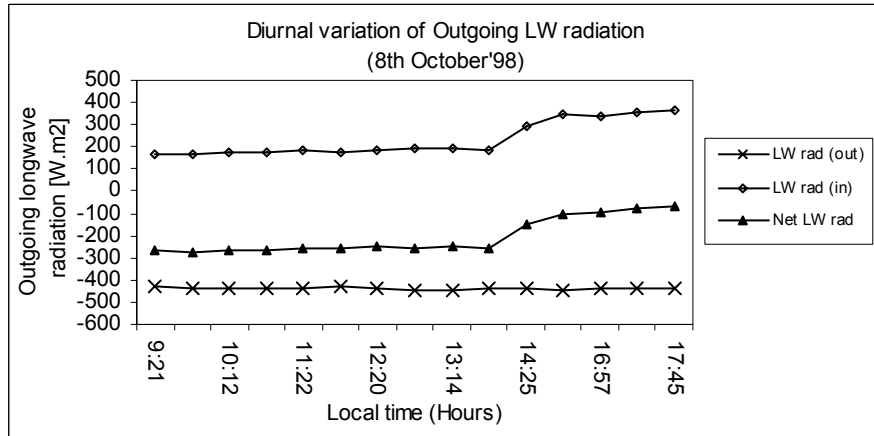


Figure 5.3: Diurnal variation of longwave (LW) radiation.

In Figure 5.3 we can see that from morning to 13:30 hours the net longwave radiation was almost constant and after wards increases, this was due to presence of cloud in the afternoon time which increases the incoming longwave radiation as well as net longwave radiation.

Net radiation was calculated from the net shortwave and the net longwave radiation. The fluctuations of the net radiation in the daytime for the lake water surface are presented in the Figure 5.4 below:

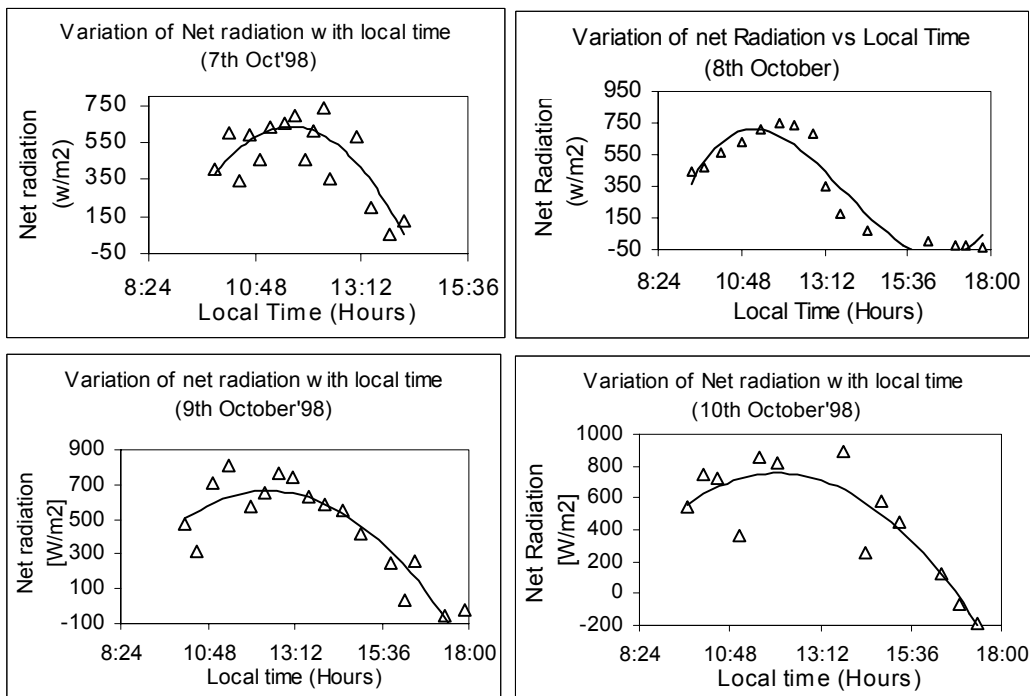


Figure 5.4: Variation of Net radiation with local time.

From the above figure we can see that in the afternoon time the net radiation was very low even negative, this was because of low incoming solar radiation, high albedo value and the effect of net longwave radiation being negative.

Slob's (after de Bruin, 1987) equation was also tested for instantaneous net radiation by comparing with the calculated net radiation from the water surface (Figure 5.5). The results shows a high correlation ($R^2 > 0.9$) between two approach and the net radiation in Slob approach gives about 25% more than the estimated value.

Figure 5.6 presents the results from the analysis of 8th of October'98 over the water surface in which all the radiation budget components are shown. The following general features emerge:

- i) The solar radiation at TOA (Computed not observed) describe a smooth symmetrical curve with peak value, 1359 W/m^2 at noon. This is slightly less than the value of solar constant (1367 W/m^2) because of the date and the latitude of the site.
- ii) Surface receipt solar radiation follows the same shape as solar radiation at top of atmosphere (TOA).
- iii) Reflected solar radiation is very small because of low albedo value of water surface.
- iv) Both longwave fluxes are relatively constant with time due to the small diurnal temperature variation of lake surface and the air temperatures respectively.
- v) Net radiation is dominated by incoming solar radiation at daytime and of course is equal to net longwave radiation at night.

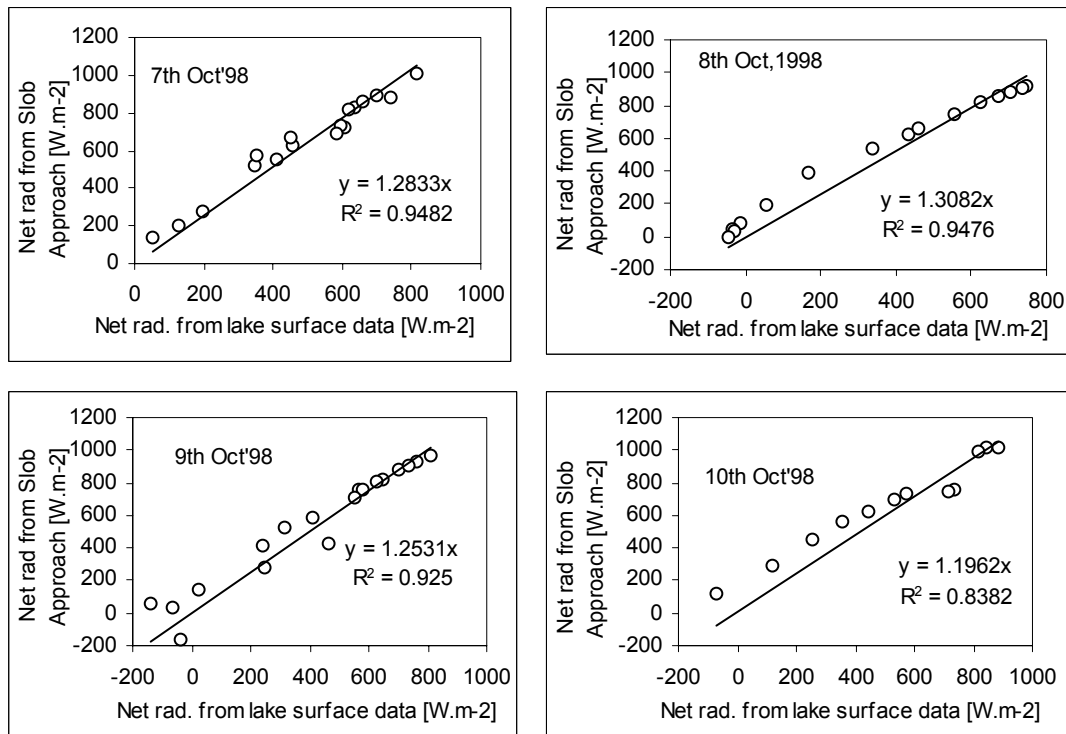


Figure 5.5: Comparison of net radiation (Slob approaches Vs Calculated)

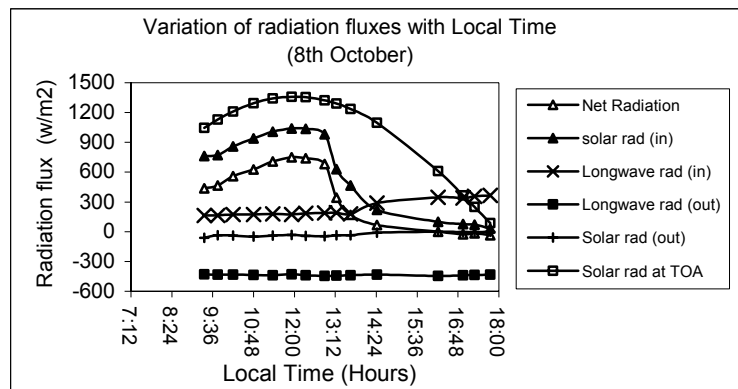


Figure 5.6: Variation of radiation fluxes with local time.

Sensible heat flux

Sensible heat flux was calculated using Equation 3.18 which shows that it is proportional to the temperature difference between the surface and the air ($T_o - T_a$) and inversely proportional to the aerodynamic resistance to heat transport, r_{ah} . The r_{ah} is again inversely proportional to the wind velocity and the roughness height. As in water surface the roughness height is very low (0.00137m as proposed by Penman) so the resistance to heat transport is very high. Some other researchers (i.e. Allen, et. al., 1996; Brutsaert, 1982) proposed even lower value for the roughness height, which will give the high value of resistance to heat transport. From the data set it was found that the temperature difference between the water surface and the air was very low which gives a negligible value of

sensible heat flux. Instantaneous daytime sensible heat flux for 8th October'1998 are presented in Table 5.1 and Figure 5.7.

Table 5.1: Sensible heat flux at different daytime (8th October 1998)

Note: Positive value indicates the heat flux leaving the surface

Local Time	Water surface Temp. T_o	Air Temp. T_a	$T_o - T_a$	Wind speed	resistance to heat transport	Sensible heat flux, H	Net Radiation	Remarks
(hours)	°C	°C	°C	(m/s)	(s/m)	(w/m ²)	(w/m ²)	[-]
9:21	19.0	19.0	0.0	0.2	1456.8	0.00	436.83	
9:45	20.6	20.4	0.2	3.5	83.2	2.28	465.78	
10:12	19.8	19.8	0.0	3.5	83.2	0.00	559.09	
10:48	20.8	20.8	0.0	5.5	53.0	0.00	627.74	
11:22	22.7	22.3	0.4	6.0	48.6	7.76	708.28	
11:55	23.1	22.9	0.2	3.5	83.2	2.26	750.62	
12:20	22.3	22.3	0.0	5.0	58.3	0.00	739.37	
12:53	23.0	22.7	0.3	4.5	64.7	4.35	680.46	
13:14	23.8	23.7	0.1	5.5	53.0	1.77	344.99	
13:39	23.7	24.0	-0.3	6.5	44.8	-6.27	170.84	Cloudy
14:25	24.2	23.7	0.5	7.0	41.6	11.26	66.46	Rainy
16:13	19.8	19.9	-0.1	1.5	194.2	-0.49	-1.00	Cloudy
16:57	20.2	20.1	0.1	2.5	116.5	0.81	-27.50	Cloudy
17:17	20.4	20.2	0.2	3.5	83.2	2.28	-17.53	Cloudy
17:45	20.2	20.0	0.2	2.0	145.7	1.30	-37.17	

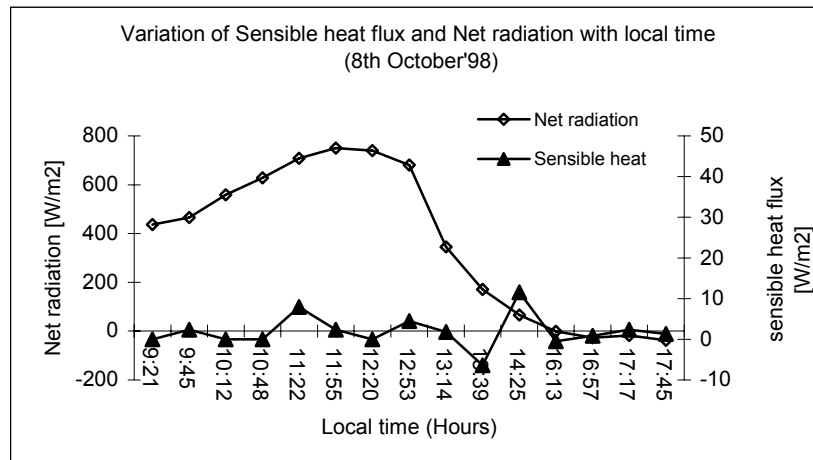


Figure 5.7: Variation of Sensible heat flux in daytime.

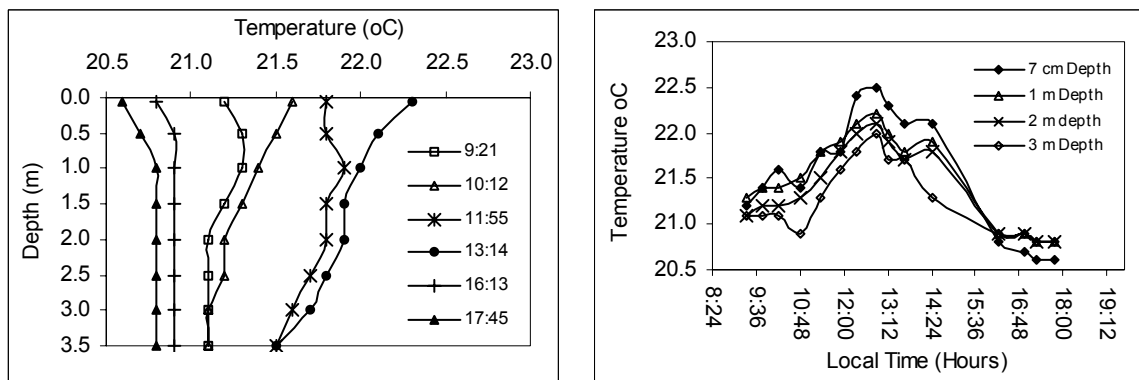
From the Table 5.1 and Figure 5.7 we can see that, the sensible heat flux is negligible with compare to the net radiation, analyses for the other days also shows the same results which are presented in Appendix G. But there was little sensible heat flux when the weather was windy and rainy because at that time the air was relatively cooler and resistance to heat transport was less because of high wind velocity. As we discussed before if there is wind (wave) in sunny midday it may reduce the net shortwave radiation which reduces the evaporation. However as there are no significant difference between the water surface temperature and the air temperature, the sensible heat flux will be always negligibly small and can be assumed as zero for water.

Water heat flux, G_o

Water heat flux (G_o) was estimated using Equation 3.17 considering the top 50-cm water depth, the results are presented in Table 5.2 for 8th October 1998. From the Table we can see that the water heat flux, G_o is very negligible as compared to net radiation. Also analysis of G_o for the other days are shows the same results which are presented in Appendix G. This is because there are negligible difference in temperature between the two depths. The variations of water temperature at different depth with local time are presented in Figure 5.8. The Figure shows a very small variation of water temperature through out the day. Also we can see that there is no heat storage within the water body because the temperature of the water body increases from morning to midday and again decreases in the afternoon time and comes to the same morning temperature. Even in the lower depth (3.5m depth) there is no increase of water temperature, hence there is no heat storage within the water body.

Table 5.2: Water heat flux in day time (8th October '98)

Local Time (hours)	Water temp. °C		Diff in water temp. °C	Water heat flux, G_o (w/m ²)	Net Radiation R_n (w/m ²)
	at 0.07m depth	at 0.5m depth			
9:21	21.2	21.3	-0.1	-0.1412	436.83
9:45	21.4	21.5	-0.1	-0.1412	465.78
10:12	21.6	21.5	0.1	0.1412	559.09
10:48	21.4	21.5	-0.1	-0.1412	627.74
11:22	21.8	21.8	0.0	0.0000	708.28
11:55	21.8	21.8	0.0	0.0000	750.62
12:20	22.4	22.2	0.2	0.2823	739.37
12:53	22.5	22.3	0.2	0.2823	680.46
13:14	22.3	22.1	0.2	0.2823	344.99
13:39	22.1	21.9	0.2	0.2823	170.84
14:25	22.1	21.9	0.2	0.2823	66.46
16:13	20.8	20.9	-0.1	-0.1412	-1.00
16:57	20.7	20.8	-0.1	-0.1412	-27.50
17:17	20.6	20.7	-0.1	-0.1412	-17.53
17:45	20.6	20.7	-0.1	-0.1412	-37.17

Figure 5.8: Variation of water temperature with depth and local time (8th October 1998).

Therefore, from the above data and results we can conclude that, for daily basis G_o is zero as there is no heat storage and even for instantaneous case G_o is very negligible. As there are no established empirical relations to get G_o from net radiation, R_n for water body to use in Remote sensing technique so for simplicity we can assume the instantaneous water heat flux is negligible for shallow water body. However for deeper water body this assumption may not be true.

Latent heat flux, λE

In energy balance approach latent heat flux (λE) was calculated as residual using Equation 3.16. As the sensible heat flux, H for the water surface is very negligible and assumed as zero (as discussed above) and the water heat flux, G_o is also negligible hence the latent heat flux, λE or evaporation is almost same as net radiation, R_n (see Table 5.3 and Figure 5.9).

Table 5.3: Variation of Latent heat flux, R_n , G_o and H with Local Time (8th October 1998)

Local Time	Net Radiation R_n	Sensible heat flux, H	Water heat flux, G_o	Latent heat flux, LE
(hours)	(w/m ²)	(w/m ²)	(w/m ²)	(w/m ²)
9:21	436.83	0.00	-0.14	436.97
9:45	465.78	2.28	-0.14	463.64
10:12	559.09	0.00	0.14	558.94
10:48	627.74	0.00	-0.14	627.88
11:22	708.28	7.76	0.00	700.52
11:55	750.62	2.26	0.00	748.36
12:20	739.37	0.00	0.28	739.09
12:53	680.46	4.35	0.28	675.82
13:14	344.99	1.77	0.28	342.94
13:39	170.84	-6.27	0.28	176.82
14:25	66.46	11.26	0.28	54.92
16:13	-1.00	-0.49	-0.14	-0.37
16:57	-27.50	0.81	-0.14	-28.18
17:17	-17.53	2.28	-0.14	-19.66
17:45	-37.17	1.30	-0.14	-38.33

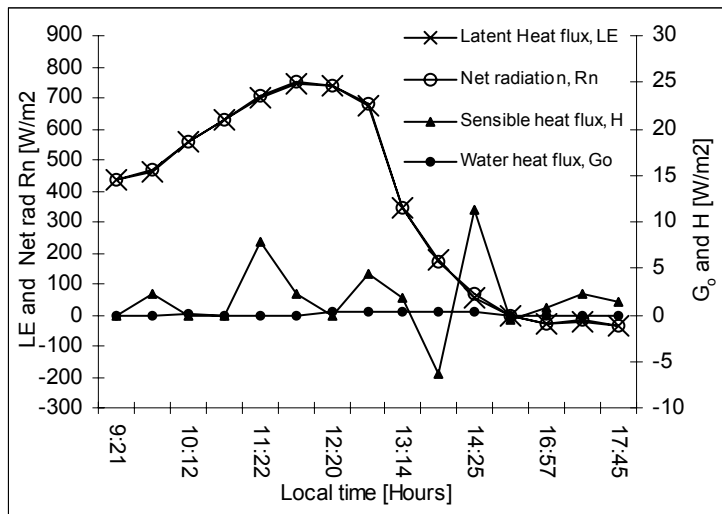


Figure 5.9: Variation of Latent heat flux, R_n , G_o and H with Local Time (8th October 1998)

To calculate daily evaporation using data from the meteorological stations, evaporative fraction approach was used. The evaporative fraction was calculated using the data from the water surface of the lake collected during the fieldwork in October 1998. The variations of evaporative fraction in the daytime are presented in Figure 5.10. The average evaporative fraction for the lake water was calculated as 0.998 which was almost 1, this means that the sensible heat flux is very negligible and closed to zero.

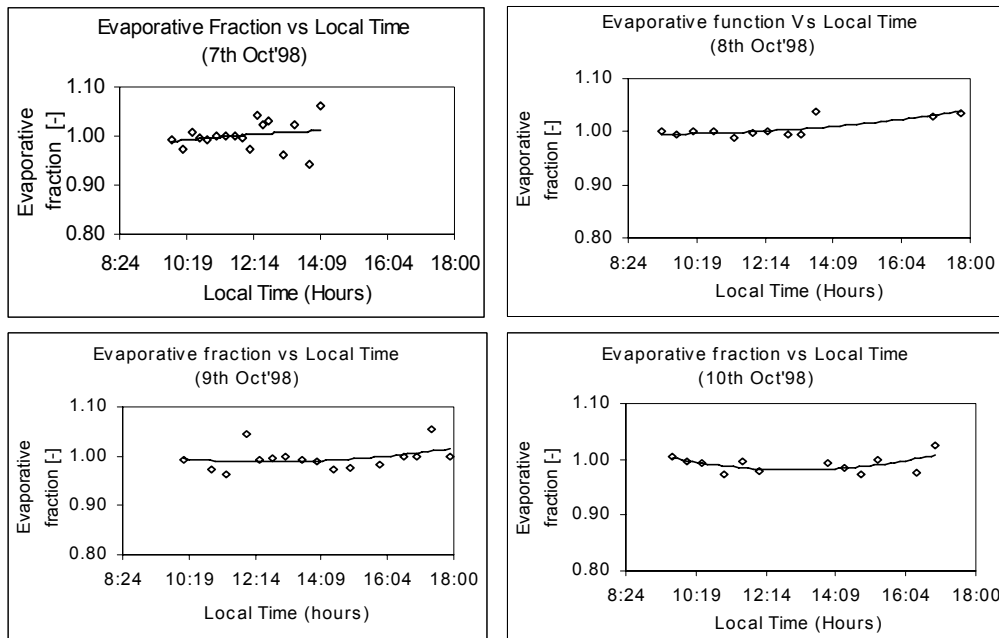


Figure 5.10: The variations of evaporative fraction with the daytime

Instantaneous value of latent heat flux was also calculated by using other three methods: Bowen ratio, Penman equation and Priestley-Taylor equation for different days and were compared with the energy balance approach (Residual approach). Analysis for 8th October are presented in Figure 5.11 and analyses for other days are presented in Table 5.4.

From the Figure 5.11 and Table 5.4 it can be concluded that the Priestley-Taylor method is better with compare to other two methods because it gives high correlation with the energy balance approach and also slope of the regression line (m) is closed to 1 although this method gives only about 5% lower value than the energy balance approach. As this method needs only temperature, radiation (R_n) and water heat flux (G_o) data that can be estimated with the satellite image, hence this method can be applied in remote sensing technique (for potential condition).

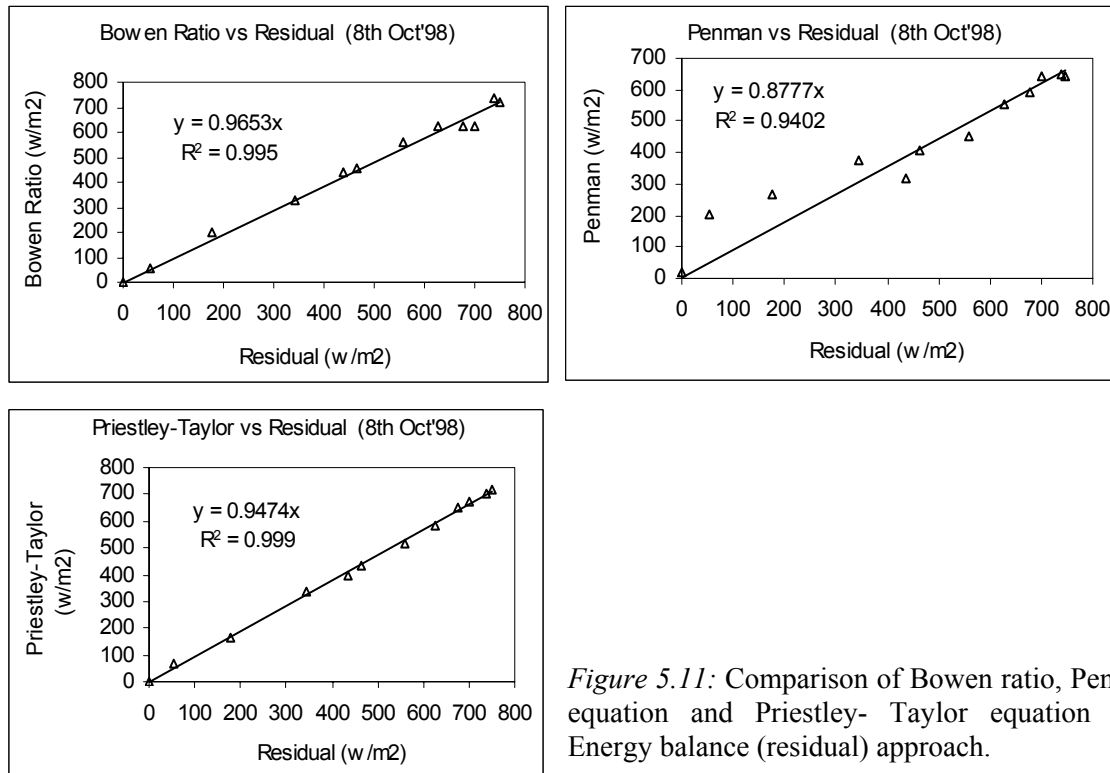


Figure 5.11: Comparison of Bowen ratio, Penman equation and Priestley- Taylor equation with Energy balance (residual) approach.

Table 5.4: Comparison of three methods with Energy balance method

Date	R ²			Regression Equation, Y = m.X (X= Energy balance approach)		
	Bowen ratio	Penman	Priestley-Taylor	Bowen ratio	Penman	Priestley-Taylor
7 th Oct'98	0.588	0.957	0.996	Y = 0.8411.X	Y = 0.7915.X	Y = 0.9469.X
8 th Oct'98	0.995	0.940	0.999	Y = 0.9653.X	Y = 0.8777.X	Y = 0.9474.X
9 th Oct'98	0.855	0.927	0.999	Y = 0.8711.X	Y = 0.8778.X	Y = 0.9507.X
10 th Oct'98	0.885	0.948	0.999	Y = 0.8246.X	Y = 0.8619.X	Y = 0.9444.X

5.2 Annual Evaporation from field data

In order to find the monthly and seasonal variation of evaporation, continuous weather data is necessary from the lake surface. However, since there are no direct offshore measurement of the water surface, so data from lakeshore station (Loldia) and from a station about 10km away from lake, Ndabibi (Location of these stations are presented in Fig. 2.4).

To estimate monthly to annual evaporation Ndabibi station data were used because of the availability of daily meteorological data. However, to check the applicability of these data to calculate lake evaporation, climatic condition of the two stations were compared by considering the shortwave and longwave radiation of the two areas.

Solar radiation sensor at Loldia station has the spectral range of 0.4-0.7 μm so the data were converted to broad band (0.305 - 2.8 μm) solar radiation by a multiplying factor 2.1 as proposed by Frouin and Pinker (1995). Then incoming solar radiation and the net longwave radiation of the two stations were compared and results are presented in Figure 5.12. The results show a little variation of incoming solar radiation and net longwave radiation for daily basis due to local cloud variations. But for long term basis there is practically no difference, which means that the climates of the two stations are similar, therefore for long-term calculation we can use Ndabibi station data. Evaporation of the two stations also shows the same result (Figure 5.13). For daily evaporation we get some fluctuations but for long term basis the variation was negligible, on average of three month period from mid of July'98 to mid of October'98 the evaporation of lakeshore station and Ndabibi station was 4.32 mm/day and 4.45 mm/day respectively.

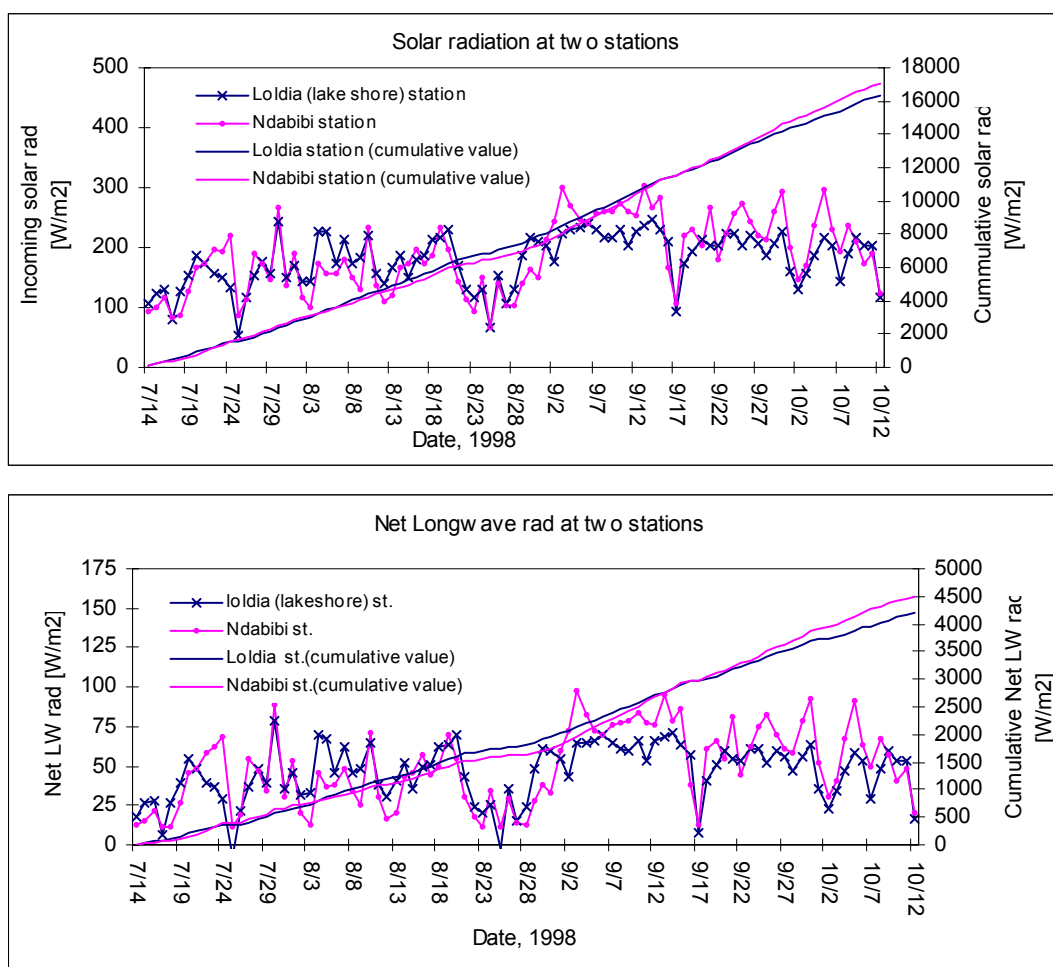


Figure 5.12: Variation of incoming solar radiation and net longwave at two stations
 Note: For longwave (LW) radiation all the values are negative.

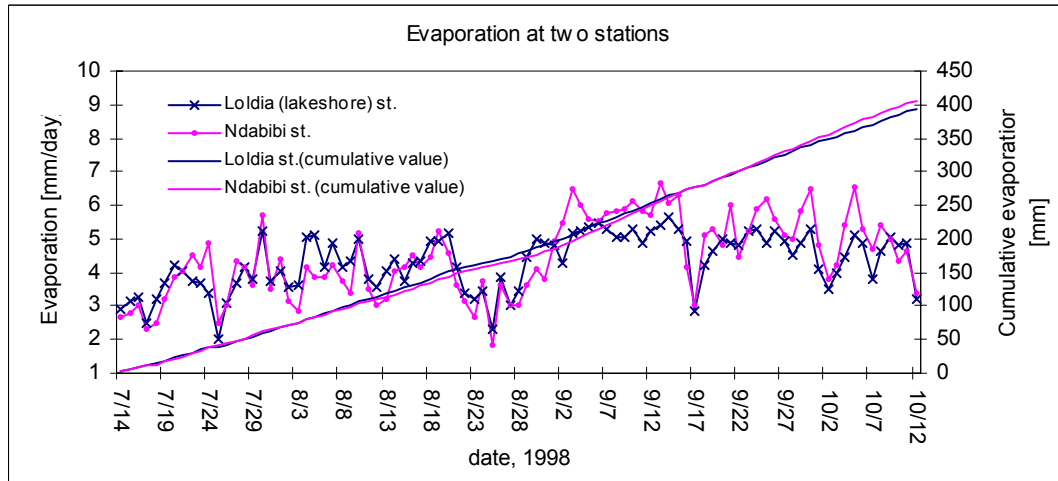


Figure 5.13: Variation of Evaporation at two stations

5.2.1 Lake Evaporation using Ndabibi station data

To get the seasonal variability of evaporation from lake, Ndabibi station data were used. Evaporation was also calculated using Slob’s approach to check the applicability of this method. The results are compared and presented in Figure 5.14 and 5.15.

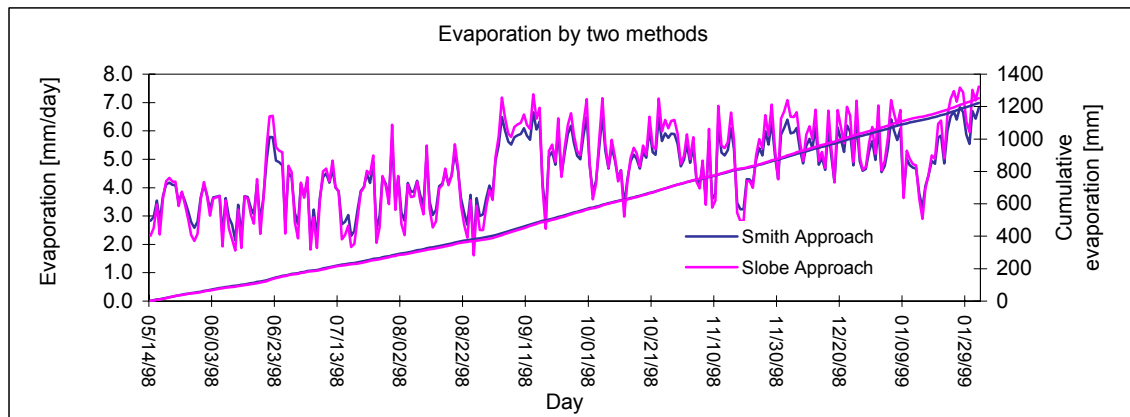


Figure 5.14: Daily evaporation by two methods.

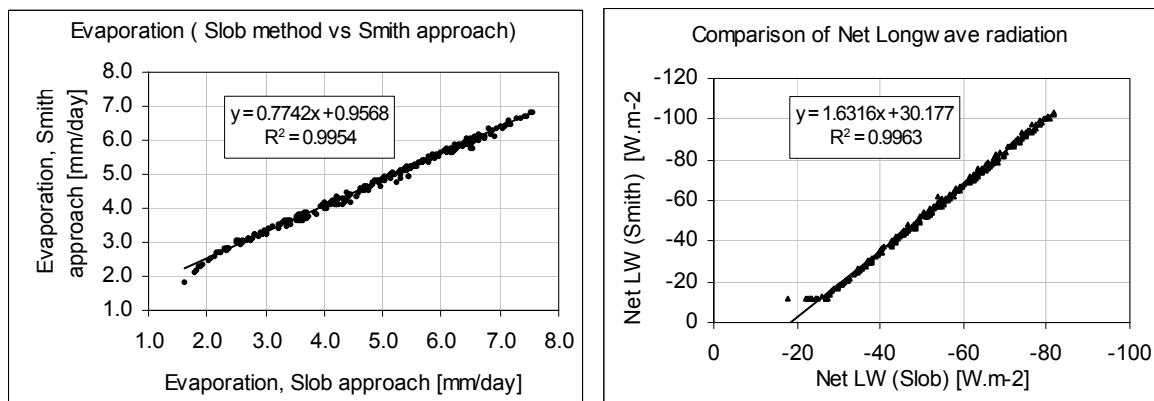


Figure 5.15: Comparison of Slob’s approach with the field (Smith approach) method.

Slob's approach for net longwave radiation calculation (Eq. 3.15) shows a high correlation with the Smith's approach (Eq. 3.14) although Slob's approach gives little higher evaporation in cloud free days with compare to smith approach. However for long term average the variation is very less and for about 9 months period (from May'98 to Jan, 1999) daily average evaporation of 4.61 and 4.72 mm/day was calculated using Smith's method and Slob's method respectively. Monthly average value of temperature, solar radiation, transmissivity and evaporation are presented in Table 5.5.

Table 5.5: Monthly average value of evaporation and other climatic parameters (Ndabibi Meteorological Station)

Month	In coming solar rad	Extra-terrestrial shortwave solar radiation	Transmissivity	Temp at 2m	Maximum possible sunshine hours	actual sunshine hour, n	Evaporation (Smith approach)	Evaporation (Slob approach)
	[<i>w/m²</i>]	[<i>wm⁻²</i>]	[<i>-</i>]	[<i>oC</i>]	(<i>hours</i>)	[<i>hour</i>]	[<i>mm.day⁻¹</i>]	[<i>mm.day⁻¹</i>]
May'98	141.73	394.35	0.36	17.25	11.96	2.42	3.46	3.30
June'98	158.46	384.22	0.41	15.75	11.96	3.56	3.68	3.64
July'98	154.20	389.81	0.40	14.76	11.96	3.23	3.67	3.57
Aug'98	149.96	411.09	0.37	14.32	11.98	2.60	3.74	3.55
Sept.'98	242.70	430.07	0.56	15.09	12.00	6.59	5.55	5.84
Oct'98	220.39	433.24	0.51	15.86	12.02	5.48	5.14	5.32
Nov.'98	206.32	423.72	0.49	15.44	12.04	5.04	4.82	4.94
Dec.'98	245.77	416.75	0.59	15.86	12.05	7.14	5.47	5.85
Jan.'99	239.75	422.88	0.57	16.83	12.04	6.67	5.39	5.74
Feb.'99	-	-	-	-	-	-	-	-
March'99	-	-	-	-	-	-	-	-
April'99	-	-	-	-	-	-	-	-

In Figure 5.14 there is a big jump of evaporation value from 2 mm/day to 7 mm/day in 3rd week of June and beginning of September, which was due to the variation of incoming solar radiation (Figure 5.16), which can be explained by the presence of clouds. This can be shown from temperature data. In a cloudy day the difference between the daily maximum and minimum temperature is comparatively less than that of sunny or cloud free day. From Figure 5.17 we can see the variation of incoming solar radiation and the difference in daily max. and min. temperature follow the same trend which confirmed the effect of cloud on evaporation.

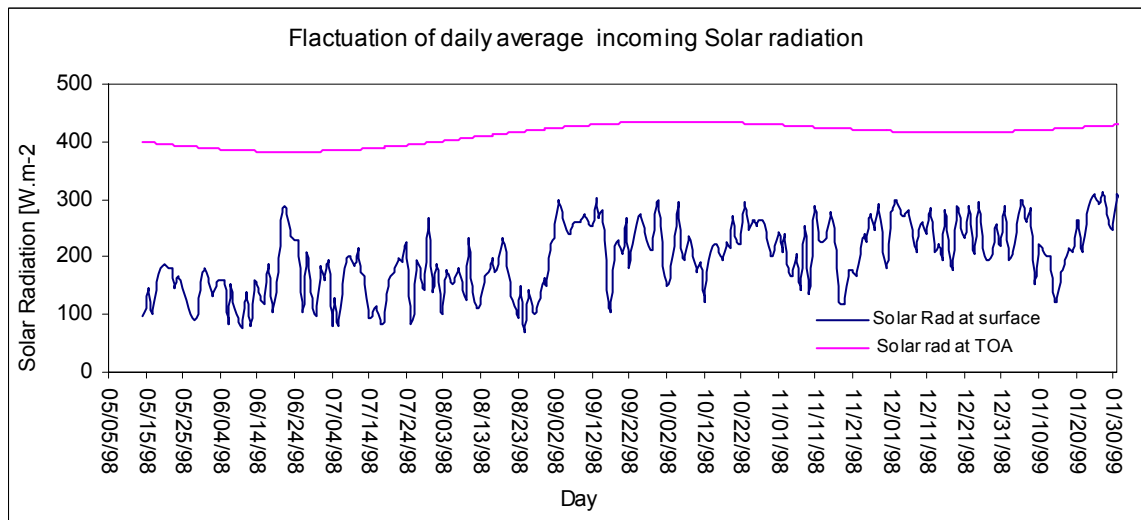


Figure 5.16: Fluctuation of daily average incoming solar radiation at Ndabibi met. Station.

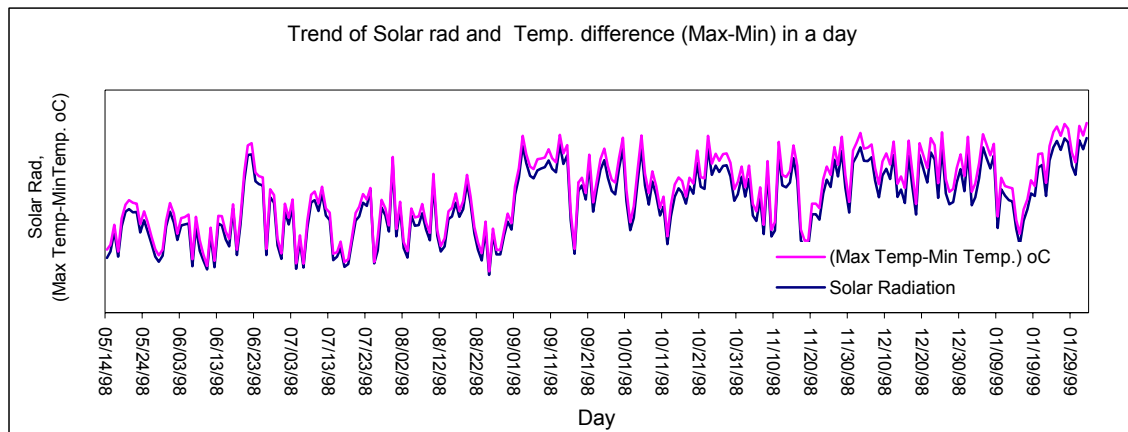


Figure 5.17: Trend of the variation of solar radiation and difference of daily max and min temperature over time at Ndabibi met station

5.2.2 Long-term evaporation from Ndabibi Met. Station data

Long-term (i.e. 7 years mean, 1961-68) solar radiation from Kedong Met. Station, which is very closed to the lake, was compared with solar radiation from Ndabibi station (few month data) and the results are presented in Table 5.6 and Figure 5.18. The monthly mean solar radiation at Ndabibi station for 1998-99 was much lower than the 7 years mean value. This is because, 1998-1999 has more cloud cover than the long-term average. Using Kedong Met. Station data, the long-term evaporation was estimated by following the Slob's approach for net longwave radiation and the results are presented in Table 5.6 and it can be observed that the long term mean evaporation value was higher than the 1998-1999 value. Monthly mean min, mean max and mean evaporation estimated from this long-term data is also presented in Table 5.6. From this Table we get the temporal variations of evaporation from the lake.

Table 5.6: Long term evaporation using Kedong Met. Station data (1961-68)

Month	Kedong Met. station (1961-68)						Ndabibi St.(1998-99)	
	Min Mean		Mean		Max Mean		Mean	
	Incoming solar rad	Evaporation	Incoming solar rad	Evaporation	Incoming solar rad	Evaporation	Incoming solar rad (mean)	Evaporation
	[W/m ²]	[mm/day]	[W/m ²]	[mm/day]	[W/m ²]	[mm/day]	[W/m ²]	[mm/day]
Jan	243.7	5.83	266.50	6.38	282.50	6.76	239.75	5.74
Feb	232.6	5.63	265.10	6.41	300.90	7.28		
Mar	196.3	4.76	250.00	6.06	276.20	6.70		
Apr	208.9	5.00	229.20	5.49	254.40	6.09		
May	175.4	4.10	210.80	4.93	248.10	5.80	141.73	3.30
Jun	179.8	4.14	203.00	4.67	251.50	5.79	158.46	3.64
July	122.1	2.83	182.70	4.23	229.70	5.32	154.20	3.57
Aug	65.9	1.56	189.00	4.47	225.80	5.34	149.96	3.55
Sep	214.2	5.16	246.70	5.94	279.10	6.72	242.70	5.84
Oct	232.6	5.62	256.80	6.20	302.40	7.30	220.39	5.32
Nov	188	4.50	232.10	5.56	263.60	6.31	206.32	4.94
Dec	224.8	5.35	239.90	5.71	263.10	6.26	245.77	5.85

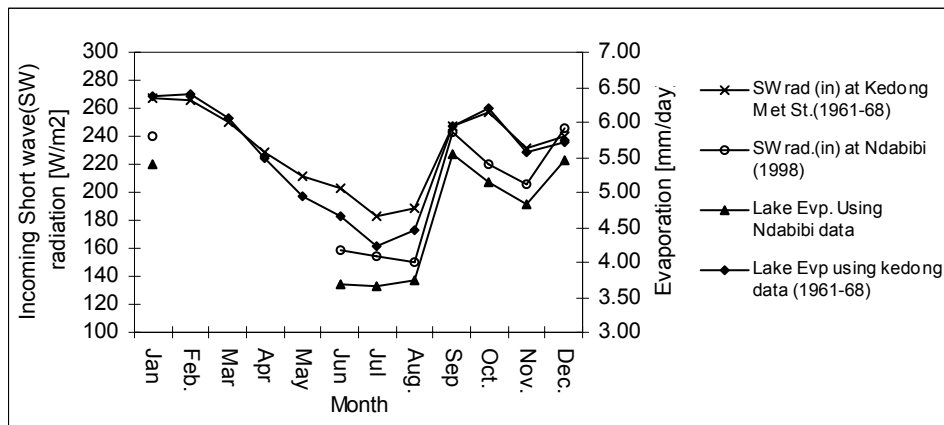


Figure 5.18: Comparison of long-term mean incoming shortwave radiation and evaporation (Kedong Met. Station, 0°55' S, 36°30' E, 1961-68) data with 1 year (1998-1999) Ndabibi data.

5.3 Remote sensing Evaporation

5.3.1 TOVS Application:

A TOVS atmospheric profile of 14th July 1998 (solar elevation = 48.27 degree) for area closed to Naivasha was used in the analysis. The profile was collected from ECMWF-MARS archive and has a resolution of 80 km (coordinate of the center of image is 0.62° N, 37.35°E with coarse accuracy). In the profile there were few missing data which were filled by interpolation. Using this profile the instantaneous incoming shortwave and longwave radiation was estimated by following the techniques described in chap 4 which

leads to a value 398.28 W/m^2 and 375.94 W/m^2 for incoming shortwave and longwave radiation respectively. For cloud transmittances factor T_C , we assume a value 0.60 (Roughly estimated from a NOAA AVHRR image of 21st May, 1998 for the same area), as there are no satellite image available for the same period of the TOVS profile. Out going longwave radiation from the lake was calculated by using Eq. 3.6 using the skin temperature given in the profile and the calculated value was 398.27 W/m^2 . Finally the net radiation in the lake was estimated using the albedo $r_o = 0.06$ which leads to a value of 352.05 W/m^2 . This value seems to be reasonable because the day was cloudy and also this value is closed to the estimated net radiation using Ndabibi met. Station data. However by using the satellite images taken at the same time of TOVS profile for the same area, it is possible to estimate net radiation more accurately.

5.3.2 Thematic Mapper Application:

To estimate evaporation from remotely sensed spectral data a TM image of 21st January 1995 was used in the analysis and algorithm proposed by Farah and Bastiaanssen (1999) was followed. In the calculations, water heat flux G_o was taken as 1% of net radiation in the instantaneous case and for daily total G_o was considered as zero and sensible heat flux, H was considered as zero in both cases. For daily total estimation, evaporative fraction approach was used and the net radiation was calculated using Equation C16 considering slob's approach for net longwave radiation. For details see Appendix F. The daily total evaporation from the lake, $E_{24\text{hours}} = 5.95 \text{ mm/day}$ was obtained from the analysis which seems to be reasonable. The spatial variation of evaporation, lake surface temperature, latent heat flux calculated using energy balance equation and Priestley-Taylor equation are presented in Figure 5.19, 5.20, 5.21 and 5.22 respectively.

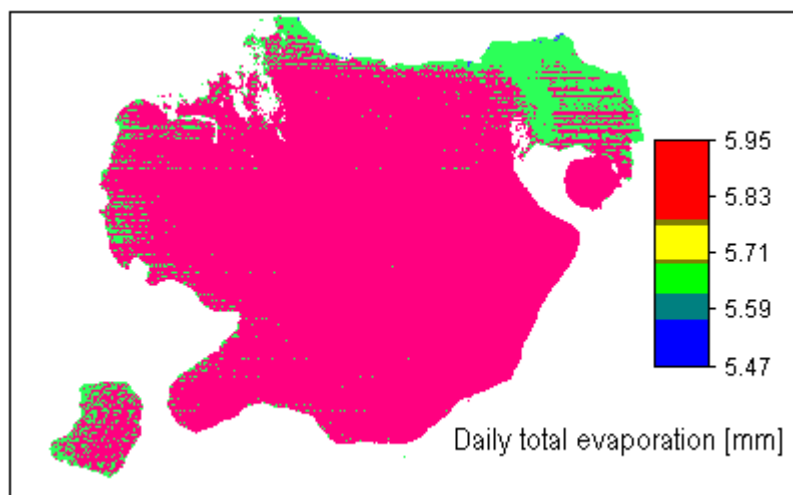


Figure 5.19: Spatial variation of daily evaporation [mm] from lake surface derived from TM image (21st January 1995)

Chapter 6

Conclusions

Results of the lake surface data analysis shows that the sensible heat flux in the lake is negligibly small and can be taken as zero. This is because of the negligible difference in air and water surface temperature in the lake and also because of very small roughness height of the water surface. However, the high wind speed may tends to increases the evaporation but on the other hand there is a possibility of reducing the net solar radiation due to the wave effect i.e. compensating each other. Hence the wind speed has little effect in the evaporative process above the lake in the daytime. As the temperature difference between the surface and the air is negligible throughout the 24 hours above the lake, so the sensible heat flux in the lake can be considered as zero even in the nighttime.

Lake surface data analysis also shows that the water heat flux in the lake is closed to zero because of negligible temperature difference in the lake water. As the lake is shallow so the water temperature increases in the early to mid day with the solar altitude and decreases again in the late after noon to night for compensating the net longwave radiation and sensible heat flux if any. Again the net longwave radiation from the water surface is significantly high in the nighttime because of water surface temperature and as the lake is shallow so there are not enough heat storage in the lake to take part in evaporation process in the nighttime after compensating the net longwave radiation. As we can see that the sensible heat flux and the water heat flux is negligibly small and considered as zero so the evaporation from the lake is equals to the net radiation.

From the comparison of three method with the energy balance residual approach for estimating lake evaporation, Priestley-Taylor method gives high correlation with the energy balance method and as this method needs only net radiation and temperature data which can be estimated using remote sensing satellite images, hence this method can be used in remote sensing evaporation for the wet condition.

From instantaneous evaporation to daily estimation, evaporative fraction method was used and an average value of evaporative fraction ≈ 1 was obtained above the lake surface that again proves that there is no sensible heat flux in the lake.

For daily net longwave radiation calculations, Slob's equation gives a high correlation ($r^2 = 0.996$) with the commonly used smith's equation and for long-term comparison and the result shows that, evaporation can be calculated within $\pm 5\%$ from the lake using this equation. As this equation is very simple and it needs only incoming solar radiation data so we can effectively use this equation for estimating net longwave radiation for potential condition. Hence we can conclude that by using only pyranometer data from the lake area one can estimate net radiation as well as evaporation from the lake by estimating net shortwave and longwave radiation.

From the results of daily evaporation we can see the effect of the clouds in the evaporative process. Presence of cloud immediately reduces the incoming solar radiation as well as evaporation. In remote sensing evaporation, normally cloud free satellite images are used for estimating evaporation which can give over estimated value for long-term calculations

if the cloud effect does not considered accurately. However for the Naivasha area, this study and the data set from Ndabibi meteorological station can be used to estimate the reduction factor for compensating the cloud effect.

For estimating evaporation using a new remote sensing approach TOVS (TIROS Operational Vertical Sounder) atmospheric profile, gives encouraging results of net longwave and shortwave radiation. Although the resolution of this data set is very low but this approach can be effectively used for large catchment, river basin or regional evaporation studies. The main advantage of this approach is that it can estimate net radiation using fully remote sensing technique and also the data up to 10-MB size can freely downloaded from the Internet with temporal resolution of 24 hours for any part of the world. Hence it is possible to retrieve the longer time series of evaporation using these data set for any part of the world.

Using energy balance residual approach and Priestley – Taylor equation, instantaneous latent heat flux from the lake was calculated from high resolution Thematic Mapper spectral data and both of the approach gives very close value. The daily total evaporation of 5.95 mm from the lake using evaporative fraction approach and Slob's equation for daily net longwave radiation seems to be good estimation because from pan data the estimated average evaporation was 5.46 mm for 21st January with a standard deviation of 1.28 mm for the period of 1957-1990. Also we get 5.83-mm evaporation for 21 January'1999, from the lake using Ndabibi Met. Station data. Hence we can conclude that for remote sensing evaporation, Slob's approach for daily net longwave radiation can be used for potential condition.

From the satellite images and field observations, negligible spatial variation of evaporation, surface temperature and albedo was found in the lake, which indicate the less effective use of remote sensing technique for evaporation calculation from this lake. However the lake evaporation can be estimated by using only pyranometer data from the surface of the lake with high accuracy.

APPENDICES

APPENDIX A: General Climatic Data of Naivasha**APPENDIX AI: Climatic Statistics Naivasha, Naivasha DO (0° 43' S, 36° 26' E; 1900m AMSL) (East African Meteorological Dept. 1964)**

Month	Temp °C (1937-54)					Relative Humidity	Rainfall (1910-62)	Wind (1938-54)	
	Max	Mean Max	Mean	Mean Min	Mn	% at 1500h	Mean, mm	at 0900h (m/s)	at 1500 h (m/s)
January	30.8	27.7	17.9	8.1	1.9	28.0	22.0	1.5	3.1
February	32.1	28.3	18.3	8.2	3.1	28.0	28.0	1.5	3.1
March	32.6	27.3	18.5	9.8	2.8	34.0	34.0	1.5	3.1
April	30.5	25.1	18.3	11.5	5.6	51.0	51.0	1.5	3.1
May	27.6	23.8	17.5	11.3	6.1	54.0	54.0	1.5	3.6
June	27.6	23.0	16.5	9.9	4.4	51.0	51.0	1.5	3.6
July	26.8	22.5	15.9	9.3	4.6	49.0	49.0	1.5	3.6
August	27.2	22.9	16.1	9.4	4.4	48.0	48.0	1.5	4.2
September	28.4	24.5	16.7	8.8	2.2	43.0	43.0	1.5	4.2
October	30.3	25.6	17.3	9.1	3.9	41.0	41.0	1.5	4.2
November	28.9	24.7	17.0	9.3	3.9	47.0	47.0	1.5	3.1
December	30.1	25.8	17.3	8.7	3.3	40.0	40.0	1.5	3.1

Source: (LNROA, 1993)

APPENDIX AII: Mean Rainfall figure (in mm) for selected station

Month	Naivasha Town, Naivasha DO (0°43' S, 36°26' E)	Naivasha vet. Station (0°39' S, 36°25'30" E)
	(mm)	(mm)
Year	42	39
Average (mm)	666	729
Altitude (m)	1900	1829
January	37.0	36.0
February	41.0	33.0
March	47.0	60.0
April	114.0	121.0
May	109.0	103.0
June	45.0	52.0
July	39.0	44.0
August	53.0	54.0
September	25.0	46.0
October	45.0	63.0
November	64.0	71.0
December	48.0	47.0

Source: (Jaetzold and Schmidt 1983, LNROA, 1993)

APPENDIX AIII: Daily Insolation, W/m² (East African Meteorological Dept)

Month	Naivasha Met station, (1970-1982)	Kedong Ranch 0°55' S, 36°30' E			Kisumu 0°06' S, 34°45' E		
		(1961-68)			1973		
	Mean	Max Min	Mean	Min Mean	Max	Mean	Min
Jan	269.9	282.5	266.5	243.7	318.9	284.5	199.6
Feb.	266.2	300.9	265.1	232.6	337.8	277.7	121.1
March	269.1	276.2	250.0	196.3	325.2	287.4	265.1
April	240.2	254.4	229.2	208.9	320.8	274.3	216.6
May	237.3	248.1	210.8	175.4	309.2	265.6	165.7
June	237.3	251.5	203.0	179.8	300.9	262.2	209.3
July	222.8	229.7	182.7	122.1	288.3	227.3	177.4
Aug.	237.3	225.8	189.0	65.9	317.9	266.5	190.0
Sept.	255.4	279.1	246.7	214.2	340.7	261.7	133.7
Oct.	256.8	302.4	256.8	232.6	333.4	278.6	227.8
Nov.	240.2	263.6	232.1	188.0	312.6	271.9	215.2
Dec.	260.4	263.1	239.9	224.8	319.3	282.0	213.7

Note: Coordinate of Naivasha Met. Station (Naivasha WDD): 0°44' S, 36°27' E and 1936 m above sea level

Source: LNROA, 1993 and Muthuri et.al, 1989.

APPENDIX AIV: Temperature Data from Naivasha Veterinary Experiment Station (0°39' S, 36° 25' 30" E)

Month	Mean Max Temp °C	Mean Temp °C	Mean Min Temp °C	Absolute Min Temp °C
January	27.7	17.5	7.3	2.8
February	28.3	17.5	6.8	2.8
March	27.8	17.8	7.9	4.4
April	26.3	17.3	8.4	2.2
May	25.1	16.9	8.8	3.3
June	24.7	16.3	8.0	2.2
July	24.7	15.9	7.2	2.2
August	24.6	16.1	7.7	2.8
September	25.7	16.3	7.0	1.7
October	26.1	16.8	7.6	4.4
November	25.5	16.6	7.8	3.3
December	25.7	16.7	7.7	4.4
Mean	26.0	16.8	7.7	1.7

Source: (Jaetzold and Schmidt 1983, after LNROA, 1993)

APPENDIX B: Water Balance of Lake Naivasha**APPENDIX BI:** Hydrologic balances for Lake Naivasha determined by Gaudet and Melack (1979)

All the value in millions of cubic meters ($m^3 \times 10^6$)

	1973	1974	1975
Surface Runoff	0.6	0.7	0.4
River discharge	90.8	204.0	240.5
Rainfall	106.1	114.2	77.1
Seepage in	37.0	42.3	50.8
Total Input	234.5	361.7	388.8
Evapotranspiration (Swamp)	14.3	13.2	13.3
Lake Evaporation	309.5	276.0	278.2
Seepage out and use for irrigation	24.6	50.6	93.3
Total Output	348.4	339.8	304.8
<i>Change in Storage (Calculated by balance)</i>	<i>-113.9</i>	<i>+21.4</i>	<i>+4.0</i>

APPENDIX BII: A rough Water balance determined by the LNROA (1993) for Lake Naivasha.

	Addition ($m^3 \times 10^6$)	Subtraction ($m^3 \times 10^6$)
Rainfall	7.296	
River discharge	150.00	
Seepage in	49.00	
Evaporation from free water		162.00
Evapotranspiration		10.8
Underground seepage		55.00
Abstraction Agriculture		32.7
Abstraction Geothermal power plant		15.2
Totals	271.96	275.70

[For this Calculation Lake level was considered 1885m a.m.s.l. and from area elevation curve a corresponding lake area 120 km² (open water 108 km², swamp area 12 km²) was taken]

APPENDIX C: EVAPORATIVE DEMAND OF THE ATMOSPHERE

Standard micro-meteorological expressions required for evaporation calculations
(Note: Equations are taken from Bastiaanssen et. al 1996b)

APPENDIX CI: WATER VAPOR

1. Saturated vapor pressure

$$e_s = 6.11 \exp \frac{17.27 \times (T_a - 273)}{(T_a - 273) + 237.3} \quad [\text{mbar}] \quad (\text{C1})$$

Where

T_a = Air temperature at observation height [K]

e_s = Saturated vapor pressure [mbar]

2. Actual vapor pressure

$$e_a = e_{s(wet)} - \gamma (T_{dry} - T_{wet}) = U \times e_s \quad [\text{mbar}] \quad (\text{C2})$$

Vapor pressure deficit

$$D = e_s - e_a \quad [\text{mbar}] \quad (\text{C2a})$$

Where,

D = Vapor pressure deficit [mbar]

e_a = actual vapor pressure [mbar]

$e_{s(wet)}$ = saturated vapor pressure at wet bulb temperature [mbar]

T_{dry} = dry bulb temperature [K]

T_{wet} = wet bulb temperature [K]

γ = Psychrometric Constant [mbar. K⁻¹]

U = Relative Humidity [-]

3. Slope of saturated vapor pressure curve

$$\Delta = 4098 \frac{e_s}{\{(T_a - 273) + 237.3\}^2} \quad [\text{mbar.K}^{-1}] \quad (\text{C3})$$

Where,

e_s = saturated vapor pressure [mbar]

T_a = air temperature [K]

4. Vapor density

$$\rho_v = \frac{e_a}{T_a \times 4.61} \quad [\text{Kg.m}^{-3}] \quad (\text{C } 4)$$

Where,

ρ_v = actual vapor density [Kg.m^{-3}]

e_a = actual vapor pressure [mbar]

T_a = air temperature at observation height [Kelvin]

5. Dry air density

$$\rho_d = \frac{P - e_a}{T_a \times 2.87} \quad [\text{Kg.m}^{-3}] \quad (\text{C } 5)$$

Where

ρ_d = dry air density [Kg. m^{-3}]

P = total pressure [mbar]

6. Moist air density

$$\rho_a = \rho_d + \rho_v \quad [\text{Kg.m}^{-3}] \quad (\text{C } 6)$$

Where

ρ_a = moist air density [Kg. m^{-3}]

7. Total air pressure

$$P = 1004 \left(\frac{293 - 0.0065Z}{293} \right)^{5.26} \quad [\text{mbar}] \quad (\text{C } 7)$$

Where

P = Total pressure [mbar]

Z = Elevation [m]

(Source: ICID Bulletin 1994, Vol. 43. No. 2)

8. Latent heat of vaporization

$$\lambda = \{2.501 - 0.002361(T - 273)\} \times 10^6 \quad [\text{J.Kg}^{-1}] \quad (\text{C } 8)$$

Where

λ = Latent heat of vaporization [J. Kg⁻¹]

T = average of surface and air temperature [K]

9. Psychrometric constant

$$\gamma = 1630 \frac{P}{\lambda} \quad [\text{mbar.K}^{-1}] \quad (\text{C } 9)$$

Where

γ = Psychrometric Constant [mbar. K⁻¹]

P = total pressure [mbar]

λ = Latent heat of vaporization [J. Kg⁻¹]

APPENDIX CII: RADIATION

10. Solar declination

$$\delta = 0.409 \sin(0.0172J - 1.39) \quad [\text{rad}] \quad (\text{C } 10)$$

Where

δ = Solar declination [rad]

J = day number of the year [-]

sin = sine function which should be in radian mode

11. Solar distance

$$d_s = 1 + 0.0167 \sin\left[\frac{2\pi(J - 93.5)}{365}\right] \quad [\text{AU}] \quad (\text{C 11a})$$

$$E_o = 1 + 0.033 \cos(0.0172 J) \quad [-] \quad (\text{C 11b})$$

Where

d_s = relative distance between earth and sun [AU]

E_o = Eccentricity correction factor of the earth orbit [-]

cos = cosine function which should be in radian mode

12. Solar hour angle

$$\omega = \arccos(-\tan(\text{lat}) \tan \delta) \quad [\text{rad}] \quad (\text{C 12a})$$

$$\omega_a = \pi(12 - \text{Local time})/12 \quad [\text{rad}] \quad (\text{C 12b})$$

ω = Solar hour angle representing the 24 hour solar radiation [rad]

ω_a = Instantaneous Solar hour angle [rad]

lat = latitude [rad]

δ = solar declination [rad]

13. Extra-terrestrial shortwave solar radiation

$$R_a = 435.2 \times E_o \times (\omega \sin(\text{lat}) \sin \delta + \cos(\text{lat}) \cos \delta \sin \omega) \quad [\text{W.m}^{-2}] \quad (\text{C 13a})$$

Where

R_a = Daily Extra-terrestrial short wave solar radiation [W.m^{-2}]

For Instantaneous Extra-terrestrial short wave solar radiation, R_{ai}

$$\begin{aligned} R_{ai} &= 1367 \times E_o \times (\sin(\text{lat}) \sin \delta + \cos(\text{lat}) \cos \delta \cos \omega_a) \quad [\text{W.m}^{-2}] \quad (\text{C 13b}) \\ &= 1367 \times \sin((\text{lat}) \sin \delta + \cos(\text{lat}) \cos \delta \cos \omega_a) / d_s^2 \\ &= 1367 \times \cos(\phi_{su}) / d_s^2 \end{aligned}$$

Where ϕ_{su} = solar zenith angle [rad]

14. Maximum possible sunshine hours

$$N = 7.64 \omega \quad [\text{Hours}] \quad (\text{C } 14)$$

Where, N = Maximum possible sunshine hours

15. At surface incoming short wave solar radiation

$$K \downarrow = (0.24 + 0.59 n/N) \cdot R_a \quad [\text{W.m}^{-2}] \quad (\text{C } 15)$$

Where

$K \downarrow$ = incoming short wave solar radiation

R_a = Extra-terrestrial short wave solar radiation [W.m^{-2}]

N = Maximum possible sunshine hours

n = actual hours of sunshine [Hours]

16. Daily Net Radiation

$$R_n = (1 - r_o) \cdot K \downarrow - 110 \cdot \frac{K \downarrow}{R_a} \quad [\text{W m}^{-2}] \quad (\text{C } 16)$$

Where $K = \tau_{sw} \cdot R_a$ and τ_{sw} [-] is the shortwave atmospheric transmissivity.

17. Penman-Monteith Equation

$$\lambda E = \frac{\Delta R_n + \rho_a c_p (e_s - e_a) / r_{ah}}{\Delta + \gamma \left(1 + \frac{r_s}{r_{ah}}\right)} \quad [\text{W.m}^{-2}] \quad (\text{C } 17)$$

Where

λE = Latent heat flux [W.m^{-2}]

e_s = saturated vapor pressure at observation height [mbar]

e_a = actual vapor pressure at observation height [mbar]

r_s = canopy resistance [s.m^{-1}]

APPENDIX D: Estimating evapotranspiration from the Water Hyacinth

To estimate evapotranspiration from the water hyacinth i.e. from the swamp area, the energy balance residual approach was used. To calculate the different components of energy balance we follow the same procedure as describe in chapter 3 but the only exception is sensible heat flux because it differ from the water surface. In to calculation of aerodynamic resistance to heat transport (Equation 3.19) we used different roughness height for momentum transport (z_{om}) and heat transport (z_{oh}) and a different value for plant displacement height (d). We consider the integrated stability function for momentum transfer and sensible heat, Ψ_{sm} and Ψ_{sh} as zero because there are not significant difference in temperature between the surface and at 1.5m height. In Table D1 some empirical equations are presented for estimating z_{om} and d .

Table D1: Empirical Equations for estimating z_{om} and d

Equations	Author(s)
$z_{om}=0.123h$ $d = 0.67h$	Allen et al. (1989)
$z_{om}=0.2h$	Thom (1975)
$z_{om}=0.14h$	Brutsaert (1982)

Where h is plant height

The roughness height heat transport z_{oh} can be calculated using the relation:

$$KB^{-1} = \ln\left(\frac{z_{om}}{z_{oh}}\right)$$

Brutsaert (1982) proposed a value for $KB^{-1} \geq 2.3$, Gratt (1978) proposed $KB^{-1} = 2$. For permeable rough surfaces such canopies, Prevot et. al., (1994) showed that KB^{-1} is in between 2 to 3. However, in our calculation we consider,

$$d = 0.67 h = 0.0469\text{m (as } h = 0.07\text{m)}$$

while

$$z_{om} = 0.123h = 0.00861\text{m}$$

and

$$z_{oh} = 0.1 z_{om} \text{ (Considering } KB^{-1} = 2.3) \\ = 0.000861\text{m}$$

From the data and the analysis (see Table D 2) we found that free water surface evaporate 25% more than the water hyacinth. This is mainly because the canopy temperature is higher than the water surface and also albedo for the water hyacinth (0.17) is much higher than the water surface (0.06). But if we use penman- Monteith equation (Eq. C17) considering canopy resistance then free water surface evaporate 50% more if canopy resistance = 0 (s/m) and 60% more if canopy resistance =50 (s/m) than the water hyacinth. Therefore it can be conclude that evapotranspiration from the swamp area (which is mainly covered by water hyacinth) must be less than the free water surface.

Table D2:

APPENDIX E: TOVS**APPENDIX EI: TOVS Sensors**

Table E1. Instrument Parameters for TOVS Sensors.

TOVS Instrument Parameters	HIRS/2	SSU	MSU
Calibration	Stable blackbodies (2) and space background	Stable blackbody and space	Hot reference body and space background each scan cycle
Cross-track scan angle (degrees from nadir)	+/- 49.5	+/- 40.0	+/- 47.35
Scan time (seconds)	6.4	32.0	25.6
Number of steps	56	8	11
Angular FOV (degrees)	1.25	10.0	7.5
Step angle (degrees)	1.8	10	9.47
Step time (seconds)	0.1	4.0	1.84
Ground IFOV at nadir (km diameter)	17.4	147.3	109.3
Ground IFOV at end of scan	58.5 km cross-track x 29.9 km along-track	244 km cross-track x 186.1 km along-track	323.1 km cross-track x 178.8 km along-track
Distance between IFOV enters (km along-track)	42.0	62.3	168.1
Swath width	+/- 1120 km	+/- 737 km	+/- 1174 km
Data rate (bits per second)	2880	480	320
Data precision (bits)	13	12	12
Time between start of each scan line	6.4 sec	32 sec	25.6 sec
Step and dwell time	0.1 sec	4.0 sec	1.81 sec
Time *	0.5 sec	2.0 sec	0.9 sec
* Time- The difference between the start of each scan and the center of the first dwell period.			

Source: NOAA POD User's Guide, 1998 (Kidwell, 1998)

TOVS-HIRS/2 Sensor:

The HIRS/2 instrument is a step-scanned multi-channel spectrometer with 20 channels primarily in the infrared region of the spectrum including both longwave (15 micron) and shortwave (4.3 micron), plus one channel in the visible (.69 micron) region. The Table E2 contains typical values of the HIRS/2 spectral characteristics and noise equivalent differential radiance (NE_dN's in units of milliWatts/m²-steradians-cm).

Table E2: Characteristics of HIR/2 Channels.

Channel	Wavelength (micrometers)	Maximum Scene Temperature (K)	Specified NEdN	Level of peak energy contribution	Principle absorbing constituents	Purpose of radiance observation
1	14.95	280	3.00	30 mbar	CO ₂	<i>Temperature sounding:</i> The 15 μm band channel provides better sensitivity to the temperature of relatively cold regions of the atmosphere than can be achieved with 4.3μm band channels. Radiance in channels 5,6 and 7 are also used to calculate the height and amounts of cloud within the HIRS field of view.
2	14.71	265	0.67	60 mbar	CO ₂	
3	14.49	240	0.50	100 mbar	CO ₂	
4	14.22	250	0.31	400 mbar	CO ₂	
5	13.97	265	0.21	600 mbar	CO ₂	
6	13.64	280	0.24	800 mbar	CO ₂ /H ₂ O	
7	13.35	290	0.20	900 mbar	CO ₂ /H ₂ O	
8	11.11	330	0.10	Surface	Window	<i>Surface Temperature</i> and cloud detection
9	9.71	270	0.15	25 mbar	O ₃	<i>Total ozone concentration</i>
10	12.47	290 310*	0.16 0.09*	900 mbar	H ₂ O	<i>Water vapor sounding.</i> Provides water vapor corrections for CO ₂ and window channels. The 6.7-μm channel is also used to detect thin cirrus cloud.
11	7.33	275	0.20	700 mbar	H ₂ O	
12	6.52	260	0.19	500 mbar	H ₂ O	
13	4.57	300	0.006	1000 mbar	N ₂ O	<i>Temperature sounding:</i> The 4.3 μm band channel provide better sensitivity to the temperature of relatively warm regions of the atmosphere than can be achieved with the 15μm band channels. Also the short-wavelength radiance is less sensitive to clouds than those for the 15μm regions.
14	4.52	290	0.003	950 mbar	N ₂ O	
15	4.47	280	0.004	700 mbar	CO ₂ /N ₂ O	
16	4.45	260	0.002	400 mbar	CO ₂ /N ₂ O	
17	4.13	280 350*	0.002	5 mbar	CO ₂	
18	4.00	340	0.002	Surface	Window	<i>Surface Temperature:</i> Much less sensitive to clouds and H ₂ O than 11 μm channel to detect cloud contamination and derive surface Temperature under partly cloudy sky conditions. Simultaneous 3.7 and 4.0 μm data enable reflected solar contribution to be eliminated from the observations.
19	3.76	340	0.001	Surface	Window	
20	0.690	100% A	0.10% A	Cloud	Window	<i>Cloud detection:</i> Used during the day with 4.0 and 11 μm window channels to define clear field of view.

* In the above table, NOAA-11 and all subsequent satellites (except NOAA-12) have channels 10 and 17 at different locations in the spectrum. An * (asterisk) indicates the values for NOAA-11.

TOVS-MSU Sensor:

The MSU instrument was designed to make passive measurements in four regions of the 5.5-micrometer oxygen region of the spectrum. The Table E3 shows the spectral frequencies, bandwidths and typical Noise Equivalent delta Temperature (NEdT) values of the four MSU channels, along with the optical scan properties of the MSU.

Table E3: Characteristics of MSU Channels.

MSU Channel number	Frequency (Ghz)	NEdT (K)	RF Bandwidth (MHz)	Principle absorbing constituents	Level of peak energy contribution	Purpose of radiance Observation
1	50.3	0.3	220	Window	Surface	<i>Surface emissivity and cloud attenuation determination</i>
2	53.74	0.3	220	O ₂	700 mbar	<i>Temperature sounding: The microwave channels probe through clouds and can be used to alleviate the influence of clouds on the 4.3 and 15 μm sounding channels.</i>
3	54.96	0.3	220	O ₂	300 mbar	
4	57.95	0.3	220	O ₂	90 mbar	

TOVS-SSU Sensor:

The SSU is a step-scanned far-infrared spectrometer with three channels in the 15-micrometer carbon dioxide absorption band. The 3 SSU channels have the same frequency but different cell pressures. The SSU instrument makes use of the pressure modulation technique to measure radiation emitted from carbon dioxide at the top of the earth's atmosphere. The primary objective of the SSU instrument is to obtain data from which stratospheric (25-50 km) temperature profiles can be determined. The SSU is used in conjunction with HIRS/2 and MSU to determine temperature profiles from the surface to the 50-km level (TOVS Sounding Product).

Table E4: Characteristics of SSU Channels:

Channel Number	Central Wave number (cm-1)	Cell Pressure (mb)	Pressure of weighting function peak	
			(mb)	Km
1	668	100	15	29
2	668	35	5	37
3	668	10	1.5	45

Advanced TIROS Operational Vertical Sounder, ATOVS

There are three separate sensors within the Advanced TIROS Operational Vertical Sounder (ATOVS) system. These are the High Resolution Infrared Radiation Sounder (HIRS/3), the Advanced Microwave Sounding Unit-A (AMSU/A), and the Advanced Microwave Sounding Unit (AMSU/B).

The High Resolution Infrared Radiation Sounder (HIRS/3):

High Resolution Infrared Radiation Sounder (HIRS/3) is a discrete stepping, line-scan instrument designed to measure scene radiance in 20 spectral bands to permit the calculation of the vertical temperature profile from Earth's surface to about 40 km. Multispectral data from one visible channel (0.69 micrometers), seven shortwave channels (3.7 to 4.6 micrometers) and twelve longwave channels (6.5 to 15 micrometers) are obtained from a single telescope and a rotating filter wheel containing twenty individual filters. The characteristics of sensors are presented in Table E5 below:

Table E5: HIRS/3 Spectral Characteristics.

HIRS/3 Channel Number	Central Wave Number (cm^{-1})	Wavelength (micrometers)	Principle absorbing constituents	Noise Equivalent Delta Radiance $\text{mW}/(\text{m}^2\text{-sr-cm}^{-1})$
1	669	14.95	CO ₂	3.00
2	680	14.71	CO ₂	0.67
3	690	14.49	CO ₂	0.50
4	703	14.22	CO ₂	0.31
5	716	13.97	CO ₂	0.21
6	733	13.64	CO ₂ /H ₂ O	0.24
7	749	13.35	CO ₂ /H ₂ O	0.20
8	900	11.11	Window	0.10
9	1,030	9.71	O ₃	0.15
10	802	12.47	H ₂ O	0.15
11	1,365	7.33	H ₂ O	0.20
12	1,533	6.52	H ₂ O	0.20
13	2,188	4.57	N ₂ O	0.006
14	2,210	4.52	N ₂ O	0.003
15	2,235	4.47	CO ₂ /N ₂ O	0.004
16	2,245	4.45	CO ₂ /N ₂ O	0.004
17	2,420	4.13	CO ₂	0.002
18	2,515	4.00	Window	0.002
19	2,660	3.76	Window	0.001
20*	14,500	0.690	Window	0.10% albedo

The Advanced Microwave Sounding (AMSU):

Advanced Microwave Sounding Unit-A (AMSU-A)

The Advanced Microwave Sounding Unit-A (AMSU-A) system is implemented in two separate modules: the AMSU-A1 and AMSU-A2. The AMSU-A is a multi-channel microwave radiometer that will be used for measuring global atmospheric temperature profiles and will provide information on atmospheric water in all of its forms (with the exception of small ice particles, which are transparent at microwave frequencies) from the NOAA KLM spacecraft.

AMSU-A1 consists of 12 V-band channels (3 through 14) and one W-band channel (15) and associated circuitry. This module provides a complete and accurate vertical temperature profile of the atmosphere from the Earth's surface to a height of approximately 45-km.

AMSU-A2 contains the two lower frequencies (K-band channel 1 and Ka-band channel 2), and the associated scanning, calibration, processing, and power control hardware and circuitry. This module is used to study atmospheric water in all of its forms with the exception of small ice particles

Advanced Microwave Sounding Unit-B (AMSU-B)

The Advanced Microwave Sounding Unit-B (AMSU-B) is a 5-channel microwave radiometer. The purpose of the instrument is to receive and measure radiation from a number of different layers of the atmosphere in order to obtain global data on humidity profiles. It works in conjunction with the AMSU-A instruments to provide a 20-channel microwave radiometer.

APPENDIX EII: Data availability, Geographic location & coverage, Parameters

Period of Record of:

TOVS data: Start Date: 1979-07-02
End Date: to present

ATOVS data: Start Date: 1998-10-26
End Date: to present

Current data available from Satellite Active Archive (SAA):

Online valid range: TOVS: 1995/06/13 to Present
ATOVS: 1998/10/26 to Present

On Tape valid range: TOVS: 1979/07/02 to Present
ATOVS: 1998/10/26 to Present

Note: Data less than 10mb can get free through online
(SAA address: <http://sit.saa.noaa.gov/saa-www-bin/tovs1b-search.sh>),

Geographic Location(s) for both TOVS and ATOVS:

Global
Boundary Layer
Troposphere
Stratosphere

Geographic Coverage for both TOVS and ATOVS:

Northernmost Latitude: 90N

Southernmost Latitude: 90S

Westernmost Longitude: 180W

Easternmost Longitude: 180E

Discipline(s):

Earth Science - Atmosphere
Earth Science - Land

Parameter(s):

- Atmospheric Composition – Aerosols
- Atmospheric Composition – Ozone
- Atmospheric Dynamics - Solar Radiation
- Atmospheric Dynamics - Atmospheric Temperature
- Earth Radiative Processes - Albedo
- Earth Radiative Processes - Brightness Temperature
- Earth Radiative Processes – Irradiance
- Earth Radiative Processes – Radiance
- Geography And Land Cover – Albedo
- Radiance And Imagery - Infrared Radiation
- Radiance And Imagery - Microwave Radiation
- Radiance And Imagery - Visible Radiation

NOTE: For further details see NOAA *POD Users Guide* (Kidwell, 1998) and NOAA *KLM Users Guide* (Goodrum, et. al., 1999).

APPENDIX EIII: Atmospheric profile derived from TOVS sensors for Naivasha area

1	SATELLITE IDENTIFICATION	206	CODE TABLE	1007
2	YEAR	1998	YEAR	
3	MONTH	7	MONTH	
4	DAY	14	DAY	
5	HOURLY	0	HOURLY	
6	MINUTE	0	MINUTE	
7	SECOND	49	SECOND	
8	LATITUDE (COARSE ACCURACY)	0.62	DEGREE	
9	LONGITUDE (COARSE ACCURACY)	37.35	DEGREE	
10	SOLAR ELEVATION	48.27	DEGREE	
11	SATELLITE CHANNEL(S) USED	12608796	FLAG TABLE	2025
12	SATELLITE DATA PROCESSING TECHNIQUE USED	32	FLAG TABLE	2022
13	SATELLITE LOCATION COUNTER	11044	NUMERIC	
14	VERTICAL SIGNIFICANCE (SATELLITE OBSERVATIONS)	7	CODE TABLE	8003
15	OZON	273	DOBSON	
16	VERTICAL SIGNIFICANCE (SATELLITE OBSERVATIONS)	2	CODE TABLE	8003
17	PRESSURE	MISSING	PA	
18	CLOUD COVER (TOTAL)	100	%	
19	VERTICAL SIGNIFICANCE (SATELLITE OBSERVATIONS)	0	CODE TABLE	8003
20	LAND/SEA QUALIFIER	0	CODE TABLE	8012
21	HEIGHT OF LAND	910	M	
22	SKIN TEMPERATURE	289.5	K	
23	PRESSURE	92000	PA	
24	VERTICAL SIGNIFICANCE (SATELLITE OBSERVATIONS)	6	CODE TABLE	8003
25	PRESSURE	92000	PA	
26	PRESSURE	85000	PA	
27	VIRTUAL TEMPERATURE	MISSING	K	
28	PRESSURE	85000	PA	
29	PRESSURE	70000	PA	
30	VIRTUAL TEMPERATURE	287.9	K	
31	PRESSURE	70000	PA	
32	PRESSURE	50000	PA	
33	VIRTUAL TEMPERATURE	275.2	K	
34	PRESSURE	50000	PA	
35	PRESSURE	40000	PA	
36	VIRTUAL TEMPERATURE	262.4	K	
37	PRESSURE	40000	PA	
38	PRESSURE	30000	PA	
39	VIRTUAL TEMPERATURE	249.6	K	
40	PRESSURE	30000	PA	
41	PRESSURE	20000	PA	
42	VIRTUAL TEMPERATURE	229.9	K	
43	PRESSURE	20000	PA	
44	PRESSURE	10000	PA	
45	VIRTUAL TEMPERATURE	206	K	
46	PRESSURE	10000	PA	
47	PRESSURE	7000	PA	
48	VIRTUAL TEMPERATURE	198.3	K	
49	PRESSURE	7000	PA	
50	PRESSURE	5000	PA	
51	VIRTUAL TEMPERATURE	204.1	K	
52	PRESSURE	5000	PA	
53	PRESSURE	3000	PA	
54	VIRTUAL TEMPERATURE	212.7	K	
55	PRESSURE	3000	PA	

56	PRESSURE	1000	PA	
57	VIRTUAL TEMPERATURE	224.5	K	
58	PRESSURE	1000	PA	
59	PRESSURE	500	PA	
60	VIRTUAL TEMPERATURE	238.2	K	
61	PRESSURE	500	PA	
62	PRESSURE	200	PA	
63	VIRTUAL TEMPERATURE	251.4	K	
64	PRESSURE	200	PA	
65	PRESSURE	100	PA	
66	VIRTUAL TEMPERATURE	258	K	
67	PRESSURE	100	PA	
68	PRESSURE	40	PA	
69	VIRTUAL TEMPERATURE	252.4	K	
70	VERTICAL SIGNIFICANCE (SATELLITE OBSERVATIONS)	4	CODE TABLE	8003
71	PRESSURE	92000	PA	
72	PRESSURE	70000	PA	
73	PRECIPITABLE WATER	22	KG/M**2	
74	PRESSURE	70000	PA	
75	PRESSURE	50000	PA	
76	PRECIPITABLE WATER	7	KG/M**2	
77	PRESSURE	50000	PA	
78	PRESSURE	30000	PA	
79	PRECIPITABLE WATER	1	KG/M**2	
80	VERTICAL SIGNIFICANCE (SATELLITE OBSERVATIONS)	5	CODE TABLE	8003
81	EQUIVALENT BLACK BODY TEMPERATURE	229.4	K	
82	EQUIVALENT BLACK BODY TEMPERATURE	216.8	K	
83	EQUIVALENT BLACK BODY TEMPERATURE	216.3	K	
84	EQUIVALENT BLACK BODY TEMPERATURE	233.9	K	
85	EQUIVALENT BLACK BODY TEMPERATURE	247.7	K	
86	EQUIVALENT BLACK BODY TEMPERATURE	260.7	K	
87	EQUIVALENT BLACK BODY TEMPERATURE	273.1	K	
88	EQUIVALENT BLACK BODY TEMPERATURE	289.5	K	
89	EQUIVALENT BLACK BODY TEMPERATURE	271.3	K	
90	EQUIVALENT BLACK BODY TEMPERATURE	284.6	K	
91	EQUIVALENT BLACK BODY TEMPERATURE	263.6	K	
92	EQUIVALENT BLACK BODY TEMPERATURE	247	K	
93	EQUIVALENT BLACK BODY TEMPERATURE	275.8	K	
94	EQUIVALENT BLACK BODY TEMPERATURE	268	K	
95	EQUIVALENT BLACK BODY TEMPERATURE	252.2	K	
96	EQUIVALENT BLACK BODY TEMPERATURE	227.7	K	
97	EQUIVALENT BLACK BODY TEMPERATURE	286.8	K	
98	EQUIVALENT BLACK BODY TEMPERATURE	290.6	K	
99	EQUIVALENT BLACK BODY TEMPERATURE	290.6	K	
100	EQUIVALENT BLACK BODY TEMPERATURE	MISSING	K	
101	EQUIVALENT BLACK BODY TEMPERATURE	279.3	K	
102	EQUIVALENT BLACK BODY TEMPERATURE	258.2	K	
103	EQUIVALENT BLACK BODY TEMPERATURE	228.2	K	
104	EQUIVALENT BLACK BODY TEMPERATURE	206.1	K	
105	EQUIVALENT BLACK BODY TEMPERATURE	226.6	K	
106	EQUIVALENT BLACK BODY TEMPERATURE	238.5	K	
107	EQUIVALENT BLACK BODY TEMPERATURE	248.6	K	
108	VERTICAL SIGNIFICANCE (SATELLITE OBSERVATIONS)	3	CODE TABLE	8003
109	PRESSURE	10200	PA	
110	TEMPERATURE/DRY	197.3	K	

APPENDIX F: Thematic Mapper Application

Estimate Evaporation using Landsat Thematic Mapper (TM) spectral data

To estimate evaporation from the lake using Landsat Thematic Mapper (TM) spectral data, algorithm proposed by Farah and Bastiaanssen W.G.M (1999) was followed. A TM scene of January 21, 1995 was used in the analysis. Landsat Thematic Mapper (TM) measures the spectral radiance in the visible, near, middle and thermal infrared spectrum at the top of the atmosphere. TM has 3 bands in the visible, 3 bands in the near- and middle infrared and 1 band in the thermal infrared spectral region. The digital values of each pixel are converted first to spectral radiance at the top of atmosphere using a radiometric calibration procedural. Digital Numbers (DN) of each pixel can be converted to spectral radiance at the top of the atmosphere as:

$$L_{\lambda_i} = a + \frac{b-a}{255} * DN \quad [\text{mW} \cdot \text{cm}^{-2} \cdot \text{sr}^{-1} \cdot \mu\text{m}^{-1}] \quad (\text{F1})$$

Where L_{λ_i} ($\text{mW} \cdot \text{cm}^{-2} \cdot \text{sr}^{-1} \cdot \mu\text{m}^{-1}$) is the spectral radiance in band i of Thematic Mapper. The constants a and b are given by Markham and Barker (1987):

Band no:	1	2	3	4	5	7
a	-0.15	-0.28	-0.12	-0.15	-0.037	-0.015
b	15.21	29.68	20.43	20.62	2.72	1.44

The thermal channel TM_6 measures the spectrally emitted radiance between 10.6 to 12.4 μm at the top of the atmosphere, L_6^{TOA} , which can be interpreted from the raw digital numbers (DN₆) in band 6:

$$L_6^{\text{TOA}} = \{0.1238 + (1.560 - 0.1238) \times \text{DN}_6/255\} \times \pi \times B \times 10 \quad [\text{W m}^{-2}] \quad (\text{F2})$$

Where B (μm) is the bandwidth of the thermal channel ($12.4-10.6=1.8 \mu\text{m}$) and DN_6 is the digital number of TM band 6.

The broad band planetary albedo at the top of the atmosphere (r_p) was calculated with a weighing scheme of the six visible and near infrared bands (TM 1,2,3,4,5 and 7). The band wise spectral reflectance at the top of the atmosphere was calculated as:

$$r_p(\lambda_i) = \frac{\pi \cdot L_{\lambda_i} \cdot d_s^2}{K(\lambda_i) \cdot \cos \phi_{su}} \quad [-] \quad (\text{F3})$$

Where $r_p(\lambda_i)$ is spectral reflectance at the top of the atmosphere of band i , d_s is the earth-sun distance in astronomical units (Iqbal, 1983), $K(\lambda_i)$ is the spectral incoming solar radiation and ϕ_{su} is the solar zenith angle. The spectral incoming solar radiation at the top of the atmosphere for the Thematic Mapper bands is as follows (Farah, 1999):

Band no:	1	2	3	4	5	7
$K(\lambda_i)$	195.8	182.8	155.9	104.5	21.9	7.5

Finally the broad band reflectance at the top of the atmosphere was estimated as:

$$r_p = \sum w_i r_p(\lambda_i) \quad [-] \quad (F4)$$

The weights for the different bands are computed as the ratio of the amount of incoming shortwave radiation from the sun in a particular band and the sum of incoming shortwave radiation for all the bands.

Using the spectrally emitted radiance of band 6, surface temperature T_o was estimated from Eq. 3.35 and Eq. 3.34. To solve Eq. 3.34 a trial and error procedure was followed.

Energy balance equation (Eq. 3.16) was used to estimate evaporation from the lake. Considering the field data analysis sensible heat flux was taken as zero and the water heat flux was considered as 1% of net radiation, R_n (i.e. $G_o = 0.01 * R_n$) and the net radiation was estimated using Eq. 3.16:

$$R_n = (1-r_o) K\downarrow + \sigma \cdot \epsilon_a \cdot T_a^4 - (1-\epsilon_o) \cdot \sigma \cdot \epsilon_a \cdot T_a^4 - \sigma \cdot \epsilon_o \cdot T_o^4 \quad [W.m^{-2}] \quad (F5)$$

Incoming solar radiation $K\downarrow$ is determined on the basis of standard astronomical equations (Iqbal, 1983) which leads to an instantaneous value of 1180 W m^{-2} at the top of the atmosphere at the lake area during Landsat overpass at 9⁴⁵ a.m. The solar zenith angle at that moment was 33.3° . From Eq. (3.30) a value for the single-way transmittance of $\tau_{sw} = 0.59$ was obtained considering water surface albedo, $r_o = 0.06$. Hence, a portion of $1180 \times 0.59 = 696 \text{ [W. m}^{-2}]$, after atmospheric absorption, scatter and transfer will reach the land surface. The apparent emissivity of the atmosphere, $\epsilon_a = 0.91$, was obtained from Eq. (3.33). Incoming long wave radiation was estimated by using air temperature ($T_a = 24.8^\circ \text{C}$) and the apparent emissivity of the atmosphere yielding a value of $\epsilon_a \cdot \sigma \cdot T_a^4 = L\downarrow = 407 \text{ [W.m}^{-2}]$. The screen height air temperature during satellite overpass was $T_a = 24.8^\circ \text{C}$ being tentatively estimated from the minimum surface temperature of lake Naivasha ($T_o = 24.8^\circ \text{C}$) assuming that $T_a \approx T_o$ above water.

From instantaneous to daily total value, evaporative fraction method was used. Daily net radiation was calculated using Eq. (C-16, Appendix C). Daily incoming solar radiation at the top of atmosphere was calculated using Eq. (C-13a, Appendix C) which was $424.68 \text{ [W.m}^{-2}]$ and applying transmissivity = 0.59, the solar radiation reaching the surface $K\downarrow = 0.59 \times 424.68 = 250.56 \text{ [W.m}^{-2}]$. For daily net longwave radiation Slob's approach was followed which leads to a value = $110 \times \tau_{sw} = 64.9 \text{ [W.m}^{-2}]$.

REFERENCES

REFERENCES

Allen, R. G., Jensen, M.E., Wright, J.L, and Bruman, R.D., 1989, Operation Estimates of evapotranspiration, *Agron. J.*, 81: 650-662.

Allen, R. G., Pruitt, W.M., Businger, J. A., Fritschen, L.J., Jensen, M.E., Quinn, F.H., 1996, Evaporation and Transpiration, Chapter 4. *Hydrology Handbook*, second Edition, ASCE, 125-234.

Ase, L. E., 1986, *Studies of Lake Naivasha, Kenya and its Drainage Area*, Stockholm University, 63: 75p.

Assouline, S., Mahrer, Y., 1993, Evaluation from lake Kinneret 1, Eddy correlation system measurements and energy budget estimates, *Water Resources Research*, 29(4), 901-910.

Bastiaanssen, W.G.M., 1995, Regionalization of surface flux densities and moisture indicators in composite terrain, A remote sensing approach under clear skies in mediterranean climates, Doctoral thesis, Wageningen Agricultural University, Wageningen, The Netherlands.

Bastiaanssen, W.G.M., Pelgrum, L., Menenti, M. and Feddes, R. A., 1996a, Estimation of surface resistance and Priestley- Taylor α -parameter at different scales, In: J. B. Stewart et. al. (eds). *Scaling up in hydrology using remote sensing*. Institute of Hydrology, Wallingford, 93-111.

Bastiaanssen, W.G.M., R. Singh, S. Kumar, J. K. Schakel and R. K. Jhorar, 1996b, Analysis and Recommendations for integrated on-farm water management in Haryana, India: a model approach. Wageningen (The Netherlands), DLO, Winand Staring Center. Report 118. 152 pp.

Breon, F., R. Frouin, and C. Gautier, 1991, Downwelling longwave irradiance at the ocean surface: An assessment of in situ measurements and parameterizations. *J. Appl. Meteorol.*, 30, 17-31.

Brind, W. and Robertson, J. K., 1958, *The Hydrology of the lake Naivasha*. (Prepared by the section of Hydrology, Ministry of Works, Kenya), 9pp + 9 plans.

Bruin, H. A. R. De, 1987, From Penman to Makkink. Committee on Hydrological Research, TNO, The Hague, *Proceedings and Information* 39: 5-31.

Bruin, H.A.R. De, 1982. Temperature and energy balance of water reservoir determined from standard weather data of a land station. *Journal of Hydrology*. 59: 261-274.

Bruin, H.A.R. De, 1981, The determination of (reference crop) evapotranspiration from routine weather data. Committee on Hydrological Research, TNO, The Hague, *Proceedings and Information* 28: 25-37.

Bruin, H. A. R. De. and Keijman, J. Q., 1979, The Priestley - Taylor evaporation model applied to a large, shallow lake in the Netherlands, *J. Appl. Meteor.*, 1979, 18: 893-903.

- Brunt, D., 1932, Notes on radiation in the atmosphere, I. Quaternary Journal of Royal Meteorological Society, 58: 389-420.
- Brutsaert, W., 1982, evaporation into Atmosphere, D. Reidel Dordrecht.
- Brutsaert, W., 1975, The roughness length for water vapor, sensible heat and other scalars. J. Atm. Sci., 32: 2028-2031
- Brutsaert, W. and Sugita, M. 1992. Application of Self-preservation in evaluation of the surface energy budget to determine daily evaporation. Journal of Geophysical Research, 37: 18377 - 18382.
- Choudhury, B.J., 1997, Global Pattern of Potential Evaporation Calculated from the Penman-Monteith Equation using Satellite and Assimilated data, Remote sensing Environment. 61: 64 – 81.
- Choudhury, B.J., 1996, Comparison of two models relating precipitable water to surface humidity using global distributed radiosonde data over land surfaces. Int. J. Climatol. 16: 663-675.
- Choudhury, B.J., 1994, Synergism of Multispectral Satellite Observation for Estimating Regional Land Surface Evaporation, Remote sensing Environment. 49: 264 -274.
- Crago, R. D. 1996, Daytime evaporation from conservation of surface flux ratios, In: J. B. Stewart et. al. (eds). Scaling up in hydrology using remote sensing. Institute of Hydrology, Wallingford, 235-244.
- Croley, T. E. II, 1989, Verifiable evaporation modeling on the Laurentian great Lakes, Water Resources Research, 25: 781-792.
- Darnell, W.L., W.F. Staylor, Gupta, S.K. et. al., 1996, A Climatology of the surface radiation budget derived from satellite data, Journal of Geophysical Research, in press.
- Darnell, W.L., W.F. Staylor, S.K. Gupta, N.A. Ritchey and A.C. Willber, 1992, Seasonal variation of surface radiation budget derieved from International satellite Cloud Climatology Project CI data, Journal of Geophysical Research 97(D14): 15745-15760.
- Darnell, W.L., W.F. Staylor, S.K.Gupta and F.M. Denn, 1988, Estimation of Surface insolation using Sun-Synchronus satellite data, J. Clim., 1, 820-835.
- Dingman, S. L., 1994, Physical Hydrology, Prentice- Hall, Inc, New Jersey.
- Doorenbos, J. and Pruitt, W.O., 1977, Crop water Requirements, Irrigation and Drainage paper 24 (rev), FAO Rome, Italy.179p.
- England, F. S. E. and Robertson, J. O., 1959, Hydrological study of the Lake Naivasha and its catchment. Hydrology section of the Ministry of Works, Kenya.

- Farah, O.H and Bastiaanssen W.G.M., 1999, Estimation variability of watershed surface parameters and evaporation from remote sensing measurements without access to ground data, *J. Of Hydrology* (submitted)
- Ferguson, H.L. and G. Den Hartog., 1975, Meteorological studies of evaporation at Perch Lake , Ontario. Hydrological studies on a small basin on the Canadian shield- Evaporation Studies, P.J. Barry (Ed.), AECL Chalk River Nuclear Laboratories, pp. 417-448.
- Frouin, R., Gautier, C. and J.J. Morcrette, 1988, Downward longwave irradiation at the ocean surface from satellite data: Methodology and in situ validation. *Journal of Geophysical Research* 93(C1): 597-619.
- Frouin, R., and Pinker, R.T., 1995, Estimating of photosynthetically active radiation (PAR) at the earth's surface from satellite observations, *Remote Sens. Environ.* 51: 98-107.
- Garrat, J. R., 1978, Transfer characteristics for a heterogeneous surface of large aerodynamic roughness, *Q. J. Roy. Met. Soc.* 104: 491-502.
- Gaudet, J. J. and Melack, J. M., 1979, Major iron chemistry and solute budget in a tropical African Lake basin. *Fresh water Biology*.
- Goodrum, G., K. B. Kidwell and W. Winston, 1999, NOAA KLM User's Guide, Washington, DC.
- Gupta, S.K., 1989, A Parameterization for Longwave Surface Radiation from Sun-Synchronous Satellite Data, *J. Clim.* 2, 305-320.
- Hargreaves, G. H. and Samani, Z. A., 1982, Estimating potential evapotranspiration, *Tech. Notes, J. Irrig. And Drain. Engrg., ASCE*, 108(3): 225-230.
- Hoyt, D. V., 1978, A model for calculation of solar global insolation. *Sol. Energy*, 21: 57-35.
- Iqbal, M., 1983, *An introduction to solar radiation*, Academic press, Canada.
- Jackson, R. D., P. J. Printer, and R. J. Reginato., 1985, Net Radiation calculated from remote multispectral and ground station meteorological data. *Agricultural and Forest Meteorology*, 35 : 153 -164.
- Keijman, J.Q., 1981, Theoretical background of some methods of determination of evaporation, *Comm. Hydro. Research, TNO, The Hague, Proceedings and Information* 28: 12-24.
- Keijman, J.Q., 1974, The estimation of energy balance of lake from simple weather data, *Boundary- layers Meteorology*, 7: 399-407.
- Kidwell, K. B., 1984, NOAA Polar Orbital Data User's guide, Washington, DC, Chap.4.
- Kidwell, K. B., 1998, NOAA Polar Orbital Data User's guide, Washington, DC.

- Koberg, G. E., 1964, Methods to compute longwave radiation from the atmosphere and reflected solar radiation from a water surface. DC: U.S. geological survey professional papers, 272-F.
- Kondrat'ev, K. Ya., 1972, Radiation process in the atmosphere. World Meteorological Organization Report WMO-309, 214pp.
- Kustas, W. P., M. S. Moran, K. S. Humes, D. I. Stannard, P. J. Printer, L. E. Hipps, E. Swiatek, and D. C. Goodrich, 1994, Surface energy balance estimates at local and regional scales using optical remote sensing from aircraft platform and atmospheric data collected over semiarid rangelands. *Water Resource Research* 30(5); 1241-1259.
- Lacis, A. A. and J. E. Hansen, 1974, A parameterization for the absorption of solar radiation in the Earth's atmosphere. *J. Atmos. Sci.* 31: 118-133.
- Li, Z., and H.G. Leighton.1993, Global climatologies of solar radiation budgets at the surface and in the atmosphere for 5 years of ERBE data. *Journal of Geophysical Research* 98(D3): 4919-4930.
- LNROA, 1996, Lake Naivasha Management Plan, July 1996.
- LNROA, 1993, A Three Phases Environmental Impact study of recent developments around Lake Naivasha, Phase I. December 1993, John Goldson Associate, Nairobi, Kenya. 75p.
- Markham, B. L. and J. L. Barker, 1987, Thematic Mapper bandpass solar exo-atmospherical irradiances, *Int. J. of Remote Sens.* 8(3): 517-523.
- Melack, J. M., 1976, Limnology and dynamics of phytoplankton in equatorial African Lakes, Ph D thesis. Dept. of Zoology, Duke University. Durham, N. C. 453p.
- Moran, M. S., R. D. Jackson, L. H. Raymond, L. W. Gay, and P. N. Slater, 1989, Mapping surface energy balance components by combining Landsat Thematic Mapper, and ground-based meteorological data. *Remote Sensing of Environment* 41: 169-184.
- Muthuri, F.M., Jones, M.B. and Imbamba, S.K., 1989, Primary productivity of Papyrus (*Cyperus papyrus*) in a tropical Swamp; Lake Naivasha, Kenya, *Biomass* 18 (1989) , 1-14.
- Nunez, M., T.L.hart, and J.D. Kalma, 1984, Estimate solar radiation in a tropical environment using satellite data. *Journal of Climatology* 4:573-585.
- Pelgrum, H., and W. G. M. Bastiaanssen, 1996, An inter comparison of techniques to determine the area averaged latent heat flux from individual in situ observations: A remote sensing approach using the European Field Experiments in a Desertification-Threatened Area data. *Water Resources Research* 32(9): 2775-2786.
- Penman, H.L., 1948a, Natural evaporation from open water, bare soil and grass, *Proceeding of Royal society, London series A*, 193: 120-146.
- Penman, H.L., 1948b *Evaporation in Nature*, *Progress in Physics* 11, p. 366-388.,

- Priestley, C.H.B. and R.J. Taylor, 1972, On the assessment of surface heat flux and evaporation using large scale parameters, *Monthly weather Review* 100; 81-92.
- Prevot, L., Y. Brunet, K. T. Paw U and B. Seguin, 1994, Canopy modeling for estimating sensible heat flux from thermal infrared measurements, in *Proc. Workshop on Thermal remote sensing of the energy and water balance*, La Londe les Maures, 20-23 Sept. France : 17-22.
- Reis, J. R. and Dias, N. L (1998), Multi- Season lake evaporation: energy- budget estimates and CRLE model assessment with limited meteorological observations. *Journal of Hydrology*, 208(1998) 135-147.
- Richardson, J. and Richardson, A., 1972, History of African Lake and its climate implications. *Ecol. Monogr.* 42: 499-534.
- Robertson, E., and P.J. Barry, 1985, The water and energy balances of perch lake (1969-1980), *Atmo. Ocean*, 23, 238-253.
- Rosenberry, D. O., A.M. Sturrock and T. C. Winter., 1993, Evaluation of the Energy budget method of determining evaporation at Williams lake, Minnesota, using alternative instruments & study approach, *Water Resources Research*, 29(8), 2473-2483.
- Rossow, W.B., and Y.C. Zhang, 1995, Calculation of surface and top of atmosphere radiative fluxes from physical quantities based on ISCCP data sets: 2. Validation and first results. *Journal of Geophysical Research- Atmosphere* 100(D1): 1167-1197.
- Schmetz, P., J. Schmetz, and E. Raschke. 1986, Estimation of daytime downward longwave radiation at the surface from satellite and grid point data. *Theoretical and applied Climatology* 37: 136-149.
- Schmugge, T., S. J. Hook and C. Coll, 1998, Recovering surface temperature and emissivity from thermal infrared multispectral data, *Rem. Sens. Env.* 65: 121-131.
- Shuttleworth, W. J., Gurney, R. J., Hsu, A. Y. and Ormsby, J. P., 1989, FIFE: The variation in energy partition at surface flux sites. *IAHS Pub. No.* 186, 67-74.
- Simons, E. and Mero. F., 1985, A simplified procedure for the evaluation of lake Kinneret evaporation, *Journal of Hydrology*, 78, 291-304.
- Smith, M., R. G. Allen, Monteith, J., Perrin, A., Perrin L., and Segeren, A., 1991, Report of the expert consultation on procedures for revision of FAO guidelines for prediction of crop water requirements. UN-FAO, Rome, Italy, 54 p.
- Stanhill, G., 1983, The distribution of global solar radiation over the land surface of the Earth. *Solar Energy* 31:95-104.
- Stewart, R. Rose W., 1976, A simple method for determining the evaporation from lakes and ponds, *Water Resources Research*, 12, 623-628.

- Stricker, J. N. M., 1981, Method of estimating evapotranspiration from meteorological data and their applicability in hydrology. Comm. Hydro. Research, TNO, The Hague, Proceedings and Information 28: 59-75.
- Stuhlmann, R., 1996, Clouds and Radiative Heating of the Earth Surface-Atmosphere system, Radiation and Water in the climate system: Remote measurements, Edited by Ehrhard Raschke, 151-174. Berlin: Springer- verlag.
- Sturrock, A.M. Winter, T.C. Rosenberry, 1992, Energy budget evaporation from William lake: A closed lake in North central Minnesota, Water Resources Research, 28(6), 1605-1607.
- Sverdrup, H. V., 1945, Oceanography for Meteorologists, London: Allen and Unwin.
- Swinbank, W.C., 1963, Longwave radiation from clear skies, Quaternary Journal of Royal Meteorological Society, 89: 339-348.
- Tarpley, J.D. 1979, Estimating incident solar radiation at the surface from geostationary satellite data. Journal of Applied Meteorology 18: 1172-1181.
- Tetley, A. E., 1948, Note on Lake Naivasha by Hydraulic engineer. Rept. From the Dir. Water Dev. of Nbi. Feb., 1948.
- Thom, A. S., 1972, Momentum mass and heat exchange of vegetation, Q. J. Royal Meteorological Society. 103: 345 -357.
- Thom, A. S., 1975, Momentum mass and heat exchange of plant communities, chapter 3 in vegetation and the atmosphere, vol.1 (J. I. Monteith, Ed.) Academic Press(Lond), 57-109.
- Thom, A. S. and H. R. Oliver, 1977, On Penman's equation for estimating regional evaporation. Quart. J. Roy. Met. Soc. 96: 67-90.
- Tuzet, A. 1990, A simple method for estimating downward longwave radiation from surface and satellite data by clear sky. International Journal of Remote sensing 11: 125-131.
- Whitlock, C. H., Charlock, T.P., Staylor, W.F., et. al., 1995, First global WCRC shortwave surface radiation budget data set. Bull. Am. Meteorol. Soc. 76: 905-922.
- Yamamoto, G., 1962, Direct absorption of solar radiation by atmospheric water vapor, carbon dioxide, and molecular oxygen. J. Atmos. Sci. 19: 182-188.
- Zhang, Y.C., W.B. Rossow, and A. A. Lacis., 1995. Calculation of surface and top of atmosphere radiative fluxes from physical quantities based on ISCCP data sets: 1. Method and sensitivity to input data uncertainties. Journal of Geophysical Research-Atmospheres 100(D1): 1149-11165.
- Zhong, Q. and Y. H. Li, 1988, Satellite observation of surface albedo over Qinghai-Xinjiang plateau region, Adv. In Atm. Sciences 5:57-65.